INFORMATION TO USERS

This manuscript has been reproduced from the microfilm master. UMI films the text directly from the original or copy submitted. Thus, some thesis and dissertation copies are in typewriter face, while others may be from any type of computer printer.

The quality of this reproduction is dependent upon the quality of the copy submitted. Broken or indistinct print, colored or poor quality illustrations and photographs, print bleedthrough, substandard margins, and improper alignment can adversely affect reproduction.

In the unlikely event that the author did not send UMI a complete manuscript and there are missing pages, these will be noted. Also, if unauthorized copyright material had to be removed, a note will indicate the deletion.

Oversize materials (e.g., maps, drawings, charts) are reproduced by sectioning the original, beginning at the upper left-hand corner and continuing from left to right in equal sections with small overlaps. Each original is also photographed in one exposure and is included in reduced form at the back of the book.

Photographs included in the original manuscript have been reproduced xerographically in this copy. Higher quality 6" x 9" black and white photographic prints are available for any photographs or illustrations appearing in this copy for an additional charge. Contact UMI directly to order.

UMI

A Bell & Howell Information Company
300 North Zeeb Road, Ann Arbor, MI 48106-1346 USA
313/761-4700 800/521-0600

UNIVERSITY OF CALIFORNIA
Santa Barbara

Nonlinear and Nonperturbative Dynamics in Quantum Wells

A Dissertation submitted in partial satisfaction
of the requirements for the degree of

Doctor of Philosophy
in
Physics
by
Bryan Galdrikian

Committee in charge:
- Professor Mark S. Sherwin, Chairperson
- Professor Björn Birnir, Co-Chairperson
- Professor Elizabeth Gwinn
- Professor James Langer

UMI Number: 9522790

UMI
300 North Zeeb Road
Ann Arbor, MI 48103

The dissertation of Bryan Galdrikian is approved:

James S. Langer

Beth Gwinn

Björn Birnir

Committee Co-Chairperson

Mark Sherwin

Committee Chairperson

August 1994

August 24, 1994

Acknowledgements

Of course it's my mother who's to blame for all of this. At that age when I was a kid full of questions, she was in college and full of answers. I became as comfortable with an Erlenmeyer flask as I was with a G. I. Joe. It seemed every question had an answer, and I began to think that everything was knowable. Someday I would know everything.

At the same time, my father would take me to the local beat café, where hippies and intellectuals played chess, read poetry, and talked about everything. Their strange words were beyond me, but hinted at mysteries to be experienced. Someday, I would experience everything.

Well, everything is a lot. It took me a while to understand that anything is possible, but not everything. However, I also learned that there are many paths to the same truth, and if I followed one path for long enough then my experiences would somehow hint at more universal truths. With no more of a plan than to learn everything by learning one thing well, I started graduate school in physics. Well, some of what I've learned I summed up in this thesis.

There are several people I'd like to thank for being helpful, and in some cases essential, to the completion of this thesis. I wish to thank Mark Sherwin, who first took me on board in his research. When I moaned and bitched, he convinced me to stay in graduate school, and I'm very grateful for that. I'm just as grateful to Björn Birnir, who gave me the opportunity to study quantum wells the way I have, as a theorist working in an experimental group. It's been a wonderful experience!

Rainer Scharf and Bala Sundaram first introduced me to Floquet states, and Frank Stiernelof and Rainer Grauer helped me develop the computer code to calculate those states. Martin Holthaus really opened up the floodgates, teaching me more about the Floquet picture than I thought I wanted to know. Chris Felix, Bill Bewley, and John Plombon were finishing their pioneering quantum well research when I started, and were always more than willing to answer my stupid and often repeated questions. Thanks and more thanks!

I feel very lucky not only to have met, but also to have worked with my friend Keith Craig. He made work a pleasure, and made me question my sanity. Woof?

James Heyman has been a friend and collaborator, and it's been a great fun simulating his experiments, and pulling my hair out over factors of two with him! Andrea Markelz and John Černe also helped to keep me out of trouble. There is no doubt in my mind who built the box of glove. Thanks to Tony Gutierreγ for keeping my stomach full of cup-o-noodle, and my head full of music!

Many, many thanks to Shirley Pepke, for her love and understanding, especially while I write this thesis. She fills my days with laughter and magic, crossword puzzles and Random walks.

And thanks to my roommates, and other friends, who always inspire me and remind me how wonderful life is. Colleen Belharrat, my guardian angel, excels at keeping me on my toes. (Sometimes literally... Olé!) Jill Katz, my best and oldest friend in Santa Barbara, has kept my head pointed toward the heavens. I love being on this planet with her.

My teachers, friends and family have encouraged and supported me for my entire life, and to them I owe everything. I love them dearly, and thank them.

To my teachers, friends and family.

Vita

June 29, 1965	Born: Fresno, California.
Sep. 1983 – Dec. 1984	Fresno City College and California State University, Fresno
Jan. 1985 – June 1988	B.S. with High Honors in Physics and Mathematics, minor in Philosophy. University of California, Davis.
Sep. 1988 – June 1990	Teaching Assistant, Dept. of Physics, University of California, Santa Barbara.
Sep. 1990 – Aug. 1991	Graduate Research Assistant, T13 and CNLS, Los Alamos National Laboratory.
Sep. 1991 – Aug. 1994	Research Assistant, Dept. of Physics, University of California, Santa Barbara.

PUBLICATIONS

"Testing for Nonlinearity in Time Series - The Method of Surrogate data," J. Theiler, S. Eubank, A. Longtin, B. Galdrikian and D. Farmer, Physica D, **58**, 77 (1992).

"Nonperturbative Resonances in Periodically Driven Quantum Wells," B. Birnir, B. Galdrikian, R. Grauer and M. S. Sherwin, Physical Review B, **47**, 6795 (1993).

"Far-Infrared Nonlinear Response of Electrons in Semiconductor Nanostructures," M. S. Sherwin, N. Asmar, W. Bewley, K. Craig, C. Felix, B. Galdrikian, E. Gwinn, A. Markelz and B. Birnir, SPIE Proceedings of OE/LASE '93, Free Electron Laser Spectroscopy in Biology, Medicine, and Materials Science, vol. 1854, pp. 36-47.

"Nonlinear Multiphoton Resonances in Quantum Wells," B. Galdrikian, B. Birnir and M. S. Sherwin, to be published in Physics Letters A.

"Resonant Harmonic Generation and Dynamic Screening in a Double Quantum Well," J. N. Heyman, K. Craig, B. Galdrikian, M. S. Sherwin, and K. Campman, P. F. Hopkins, S. Fafard, A. C. Gossard, Physical Review Letters, **72**, 2183 (1994).

"Self-Consistent Floquet States for Periodically-Driven Quantum Wells," B. Galdrikian, B. Birnir and M. S. Sherwin, Physical Review B, **49**, 13744 (1994).

Abstract

Nonlinear and Nonperturbative Dynamics in Quantum Wells

by

Bryan Galdrikian

Quantum well studies at the Free Electron Laser facility at the University of California, Santa Barbara, motivate a program for the theoretical study of the interaction of intense radiation with electrons in semiconductor heterostructures. Confined in one dimension, and free in the other two, electrons in quantum wells have their energies quantized in parabolic subbands. When laser light is coupled into the well, with polarization in the confinement direction, the matter-radiation system can be approximated as a one dimensional man-made "atom." The optical properties of this system are studied here, both in the perturbative and nonperturbative (weak and strong laser field) regimes.

Whereas the classical analog of a driven quantum well has a phase-space which is typically a mixture of resonances and chaotic trajectories (Hamiltonian chaos), the quantum system may be characterized by a time-dependent basis set known as Floquet states. These states' coarse-grained Wigner distributions are ghostly likenesses of the classical phase space structures. The nonintegrability of the classically chaotic system manifests itself quantum mechanically with the appearance of avoided crossings in the spectrum of eigenvalues associated with the Floquet states. Avoided crossings correspond to multi-photon resonances and harmonic generation.

The presence of electron-electron interactions provides interesting behavior as well, introducing nonlinearities into the dynamics (in the mean-field approximation). In the weak field regime, perturbation theory predicts an optical response function whose poles do not reside at the intersubband energy spacings, due to dressing of the field by the electron-electron interactions. Dressed optical response formulae are derived in this work up to second order. In the strong field regime, perturbation theory breaks down. However, one may directly integrate the quantum equations of motion to find a strong field steady-state response, if there is dissipation present. When dissipation can be neglected, the dynamics become sensitive to initial conditions, and the nonlinearity due to electron-electron interactions may even lead to chaos.

Contents

List of Figures

Chapter 1

Introduction

What is essential is invisible to the eye.

- Antoine de Saint-Exupéry

This work is an attempt to understand the interaction of intense radiation with matter, in particular the response of quantum systems when subjected to a powerful source of electro-magnetic radiation. Most of the work has been done in direct conjunction with experiments performed at the UC Santa Barbara Free Electron Laser (FEL) on doped quantum well structures. Quantum wells are layered semiconductor devices, which tend to confine conduction-band electrons in a plane. The confinement quantizes the allowed energies of the electrons into ***subbands***. Transitions between subbands may be probed optically, and occur typically in the Far-Infrared (FIR), or about $\hbar\omega \sim$ 5-50 meV. The UCSB FEL at present is continuously tunable in the $\hbar\omega =$ 0.5-15 meV range. Thus, it can probe inter-subband transitions in wider quantum wells (on the order of hundreds of Angstroms).

Experiments are being carried out on quantum well structures at the UCSB FEL by several groups, including those headed by Mark Sherwin, Elizabeth Gwinn, and S.

James Allen. These experiments include measurements optical absorption, harmonic generation, and optical rectification. Keith Craig has had success in measuring intensity-dependent absorption spectra in a quantum well, while James N. Heyman has measured second and third harmonic generation, as well as optical rectification (a second-order static displacement of the electrons) in a quantum well. Quantum well structures have been found to have extremely strong harmonic responses, as much as 5 or 6 orders of magnitude higher than the bulk semiconductor.

The quantum wells studied are grown, atomic layer by atomic layer, with a method called Molecular Beam Epitaxy (MBE). This method allows one to specify the chemical makeup of each atomic layer, thus providing control over the band structure of the solid in the direction of growth. (From now on, the growth direction will be labeled z, so the atomic layers just mentioned lie in the $x - y$ plane.) In the wells studied, each atomic layer consisted of $Al_xGa_{1-x}As$, with x varying from 0 to 0.3 as a function of z. Figure 1.1 schematically depicts such a quantum well structure. $Al_{0.3}Ga_{0.7}As$ has a conduction band energy which is about 250 meV higher than $GaAs$, providing that much control of the conduction band profile. The band structure is approximately uniform in the $x - y$ plane, so that electrons are free to move in the plane. This gives us an effectively one-dimensional system, since translational symmetry in the plane allows us to ignore, to a good approximation, the dynamics in the plane[1]

In order to populate the quantum well with electrons, Silicon doping regions are laid down during the growth process, usually hundreds of atomic layers from the region of the well. Electrons donated by the Silicon "fall" into the low-potential

---

[1] The present accuracy of MBE allows control of the growth with an error of about one atomic layer.

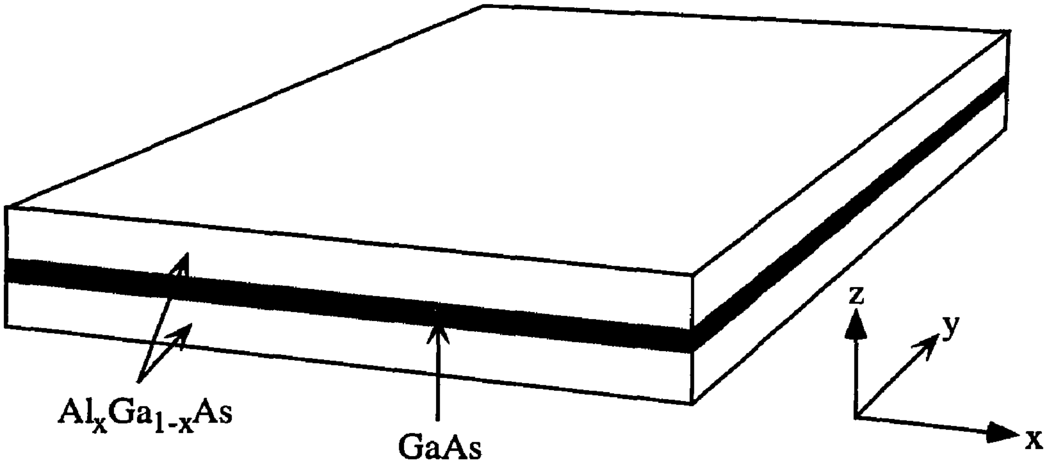

Figure 1.1: Schematic of the quantum well.

region of the well. The electron sheet density in the well, along with the profile of the well itself, are all able to be rather faithfully supplied by the growers, given the specification of the well designer. Thus, we have what seems a theorist's dream come true, that is a simple one-dimensional quantum system, which may be probed by a highly tunable source of long-wavelength radiation. Such systems are not just for textbooks any more!

Of course, these systems are actually three-dimensional, and consist of a large number of interacting electrons. They are also dissipative, due to inelastic scattering of the electrons with phonons in the solid. The dissipation may be reduced by studying transitions *below* the Longitudinal-Optical phonon energy, which for $GaAs$ is 36 meV, thus eliminating the possibility of exciting these phonons. (Acoustic phonons will still be excited, as their energies range down to zero.) The electron-electron interaction must be accounted for in order to accurately model wider quantum wells. This interaction may be treated in a variety of ways, and in this work the electron-electron interactions will be treated by the mean-field approach, that is, using an effective potential which approximates the effect of all other electrons on a single typical electron [29]. In this approximation, we will see that the effect of the electron-electron interaction can range from trivial, as in the case of linear response, where the effect is a shift of the optical absorption frequency, to spectacular in the case of strongly-driven systems, which can give rise to chaotic dynamics in the well.

This work proceeds in stages, modeling the quantum well more accurately with each stage. First we will look at classical model of a quantum well structure. We will see that classically, a single electron in a quantum well will exhibit chaotic motion when driven strongly. This interesting classical behavior has quantum manifestations, which will be explored in the second section. There we will examine the quantum manifestations of classical chaos in simple one-dimensional systems, and after that treat the effects of dissipation and electron-electron interactions. We will then be able to derive the perturbative response of doped quantum wells, and we will derive many-body second-order response functions which are used to model the experiments of Heyman et al.

Throughout this work, we will take advantage of the fact that the wavelength of the driving radiation is much larger than the system being studied, so that a good approximation to the effect of the radiation is the Electric Dipole Approximation (for a derivation, see [31]), which enters the Hamiltonian as a time-dependent potential:

$$V_L(z,t) = e\mathcal{E}z\sin\omega t, \tag{1.1}$$

where e is the electron charge, and $\mathcal{E}$ and ω are the magnitude and frequency of the electric field. The effective potential seen by a single electron, due to the presence of other electrons, will be denoted as $v(z,t)$. These two potentials, along with the conduction band profile in the z direction, $W(z)$, comprise the total potential seen by a single electron (see figure 1.2, for example). Thus the general Hamiltonian being studied is

$$H(p_z, z, t) = \frac{p_z^2}{2m^*} + W(z) + V_L(z,t) + v(z,t), \tag{1.2}$$

where p_z is the conjugate momentum to the coördinate z, and m^* is the effective mass of the electron, in the z direction. Again, we have ignored the dynamics in the $x - y$ plane, assuming they separate trivially from the z-coördinate, owing to translational symmetry in the plane.

A large body of work in the physics literature is devoted to calculating perturbative *response functions* of driven systems such as the one described by the Hamiltonian 1.2. These response functions are valid when the driving field is relatively weak, i.e. when

$$e\mathcal{E}a \ll \hbar\omega, \tag{1.3}$$

where a is a relevant length scale in the system. In general, any observable O can be used to define the response $\langle O(t)\rangle \equiv \langle\psi(t)|O|\psi(t)\rangle$, where $|\psi(t)\rangle$ is the solution to Schrödinger's equation

$$i\hbar\frac{\partial\psi}{\partial t} = H(t)\psi(t). \tag{1.4}$$

(Here we have suppressed the z- and p_z-dependence, making the equation basis independent.) In order to calculate a unique and well-defined response function, it is the usual convention to ramp up the driving field (1.1) slowly, by introducing an exponential envelope,

$$V_L(z,t) = e\mathcal{E}ze^{\eta t}\sin\omega t, \tag{1.5}$$

and then taking the limit $\eta \to 0$ in deriving the response,

$$O(t) \equiv \lim_{\eta\to 0}\langle\psi(t)|O|\psi(t)\rangle.$$

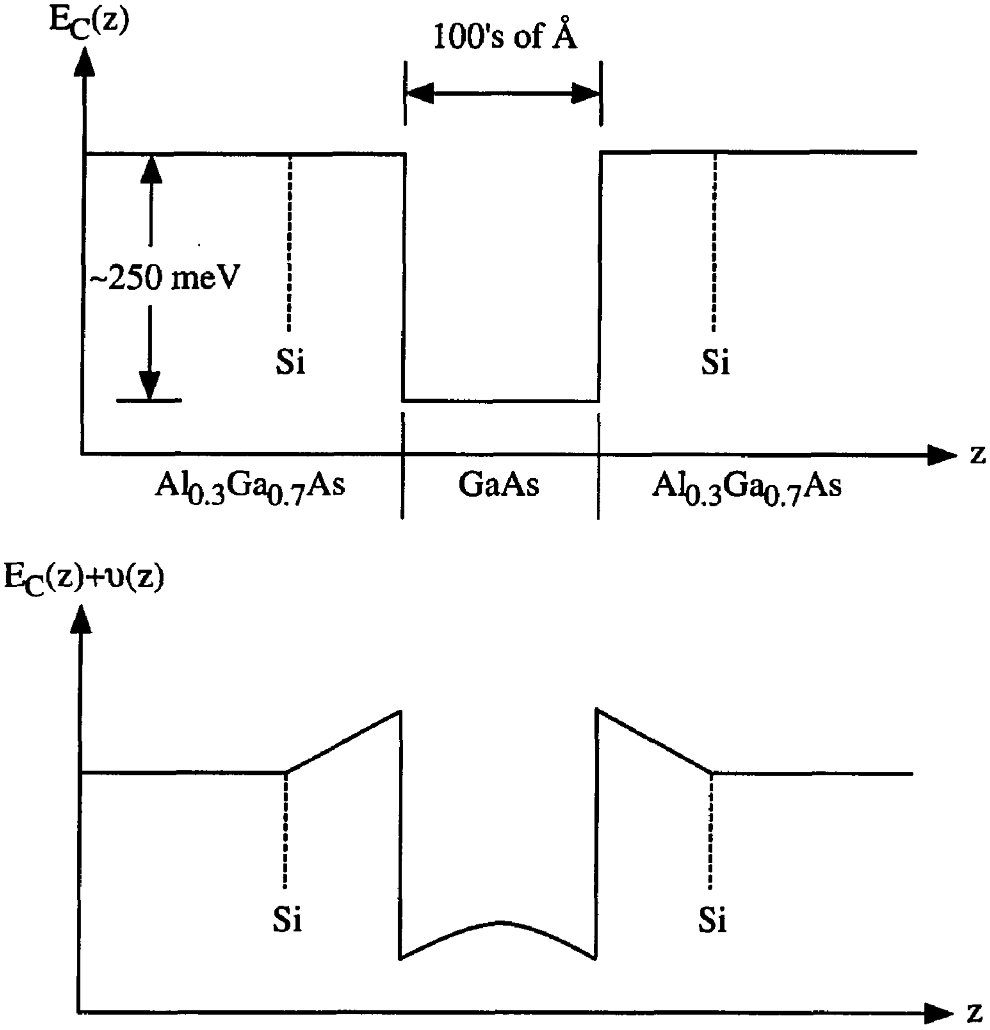

Figure 1.2: A simple square well, empty (top) and full (bottom). The well is populated by electrons from the silicon donors outside of the well.

This has the effect of eliminating all "transients" from the system's response, thus producing what we would expect to be the system's long-time behavior.

As we will see in chapter 3, there are cases where no such well-defined, unique response function exists, when (1.3) is not true. For strongly driven systems, the behavior of $|\psi(t)\rangle$ (and any observable derived from it) may depend on the *past history* of the system (that is, what the driving on the system was *before* equation 1.1 holds). The past history, for example whether or not the driving field was turned on slowly, or suddenly switched on, can have a permanent effect on the behavior of the system *even* in the long-time limit. One might think that this history dependence can be eliminated by ramping up the field in a well-defined way, as in equation 1.5, but this will not work for a strongly driven system in general. In some cases, when dissipation may be neglected, the limit

$$\lim_{\eta \to 0} |\psi(t)\rangle$$

does not even exist! We will explore examples of such history-dependence in chapter 6, and the interesting effect of many-body interactions, which can give the system a *sensitive* dependence to its history. We will also see that when dissipation is important, as it is in an actual quantum well, much of this history-dependence disappears, giving way to more robust behavior as one might expect in a real system.

We will now embark on a journey through the physics of the systems described by (1.2), from the classical regime to quantum, and from the very simple to the very complex.

Chapter 2

The Classical Picture

The dynamics of a dissipationless, driven classical particle in a potential well can be divided into two classes: regular and chaotic [15]. The chaotic regime is distinguished from the regular by sensitive dependence on initial conditions, that is, two nearby initial conditions will quickly diverge from each other. Consider now such a system, for example a square [30, 9, 33] or triangular [5] well. (We exclude the few integrable systems, where solutions to the time-evolution may be written in closed form.) With no driving, the classical phase space consists of invariant surfaces (time-evolution maps an invariant surface to itself) of constant energy. As the driving amplitude is turned up, many of these surfaces remain, but are distorted, and are now named "Kolmogorov-Arnold-Moser" (KAM) invariant surfaces. Resonances occur, between the particle's natural frequency in its potential and the drive frequency. Resonances are closed trajectories, periodic with some multiple of the drive period. If a resonance is "stable,"[1] then nearby trajectories circle about the resonant trajectory. This creates an "island" of regular motion. If the resonance is "unstable," then nearly all nearby trajectories diverge exponentially from the resonance. "Chaotic" homoclinic

---

[1] Stable here means marginally stable, as this terminology is conventional for Hamiltonian (i.e. dissipationless) systems.

tangles surround the unstable resonances, for any amount of drive. As the drive is increased, stable trajectories turn unstable, and the size of the chaotic regime grows. The growth is accompanied by the destruction of KAM surfaces, and thus regular motion is systematically replaced by chaotic motion with increased driving. The qualitative analysis is similar for all the non-integrable wells whose dynamics can be reduced to a twist map[2]. These wells are generic, in contrast to integrable wells such as parabolic wells, which are exceptional. We chose to work with the square well because it is analytically simple and experimentally easy to make. In the case of the square well, after the last of the main stable resonances goes unstable, the phase space consists of nearly entirely chaotic trajectories at low momentum, bounded by KAM surfaces beyond some particular momentum value.

In this chapter we will model the square well, scaling the system to have only one free parameter for simplicity, which we have chosen to be the scaled drive amplitude. The sequential destruction of the KAM surfaces *between* the resonances as drive amplitude is increased gives rise to non-trivial stochastic behavior as a function of drive amplitude. In the driven square well, a particle with low momentum lies in a chaotic regime, and may explore low momenta, bounded by KAM surfaces at some point. As the drive is increased, fewer resonances are separated by KAM surfaces, and the energy obtainable by the system sharply increases when the last KAM surface disappears between two resonances. This signature of chaotic transport will be seen in a simulation performed in this section. To predict when KAM surfaces disappear, we will compare the Chirikov resonance overlap criterion [15] with a

---

[2] i.e., wells for which, in the absence of driving, the oscillation frequency changes with the amplitude of oscillation. Piecewise parabolic wells have no twist, and analysis is fundamentally different in this case [37].

criterion introduced by J. M. Greene [23]. The latter criterion requires a calculation of the stability of fixed points near the KAM surface in question. We use this criterion crudely and only consider the main $n : 1$ fixed points, but the results are considerably better than Chirikov's method. The exact stability calculations will be derived in this chapter.

2.1 The Hamiltonian and Poincaré Section

We begin with the Hamiltonian (1.2), neglecting the electron-electron interactions ($v(z,t) = 0$), for an electron in a 1-D infinite square potential of half-width a:

$$H(p_z, z, t) = \frac{p_z^2}{2m^*} + W(z) + e\mathcal{E} z \sin(\omega t), \qquad W(z) = \begin{cases} 0, & |z| < a \\ \infty, & |z| \geq a \end{cases} .$$

We shall put the Hamiltonian into unitless form with the following substitutions:

$$\tau \equiv \omega t, \qquad q \equiv a^{-1} z, \qquad \lambda \equiv (m^* \omega^2 a)^{-1} e\mathcal{E}, \tag{2.1}$$

It follows that momentum is scaled by the quantity $m^*\omega a$, and energy by the quantity $m^*\omega^2 a^2$. Thus, defining

$$p \equiv (m^* \omega a)^{-1} p_z, \qquad h(p, q, \tau) \equiv (m^* \omega^2 a^2)^{-1} H(p_z, z, t),$$

we arrive at the unitless Hamiltonian

$$h(p, q, \tau) = \tfrac{1}{2} p^2 + W(q) + \lambda q \sin(\tau). \tag{2.2}$$

From (2.2), the equation of motion is integrated to give the trajectory

$$q(\tau) = \lambda[\sin(\tau) - \sin(\tau_0)] + [p_0 - \lambda \cos(\tau_0)](\tau - \tau_0) + q_0. \tag{2.3}$$

(We define $q_0 = q(\tau_0)$ and $p_0 = p(\tau_0)$.) To account for the presence of the walls, a root finder is used to find when the electron hits either wall (i.e., τ such that $q(\tau) = \pm 1$). This value of τ is then taken as τ_0, the momentum reversed, and the process is iterated. Viewed this way, it is the *boundary conditions* which give rise to the system's non-integrability. Alternatively, one can describe the potential as $W(q) = q^{2n}$, where n is an integer. For $n > 1$, the system is nonintegrable, and we retrieve our system in the limit as $n \rightarrow \infty$.

As described previously, nonintegrable Hamiltonian systems consist of two types of trajectories, regular and chaotic. Typically, there are islands of regular motion within a chaotic region of phase space. These are called resonance islands, because they consist of regular trajectories circulating around a (stable) closed trajectory. Closed trajectories with period nT/m, where T is the period of the drive, and n and m are integers, are called $n : m$ resonances.

These trajectories can be seen clearly if one views a cross-section of them in phase space, otherwise known as a Poincaré section. We will define Poincaré section to mean a sampling of the trajectories once every period of drive. Therefore an n^{th} order (period nT) resonance intersects the Poincaré section in n places. By the Poincaré map, we mean an operator $\mathcal{P}$ which evolves an initial condition through one cycle of drive, along its trajectory as defined by the Hamiltonian flow. Thus an n^{th} order resonance corresponds to an initial condition being mapped to n different locations under $\mathcal{P}$, before returning to its original value.

A typical Poincaré section for the system described by the Hamiltonian (2.2) with drive amplitude $\lambda = 0.05$ is shown in figure 2.1. In this figure, several initial conditions were chosen so that the phase space structure is clear. The subsequent trajectories are sampled at $\tau \equiv_{2\pi} \pi$. The $1 : 1$ resonance is clearly visible, surrounded by a large stable island in the upper center of the figure, and wrapping around to the bottom of the figure. (On the walls of the box, at $q = \pm 1$, trajectories at $+p$ and $-p$ continuously join together, since the particle reflects of of the walls.) Two 2 : 1 resonances can be seen, as pairs of islands around their period two fixed points. They lie at lower momentum than the 1 : 1, surrounded by the chaotic ocean formed by the tangles associated with all of unstable fixed points. All other $n : 1$ resonances have become unstable at this value of λ. Some $n : m$ resonance islands are also visible in the figure. One can make out the 1 : 6 resonance, as six islands surrounding the 1 : 1 (four of which are flattened). At high values of momentum, the dynamics are again regular, and resemble more the constant energy surfaces of the undriven system for large momenta. These invariant KAM surfaces bound the energy of the chaotic trajectories.

2.2 Classical Simulation and Energy Absorption

A poor man's quantum simulation may be carried out by iterating a "cloud" of trajectories, arising from a distribution of initial conditions in phase space. Whereas a quantum state carries phase information, a cloud of classical trajectories is a probability distribution and does not take into account phase cancellation. That is, a coarse-grained probability distribution would simply add magnitudes (number of trajectories per sector), though we know that the true quantum prescription is to add the complex amplitudes associated with given trajectories and then take the modulus.

To demonstrate the character of the stochastic dynamics of trajectories in the low-momentum chaotic region, we chose one hundred arbitrary initial conditions

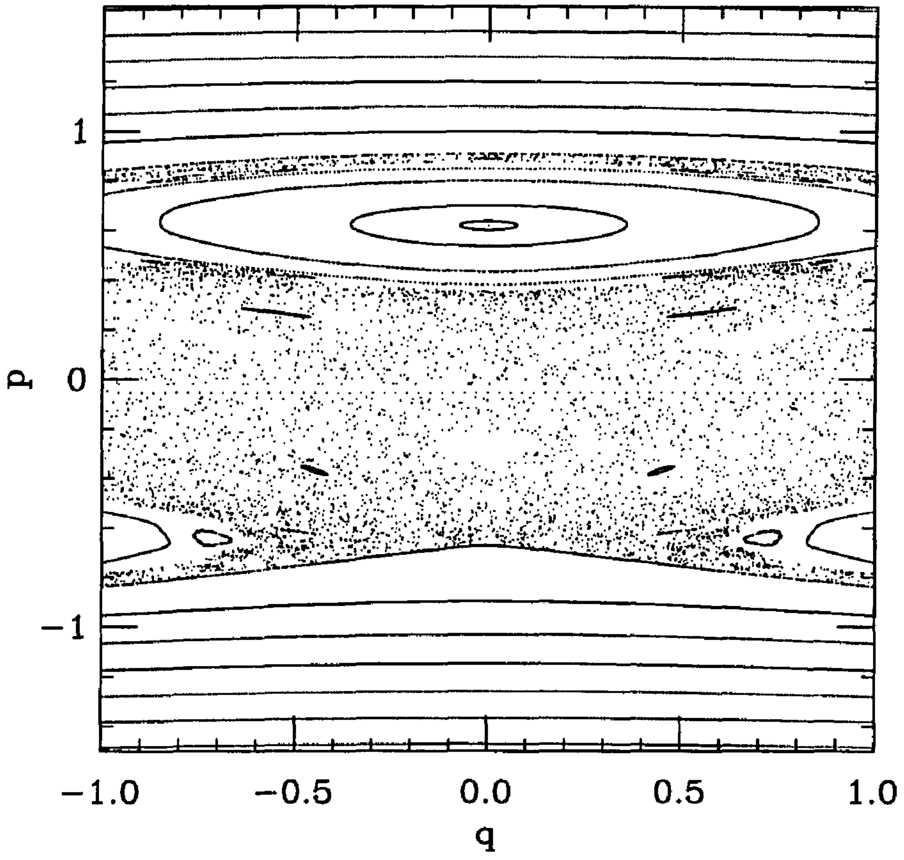

Figure 2.1: Poincaré section for the system described by the Hamiltonian (2.2) with $\lambda = 0.05$. Trajectories are sampled at $\tau \equiv_{2\pi} \pi$.

at low momentum and iterated them through the Poincaré map. By recording the ensemble energy $\langle E\rangle = \frac{1}{2}\sum_i p_i^2$ after each Poincaré iterate, we computed the statistics $max(\langle E\rangle)$ and $ave(\langle E\rangle)$ over ten thousand cycles of drive. Only the kinetic energy needs to be calculated, since our Poincaré section samples the motion at $\tau \equiv_{2\pi} \pi$, when the potential energy is exactly zero in the well. Since the motion within a chaotic region is ergodic, such a long time average is a valid representation of the dynamics of an ensemble.

The result of such calculations, as the unitless driving amplitude λ is varied, is shown in figure 2.2. The solid curve is the maximum ensemble energy, and the dotted curve is the mean ensemble energy. The dashed smooth horizontal curves are the tops of the 1:1, 2:1, and 3:1 resonances, denoted on the right. The vertical lines mark the value of λ where the indicated even resonances become unstable. If one assumes a fixed physical drive amplitude, the effects of varying the drive frequency can easily be obtained from a transformation of figure 2.2, using the scaling in equations 2.1.

The most notable features of such a simulation are the plateaus in the maximum ensemble energy. They correspond to the tops of particular resonances, where KAM surfaces block transport to the next resonance, and higher momenta. As λ is increased, the size of each resonance increases (as $\sqrt{\lambda}$, see Chirikov [15]). Eventually they grow to such an extent that the KAM surfaces between resonances are destroyed, and transport is allowed to the next resonance island. Thus we see sharp increases in energy from one plateau to the next.

The Chirikov criterion exploits what we just explained to predict the destruction of KAM surfaces [15]. The criterion uses first order perturbation theory to calculate the positions and half-widths of each resonance. Because of the symmetric nature

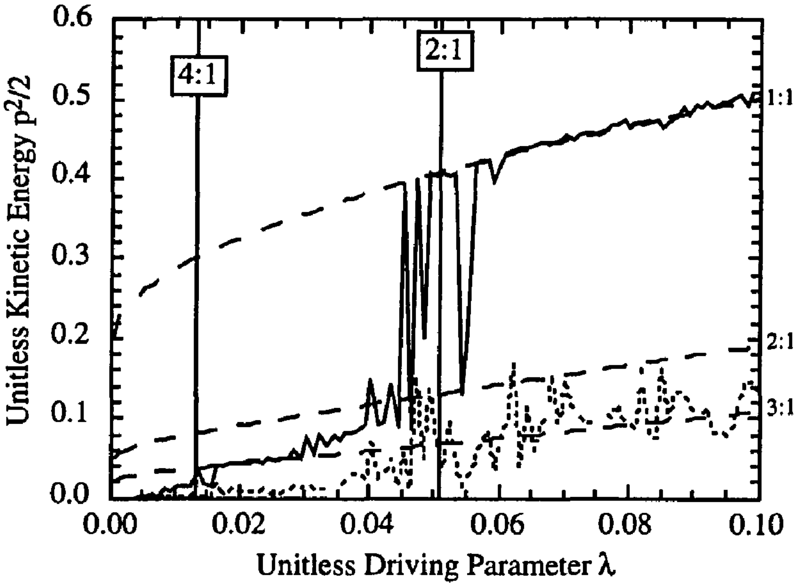

Figure 2.2: Classical energy absorption over many drive cycles as a function of the unitless driving parameter λ.

of the well, only the odd resonances are predicted to first order. In fact, the even resonances exist, but are in general much smaller than the odd ones. The criterion simply states that the KAM surfaces will be destroyed between two resonances when the sum of half-widths of the resonances exceeds the distance between them. Without performing the calculation, (see [15, 33]), the positions and half-widths in phase space of the odd resonances (to first order) are:

$$p_n = \frac{2}{n\pi}, \qquad \Delta p_n = \frac{4\sqrt{\lambda}}{n\pi}, \qquad n = 1, 3, 5, \ldots \tag{2.4}$$

This gives an overlap criterion between the n^{th} and the $(n+2)^{nd}$ resonances:

$$(\Delta p_n + \Delta p_{n+2}) \geq (p_n - p_{n+2}), \quad \text{implying} \quad \lambda \geq \frac{1}{4(n+1)^2}.$$

This result would imply an overlap between the 1 : 1 and 3 : 1 resonances at

$\lambda = 1/16$. It is an overestimate, as is common when one uses this criterion, however the predictions are much better for higher-ordered resonances.

A better analytic method for predicting the destruction of KAM surfaces between resonances is a method introduced by Greene [23, 32]. He noted, through numerical study, that KAM destruction seemed to correspond to a nearby chain of $n : m$ resonance islands making the transition from being stable to being unstable. Moreover, he was able to prove this to be true for a simple map called the standard map where stability criteria could be found for arbitrarily high-order resonance island chains. Using a renormalization scheme, he pinpointed the parameter value where *all* resonances would go unstable in a particular region, and thus when all KAM surfaces in that region would disappear.

We have naively used this criterion to analyze the driven square well. By only looking at the stability of the main *even-ordered* $n : 1$ resonances, one can approximate the value when the KAM surfaces will disappear between the odd resonances. This is confirmed by plotting the values where the even resonances turn unstable, and comparing them with the jumps in energy due to KAM line destruction. As seen in figure 2.2, this works for most resonances (again, the worst case being the destruction of KAM surfaces between the 3:1 and 1:1). Of course, the destruction of the lowest lying KAM surfaces is impossible to see because of the width of the initial cloud of states, coarse statistics, and numerical noise.

Greene's method is in principle exact, however one must determine the stability of *all* $n : m$ resonances in order to determine the exact value of some parameter at which the last KAM surface is truly destroyed. Renormalization calculations which yield very accurate predictions of KAM surface destruction were done by Lin and Reichl [30].

2.3 $n:1$ Resonances and Their Stabilities

We now calculate the phase-space locations and stability of all $n:1$ resonances in the driven square well, which were used in predicting the absorption plateaus and transitions in the classical simulation of section 2.2. In principle, this can be accomplished using the Poincaré map, $\mathcal{P}$. However, since an $n:1$ resonant trajectory is a fixed point of the map $\mathcal{P}^n$, analysis of such a resonance can become unwieldy for any value of n greater than one or two.

Instead, we use a slightly different map to achieve this goal. This new map, which we will call $\mathcal{M}$, is obtained by time-evolving the particle with equation (2.3), but only up to the time when it bounces off of a particular wall, which we choose to be the left wall at $q=-1$. Therefore, the iteration scheme goes just as before, only we sample the dynamics *at* a wall collision. Thus, $\mathcal{M}:(\tau_{\text{mod}2\pi},p)\to(\tau'_{\text{mod}2\pi},p')$, whereas $\mathcal{P}:(q,p)\to(q',p')$. This has the advantage that all $n:1$ resonances show up as fixed points of $\mathcal{M}$. On a resonant trajectory, the particle simply gets wiggled n times during its flight from wall to wall, and in fact has the same magnitude of velocity when it bounces off either wall. It is this observation about the particle's trajectory that allows us to explicitly calculate these resonances.

Taking the τ-derivative of equation (2.3) gives:

$$p(\tau)=\lambda[\cos(\tau)-\cos(\tau_0)]+p_0. \tag{2.5}$$

We seek a condition where the electron leaves the left wall at time τ_0, and arrives at the right wall at time $\tau_R=n\pi+\tau_0$, with $p(\tau_R)=p_0$. From equation (2.5), this requires:

$$\tau_0=\tau^*\equiv\pm\tfrac{1}{2}\pi.$$

The two cases (corresponding to either sign of τ^*) will be treated separately, as both correspond to fixed points of $\mathcal{M}$. Using equation (2.3), setting $q(\tau_R) = 1$ and $q_0 = -1$, and solving for p_0, we find our resonant momenta[3]:

$$p_0 = p^* \equiv \frac{2 \pm \lambda((-1)^n - 1)}{n\pi}.$$

Reversing the momentum at $\tau = \tau_R$, it is clear from equation (2.5) that at time $\tau_1 = 2n\pi + \tau^*$, the momentum has returned to its original value: $p(\tau_1) = p(\tau_R) = p^*$. Also, from equation (2.3), the electron has returned to the left wall. Thus $\mathcal{M} : (\tau^*, p^*) \to (\tau^*, p^*)$. At this time, the system has undergone n cycles of drive, so we have found an $n : 1$ resonant trajectory.

Now that we have found the locations of these fixed points of $\mathcal{M}$, the next step is to determine their stabilities. For this we must linearize $\mathcal{M}$ about the fixed points, and use standard linear stability analysis. Linearizing $\mathcal{M}$ about (τ^*, p^*),

$$\mathcal{M}(\tau, p) = \begin{pmatrix} \tau^* \\ p^* \end{pmatrix} + M \begin{pmatrix} \tau - \tau^* \\ p - p^* \end{pmatrix} + \cdots$$

where

$$M = \left. \begin{pmatrix} \frac{\partial \tau_1}{\partial \tau_0} & \frac{\partial p_1}{\partial \tau_0} \\ \frac{\partial \tau_1}{\partial p_0} & \frac{\partial p_1}{\partial p_0} \end{pmatrix} \right|_{(\tau_0, p_0) = (\tau^*, p^*)}$$

is the Jacobian of $\mathcal{M}$ evaluated at (τ^*, p^*). The stability of the fixed point at $(0, 0)$ of M is identical with that of the fixed point (τ^*, p^*) of $\mathcal{M}$.

The elements of M can be obtained from equations (2.3) and (2.5), by first

---

[3] Notice that for odd n these momenta differ from the perturbative calculation used in the Chirikov criterion (Eq. 2.4) only by a factor proportional to λ. These exact momenta, plus the perturbatively calculated half-widths, give us the estimate for the tops of the resonances seen in figure 2.2. The even resonances are small, so their half-widths are taken to be zero.

setting $q(\tau_R) = 1$ and $q(\tau_1) = q_0 = -1$ to obtain the four equations:

$$\begin{aligned}
1 &= \lambda[\sin(\tau_R) - \sin(\tau_0)] + [p_0 - \lambda\cos(\tau_0)](\tau_R - \tau_0) - 1 \\
p_R &= -(\lambda[\cos(\tau_R) - \cos(\tau_0)] + p_0) \\
-1 &= \lambda[\sin(\tau_1) - \sin(\tau_R)] + [p_R - \lambda\cos(\tau_R)](\tau_1 - \tau_R) + 1 \\
p_1 &= -(\lambda[\cos(\tau_1) - \cos(\tau_R)] + p_R).
\end{aligned} \tag{2.6}$$

(From now on we define $p_R \equiv p(\tau_R)$ and $p_1 \equiv p(\tau_1)$.) These equations correspond to motion from the left wall to the right wall, reversing momentum (thus the overall minus signs in the momentum equations), and returning to the left wall, where the momentum is once again reversed, so that the process is ready for re-iteration.

Taking the derivatives of all four equations (2.6) with respect to τ_0 and p_0, one obtains eight equations which not only contain the elements of M, but also the four partial derivatives of τ_R and p_R with respect to τ_0 and p_0. Substituting in the resonant values for τ_0, τ_R, τ_1, and $p_0(= p_R = p_1)$, the eight equations can be inverted to find an explicit form for M.

Linear stability theory gives a simple condition for fixed-point stability when the map is two-dimensional, and area-preserving. This is the case here, since $\det(M) = 1$, which can be readily checked. In this case, the fixed point $(0,0)$ is stable if and only if $|\mathbf{Tr}M| \leq 2$.

For even n,

$$\mathbf{Tr}M = 2 - \lambda^2 n^4 \pi^4,$$

for both $\tau^* = \pm\frac{1}{2}\pi$. Thus the even resonances are stable if and only if

$$|\lambda| \leq \frac{2}{n^2\pi^2}. \tag{2.7}$$

For odd n,

$$\mathbf{Tr}M = 2 - \left[\frac{4\lambda n^2\pi^2}{\lambda \pm 1} - \frac{\lambda^2 n^4 \pi^4}{(\lambda \pm 1)^2}\right].$$

If $\tau^* = -\frac{1}{2}\pi$, the signs in the denominator are plus signs, and $\mathbf{Tr}M > 2$ for any positive λ. Thus half of the odd resonances are always unstable. If $\tau^* = +\frac{1}{2}\pi$, the signs in the denominator are minus, and some algebra reveals that these odd resonances are stable if and only if

$$|\lambda| \leq \frac{1}{(\frac{n\pi}{2})^2 - 1}. \tag{2.8}$$

Thus we have determined the (τ, p) locations and stabilities of all of the $n : 1$ resonant trajectories of $\mathcal{M}$. These trajectories show up as n^{th} order fixed points of the Poincaré map $\mathcal{P}$, with identical stability criteria. To find the (q, p) intersections of these trajectories given by $\mathcal{P}$, one needs only to evaluate equations (2.3) and (2.5) at each cycle of drive.

This ends our classical exploration of driven systems. This chapter was meant to give the reader a feel for the phase space structure of a driven, confined system. As we will see in the next chapter, many of the classical phase space features will persist into the quantum regime. In addition, the system's nonintegrability will give rise to a surprising new feature, which is purely a quantum-mechanical in nature. Let us now proceed to quantize the driven square well.

Chapter 3

Quantum Mechanics: The Floquet Picture

In this chapter we will quantize a driven system and examine its dynamics. Whereas the classical system's nonintegrability led to chaos, in the quantum system nonintegrability leads to absorption anomalies, which can be seen in energy-absorption calculations analogous to those done for the classical system. The Floquet theory necessary to understand strongly driven quantum systems will be developed in this chapter, and we view the effect of the drive on the quantum system through quantum phase portraits. The absorption anomalies are nonperturbative resonances, which are caused by multi-photon processes between Floquet states (eigenstates of the one period propagator). These multi-photon processes occur at avoided crossings in the quasienergy spectrum, which is the spectrum of eigenvalues corresponding to the Floquet states. Avoided crossings only occur in non-integrable quantum systems, and manifest themselves as a form of nonlinear transport in the quantum system. To conclude this chapter, we will look at the instructive case of a driven two state system, in order to disect an avoided crossing.

We begin by quantizing the driven particle in a square potential, which was examined classically in the last chapter. This introduces one new parameter to the system, a scaled Planck's constant. The other parameter, the scaled drive amplitude, remains the same. We may examine the quantum system in an analogous fashion to the classical Poincaré section, using a phase portrait of quantum states called Floquet states. These are eigenstates of the one-period time-evolution operator, which is obtained by integration of Schrödinger's equation. Floquet states are therefore invariant states of the driven system, and their phase space portraits show them to have maximal density in regions of phase space where invariant classical surfaces exist. The dynamics of the quantum system therefore resemble the classical system, if the scaled Planck's constant is small so that many states exist in a given region of phase space. However, an energy absorption simulation like the one done for the classical system shows an entirely new feature, a resonance peak which has no apparent classical analogy. This is a multiphoton absorption, coupling two Floquet states. These absorptions can be predicted by examining the eigenvalue spectrum of the Floquet states. If two states have the correct parity, the drive will couple them at an attempted spectral crossing, breaking the degeneracy. This coupling causes the spectral lines to avoid each other, and allows transport between the basis states which comprise the coupled Floquet states. The multiphoton process, and the extended states formed from previously localized states, can be seen explicitly by viewing the phase portraits of Floquet states on and off of the resonance.

3.1 Schrödinger's Equation and Phase Portraits

The quantum dynamics of the system are found by solving Schrödinger's equation

$$i\hbar\frac{\partial\psi}{\partial\tau} = -\frac{\hbar^2}{2}\frac{\partial^2\psi}{\partial q^2} + \lambda q \sin\tau\psi(q,\tau), \qquad (3.1)$$

obtained from the Hamiltonian (2.2), with the boundary conditions $\psi(|q| \geq 1, \tau) = 0$. Here $\hbar$ is a *unitless* free parameter, related to the physical Planck's constant by

$$\hbar \equiv (m\omega a^2)^{-1}\hbar_{phys}. \tag{3.2}$$

Thus in addition to the purely classical parameter λ, we now have the purely quantum mechanical parameter $\hbar$.

The Hamiltonian (2.2) is explicitly time-dependent, so there are no stationary states or energy eigenvalues. Instead, since the time dependence is periodic, one may invoke Floquet theory[1]. Floquet's theorem, applied to the Schrödinger equation, states that if $H(\tau) = H(\tau + T)$, then there exists a complete orthonormal set of solutions to $i\hbar\dot{\psi} = H\psi$ of the form

$$\varphi_n(\tau) = e^{-i\varepsilon_n\tau/\hbar}u_n(\tau), \tag{3.3}$$

where $u_n(\tau + T) = u_n(\tau)$. These are completely analogous to Bloch states, (Bloch theory is just the special case of Floquet theory when the periodic variable is the spatial coördinate), and therefore it should be no surprise that the ε_n are quasienergies, which are conjugate variables of τ, and are only defined up to an additive constant: $\varepsilon_{nm} = \varepsilon_n + 2\pi\hbar m/T$. Thus the spectrum of quasienergies lives in Brillouin zones determined by m.

The quasienergy differences $2\pi\hbar m/T$ wash out when multiplied by $-i\tau/\hbar$ and exponentiated, and since (3.3) is independent of the Brillouin zone number m, we must have

$$u_{nm} = e^{i2\pi m\tau/T}u_n. \tag{3.4}$$

---

[1] For a rigorous introduction to Floquet theory, see for example Coddington and Levinson [16]. A good practical introduction is given in a Physical Review article by J. H. Shirley.

where u_{nm} is the Floquet state in the m^{th} zone. Thus although we have an infinite number of u_{nm}'s associated with each quantum number n, each represents the *same* physical state φ_n.

How can these quasienergies be interpreted? In some sense, they represent the perturbed energy levels of the system. This can be seen if one imagines reducing the time-dependent part of H to zero. Then Schrödinger's equation is integrable, with an orthonormal set of solutions of the form:

$$\varphi_n(\tau) = e^{-iE_n\tau/\hbar}u_n,$$

where the u_n are time-independent eigenstates of H, and E_n are the energy eigenvalues. Thus, in the limit of zero driving, the Floquet states become the stationary states, and the quasienergies become the real energies, in the $m = 0$ Brillouin zone.

Without going into the details of Floquet's theorem, one can see how the Floquet states (3.3) and quasienergies can be calculated. We first calculate the unitary propagator U_T, which takes a state from time τ to time $\tau + T$,

$$U_T\psi(\tau) = \psi(\tau + T), \tag{3.5}$$

Note that the eigenvalues of U_T must be of unit modulus, since U_T is unitary. The eigenvalue equation for U_T is then

$$U_T\psi_n(\tau) = e^{i\theta_n}\psi_n(\tau). \tag{3.6}$$

Evaluating the Floquet states (3.3) at times τ and $\tau + T$, we see that the Floquet states are in fact the eigenstates of U_T, and combining (3.5) and (3.6) we see that the quasienergies are

$$\varepsilon_n = -\frac{\hbar}{T}\theta_n.$$

U_T is in fact the Poincaré operator for the quantum system. Moreover, the Floquet states are localized about the *classical* invariant structures in phase space! This will now be demonstrated, as we calculate the Floquet states and quasienergy spectra of our system.

Of course, we must make a truncation, or N-level approximation, to our system in order to do numerics. We believe that a large enough basis will model our system accurately, especially if the omitted states do not couple significantly with the states we choose to keep. The square well is a good system to model, since energy level spacing increases with increasing energy, thus effectively decoupling higher states, no matter how large the drive. (This should be compared with the classical system, where invariant energy curves become less and less affected by the drive for high enough energy.) However, one must beware of a systematic error which arises from an artificial conservation rule introduced by basis truncation, and will *always* lead to an incorrect quasienergy spectrum from diagonalization of U_T. For a harmonically driven system with a finite number of states N, the constraint

$$\sum_{j=1}^{N} \varepsilon_j = \sum_{j=1}^{N} E_j \pmod{\hbar\omega} \tag{3.7}$$

holds for any drive strength, where the left-hand side is the sum of over the quasienergies, and the right-hand side is the sum over the undriven energy eigenvalues of the system [12]. Take for example the driven harmonic oscillator, an integrable system with exactly calculable quasienergies. The exact calculation shows no avoided crossings, as it must, yet the truncated system's quasienergy spectrum is filled with avoided crossings. In that system, most of the spectrum becomes garbage for moderate drive strengths, as the artificially imposed constraint (3.7) forces the quasienergy lines to bend into one another, and thus produce avoided crossings. A way to test one's results is to increase the basis size and see if the part of the spectrum one is interested in has converged. For the driven particle in a box the problem is not nearly so bad, and we will mainly be interested in the bottom half of our spectrum. In any system where the states of interest do not couple strongly with the rest of the states, a finite basis truncation which includes all of the states of interest will in general be a good approximation to the full system. This is the case with a nonintegrable Hamiltonian system, such as the one we are studying here, where the classical phase space consists of a region of chaos is surrounded by KAM surfaces, and in the corresponding quantum system a finite number basis states will be strongly coupled in the chaotic regime. How this works in detail will be described shortly.

We choose as a spatial basis set the eigenstates of the undriven particle in a box. Using the first N of these basis states, we integrate equation (3.1) through one cycle of drive, with pure basis states as initial conditions. After all basis states are propagated through one drive cycle, the resultant vectors are put together to form the matrix[2] U_T.

In order to visualize the correspondence between the Floquet states and the classical phase space structures, and to be able to reference *any* state to the classical phase space, we expand states using a mock phase space distribution [26]. It is impossible to construct a true probability distribution of a quantum state ψ over position and momentum, owing to the uncertainty principle. However, we may do the next best thing, and construct a function $H(q_0, p_0)$ which is the squared modulus of the overlap of ψ with a coherent state $\alpha(q_0, p_0)$, which is centered at

---

[2] Actually, because of symmetries of the system, only the one-quarter cycle propagator $U_{T/4}$ needs to be calculated. Then the half-cycle propagator is $U_{T/2} = \text{Transpose}(U_{T/4})U_{T/4}$, and the full-cycle is $U_T = (SU_{T/2})^2$. Here S is the diagonal spatial symmetry operator: $S_{nn} = -(-1)^n$.

(q_0, p_0). This is a Husimi distribution. Coherent states are maximally localized in q and p, that is, they satisfy the minimum uncertainty relation $\Delta q \Delta p = \frac{1}{2}\hbar$. Thus a Husimi distribution tells us the extent of a state's localization at any point in phase space. This distribution is somewhat ambiguous since there are many different coherent states, all of which are solutions to a harmonic oscillator Schrödinger's equation. We chose the coherent states $\alpha(q_0, p_0)$ to have Gaussian modulus in both q and p representations, centered at q_0 and p_0 respectively. The product of the standard deviations in position and momentum is of course $\frac{1}{2}\hbar$, but the ratio of α's momentum distribution width to its position distribution width is Ω, the frequency of the harmonic oscillator to which α is a solution. We will use $\Omega = 1$, but other values will bring out more detail in either the q or the p direction. Thus our coherent states, in the position representation, are

$$\langle q | \alpha(q_0, p_0) \rangle = \left(\frac{1}{\pi \hbar} \right)^{\frac{1}{4}} e^{-[(q-q_0)^2 + i p_0 (2q - q_0)]/2\hbar}.$$

For example, Husimi distributions of several Floquet states of the Schrödinger equation (3.1) are shown in figure 3.1, for $\lambda = 0.05$, so a comparison can be made to the classical phase portrait in figure 2.1. In figure 3.1, $\hbar = 0.025$.

Notice the high-momentum states which resemble KAM surfaces. They are each comprised mainly of a single undriven basis state, and couple with other states less and less for higher momentum. Thus we can feel justified in truncating the basis to N states, such that the root mean square momentum of the N^{th} basis state is well into the KAM region of the classical phase space. Then, all of the low-momentum dynamics, taking place in the chaotic and resonant regions of the classical phase space will be fairly accurate.

As mentioned earlier, classical resonances, both stable and unstable, have Floquet states localized upon them. The chaotic region is filled with a number of Floquet states, and Floquet states also lie along KAM surfaces. The smaller $\hbar$, the more states fit in a region of phase space, and more features of the classical phase space are resolved in the Husimi distributions of the Floquet states.

In figure 3.1, we see the Husimi distributions of the first twenty-three Floquet states of the quantum system with $\lambda = 0.05$ and $\hbar = 0.025$, in order of increasing mean energy. For reference to the classical phase space at this value of λ, figure 2.1 is reproduced in this figure. Notice that the region below the KAM surfaces in the classical portrait has an area of approximately 3.4, so that we expect about $3.4/2\pi\hbar \approx 22$ quantum states to fit in this region. Indeed, we see at least twenty, and perhaps twenty-one. The higher energy states all lie on KAM surfaces[3], and are composed of fewer and fewer energy eigenstates of the undriven system. The first four states at low energy also resemble basis states, but are slightly mixed. States 5-7 are associated with the third resonance (5 and 7 lie on the just-turned unstable three-cycle, and 6 lies on the always unstable three-cycle.) States 8, 9, and perhaps 10 lie on the second resonance. States 10 and 11 resemble KAM surfaces, which existed there in the classical system for lower values of λ. At this level of quantization, the dynamics are still bounded by these states, as if the KAM surfaces still existed. State 12 lies on the $1:1$ unstable fixed point, and has ghostly "arms" reaching around the stable resonance. This is an example of localization upon the stable and unstable manifolds associated with an unstable fixed point [28]. States 13-20 are all associated with the island around the stable $1:1$ fixed point. Notice the increasing number of nodes in the states, outward from the fixed point. These

---

[3] When we say that a quantum state "lies on" a classical surface, we mean that the density of that state is maximal in the region of phase space where the classical surface lies.

states provide a basis for the harmonic-oscillator like dynamics near the fixed point.

This rich detail disappears for larger $\hbar$, as will be seen later in the system shown in figure 3.3.

3.2 Quantum Simulation and Energy Absorption

We now perform a true quantum simulation of the driven particle in a box. This is quite easy to do with the basis of Floquet states above. In order to start in the unperturbed ground state, we simply set $\psi(\tau = 0) = (1, 0, 0, \ldots, 0)$. We can propagate the system through one drive cycle, $T = 2\pi$, with our propagator:

$$\psi(\tau = 2\pi n) = (U_{2\pi})^n \psi(\tau = 0).$$

After each application of $U_{2\pi}$, we find the ensemble energy of the system:

$$\langle E(\tau = 2\pi n)\rangle = \langle \psi(\tau = 2\pi n)|H_0|\psi(\tau = 2\pi n)\rangle,$$

where $H_0 = \frac{1}{2}p^2$. Again, we are sampling the dynamics at $\tau \equiv_{2\pi} 0$, when $H = H_0$.

Propagating through 1,000 cycles of drive, $max(\langle E\rangle)$ and $ave(\langle E\rangle)$ are calculated for various parameter values. An example is seen in figure 3.2. In this figure, $\hbar = 0.06875$, and λ is swept from 0 to 0.05. Besides a more or less featureless response, a sharp resonance occurs at $\lambda = 0.0395$. The reader is reminded that this resonance occurs as the field *intensity*, not frequency, is varied! This resonance is not predicted by standard time-dependent perturbation theory, as the driving strength is far too strong here for it to be valid. Indeed, this is a nonperturbative multi-photon absorption, and the mechanism behind it will be examined in the next section.

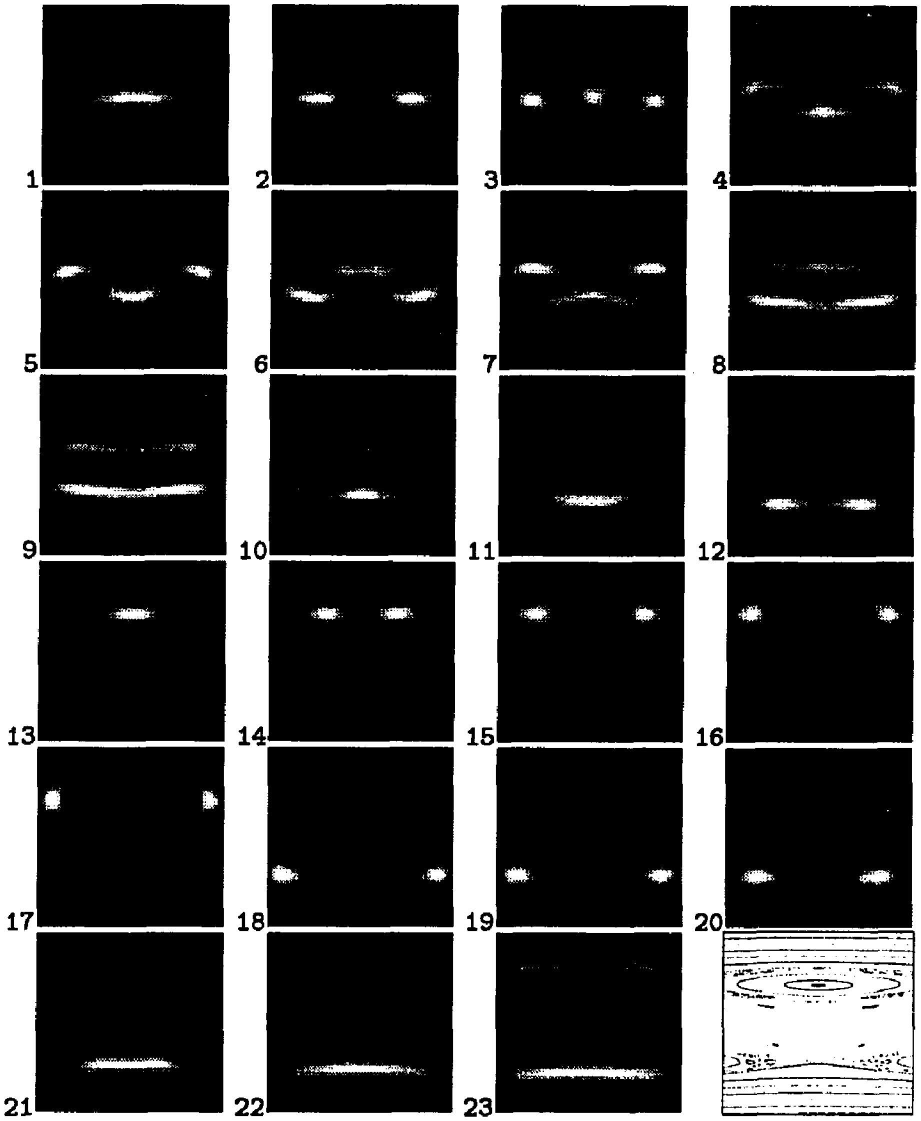

Figure 3.1: Several Floquet states of the driven particle in a box, in order of increasing mean energy, $\lambda = 0.05$ and $\hbar = 0.025$. The axes on each picture are identical with those of figure 2.1, which is reproduced on the lower right.

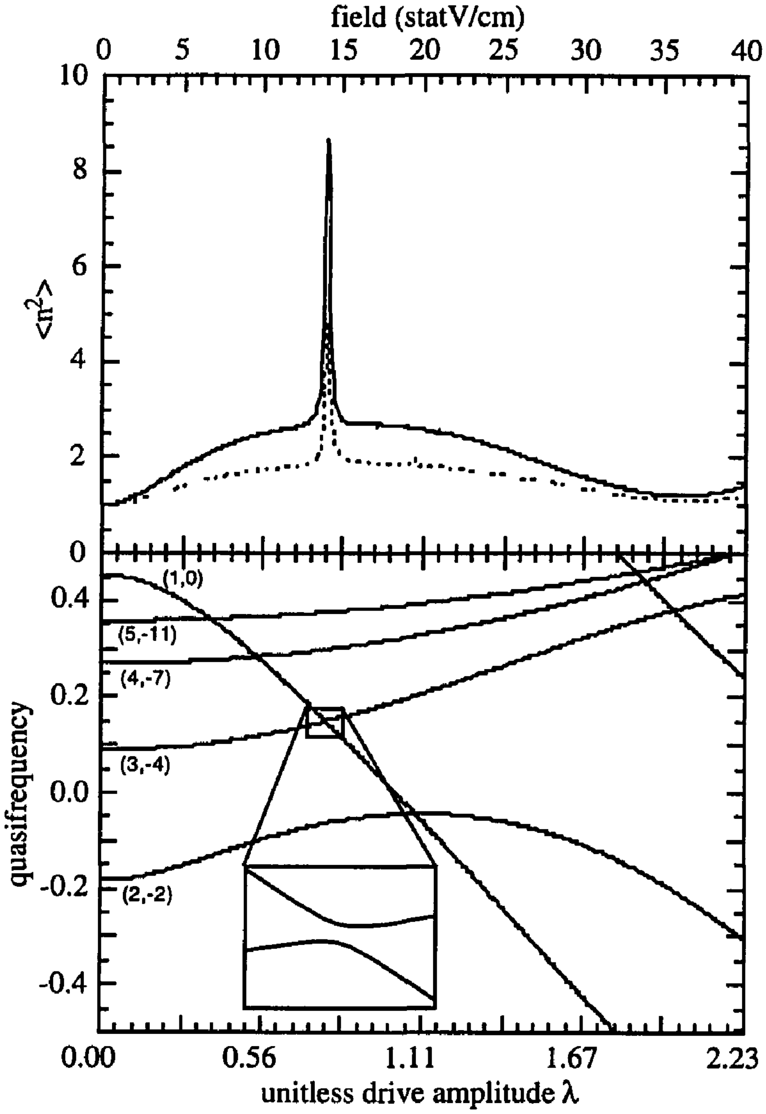

Figure 3.2: The maximum (solid) and mean (dashed) ensemble energy of the quantum system, at $\hbar = 0.06875$, sweeping through λ. Below, selected lines from the quasienergy spectrum. The lines are labeled (n, m), where n is the unperturbed basis state from which the Floquet state evolves, and m is the "photon" index number.

3.3 Nonperturbative Resonances

The mechanism behind the nonperturbative resonances is revealed upon examining the quasienergy spectrum as a function of a varied parameter, in our case λ. Varying λ while keeping $\hbar$ fixed corresponds to varying the laser intensity while keeping the frequency fixed. Since quasienergies are ambiguous up to an integer multiple of $\hbar\omega$, our quasifrequencies are ambiguous up to an integer. (We have scaled the drive frequency so that $\omega = 1$.) In order to establish an absolute reference frame in quasienergy, we let the absolute quasienergy ε_n be defined such that $\varepsilon_n \to E_n$ as $\lambda \to 0$. Then, $\varepsilon_{nm} = \varepsilon_n + m\hbar$. We have labeled the quasienergy lines as (n, m) in figure 3.2, for $n = 1 \to 5$.

It is apparent from the spectrum in figure 3.2 that nonperturbative resonances correspond to avoided crossings in the quasienergy spectrum (see the inset in this figure.) This was first noticed by Shirley [36] in the context of two-state systems. Avoided crossings occur between the quasienergies of two Floquet states whenever there is a non-zero matrix element coupling those states at a potential degeneracy. In that case, the coupling lifts the degeneracy, and as in standard degenerate perturbation theory, a new basis is formed out of the two Floquet states [10, 11]. This new basis can be a channel of transport from low to high momentum states, causing a pronounced increase in absorption at the avoided crossing.

To determine whether or not two spectral lines of a spatially symmetric system may cross, one has only to calculate a spatio-temporal parity of the Floquet states in question. The Schrödinger equation (3.1) is invariant under the parity operator

$$S_P : \begin{cases} \tau & \to \quad \tau + \pi \\ q & \to \quad -q \end{cases}$$

The states u_{nm}, as defined by equations (3.3) and (3.4) are eigenstates of S_P, and $S_P u_{nm} = (-1)^{n+m+1} u_{nm}$ [13]. The spectral lines of two states with the same S_P parity will avoid each other instead of crossing, breaking their degeneracy through the coupling of the drive. Since the crossing takes place in the same Brillouin zone in energy, the coupling is actually occurring between two states $m\hbar$ apart in quasienergy. Now since each Brillouin zone represents one photon energy from the field, we can think of the absorption at an avoided crossing as an m-photon absorption. These are strong resonances, not predicted by standard time-dependent perturbation theory.

This brings about an important notational point. In order that an avoided crossing between two quasienergies with zone-index difference Δm always correspond to a m-photon difference between quasienergies, we must label the Floquet states and quasienergies *as if the spectral lines* had *crossed*! Since the physical characteristics of the Floquet states also behave this way, the indexing makes intuitive sense. Only when we wish to follow a Floquet state along a continuous quasienergy line will this notation have difficulties.

The mixing of Floquet states at an avoided crossing is obvious upon examination of the states' Husimi distributions. Figure 3.3(a) shows the Husimi distributions of the Floquet states which arise from the first twelve basis states in a box driven with $\lambda = 0.0500$ and $\hbar = 0.06875$. Figure 3.3(b) shows the corresponding states at $\lambda = 0.0395$, and we have an explicit view of the multi-photon process taking place at the avoided crossing, and causing the nonperturbative resonance in the energy. These states are mostly identical in appearance to those in the top half of the figure, with the exception of the $n = 1$ and $n = 5$ states. These have married to form the two new states seen, which are both more extended in momentum than the corresponding Floquet states off the avoided crossing.

Nonperturbative resonances, and the avoided crossings with which they are associated, are dominant in the Floquet states which are most perturbed from the undriven basis states. This implies that the regions where KAM surfaces are most distorted or destroyed support Floquet states which interact strongly through multiphoton processes at avoided crossings. Thus these resonances constitute a concrete manifestation of classical chaos in driven quantum systems.

3.4 History-Dependence and Avoided Crossings

A useful system for understanding the Floquet picture and the quasienergy spectrum is the driven two-state system. There, the spectrum contains only two quasienergies, and so avoided crossings are isolated. Consider the Hamiltonian

$$H(t) = H_0 + V_L(t), \tag{3.8}$$

where H_0 is the undriven (single-particle) Hamiltonian, and $V_L(t)$ is the external driving field. If we work in the basis of eigenstates of H_0,

$$H_0|\xi_n\rangle = E_n|\xi_n\rangle, \qquad n = 0, 1$$

and set our energy scale such that $E_0 = -E_1$, then (3.8) becomes

$$H(t) = \tfrac{1}{2}\hbar\omega_{10}\begin{pmatrix} -1 & 0 \\ 0 & 1 \end{pmatrix} + \hbar\omega_D\begin{pmatrix} 0 & 1 \\ 1 & \zeta \end{pmatrix}\sin\omega t, \tag{3.9}$$

where

$$\hbar\omega_D = e\mathcal{E}z_{10}, \tag{3.10}$$

$\hbar\omega_{10} = E_1 - E_0$, $\zeta = (z_{11} - z_{00})/z_{10}$, and $z_{mn} = \langle\xi_m|z|\xi_n\rangle$. We have set our coördinate system such that $z_{00} = 0$.

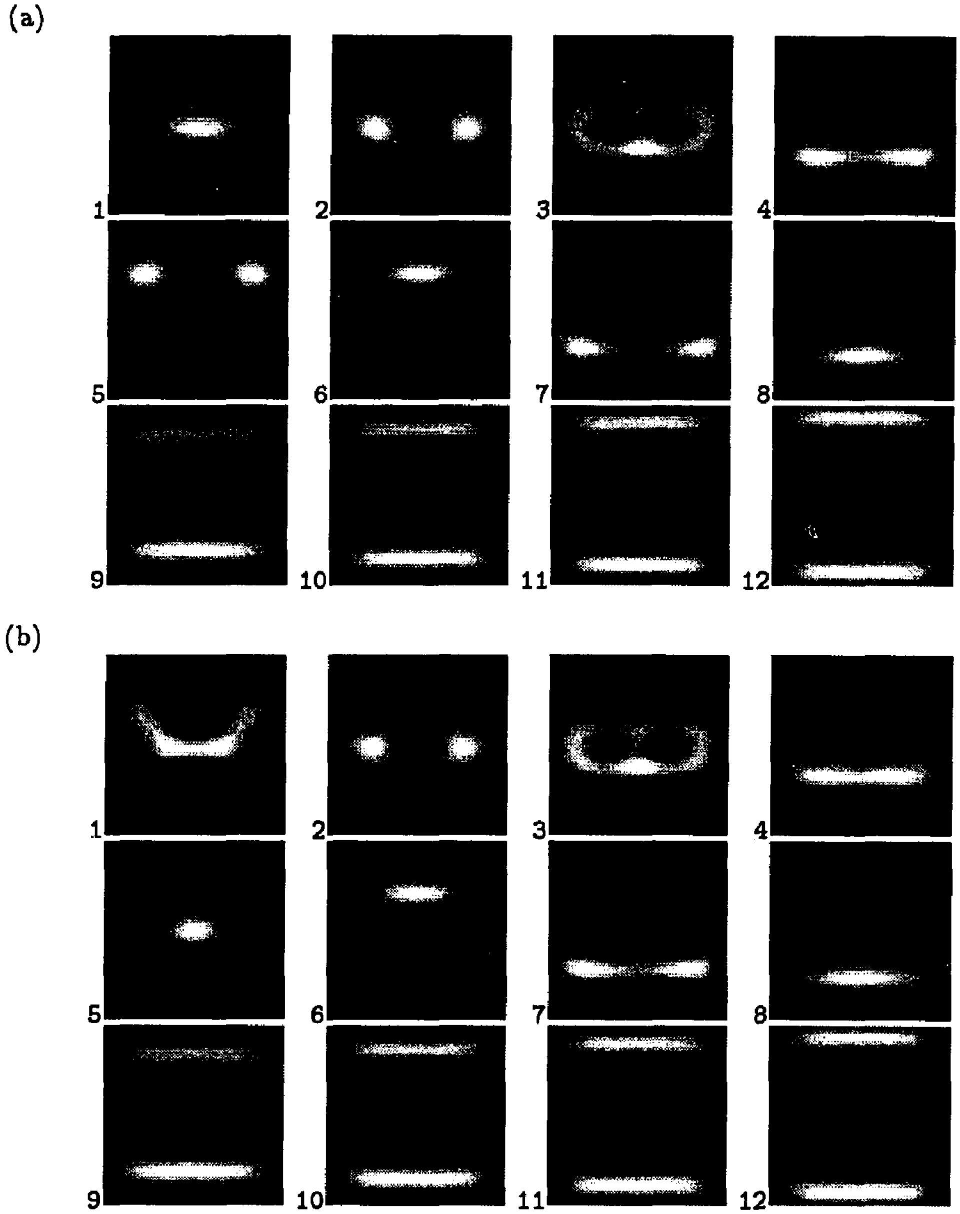

Figure 3.3: Floquet states, in order of increasing mean energy, $\hbar = 0.06875$. (a) $\lambda = 0.0500$, (b) $\lambda = 0.0395$. The axes in each picture are identical with those of figure 2.1.

Now, we may integrate Schrödinger's equation for this Hamiltonian to find the one-period propagator $\mathcal{P}$, and diagonalize to find the quasienergies as a function of the field strength (or, equivalently, as a function of ω_D). Choosing $\omega/\omega_{10} = 0.33$ (for no particular reason, other than to demonstrate a particular example), and $\zeta = 0$, and sweeping through ω_D, we arrive at the quasi-energy plot in figure 3.4.

The avoided crossings between the quasienergy levels are easily seen. We have labeled the second "Brillouin" zone index m of each state as described in the last section. Let us explore the behavior of the two-state system through this example, as we vary the effective drive amplitude ω_D. We will see that the behavior of the system is strongly dependent on the *history* of ω_D, that is, how we take the system from $\omega_D = 0$ to its final value. Keep in mind that this example is without damping - the effects of damping will be explored in later chapters.

If we ramp up the drive very slowly, then the system will adiabatically evolve from its initial state. That is, if it starts in the ground state, the system will be in the Floquet state which evolves from the ground state and whose quasienergy evolves continuously from the ground state energy. If one turns on the drive instantly, the system will be in a linear combination of Floquet states, given by the overlap of the two Floquet states and the initial state.

If one ramps through an avoided crossing, then the final state of the system again depends on the ramping speed, in which case one finds that the system "jumps the gap" at an avoided crossing if the ramping speed is fast enough. For slow ramping, as the system evolves adaibatically along one continuous spectral line, it will "turn the corner" at an avoided crossing. The wider the gap at an avoided crossing, the faster one must ramp to jump over it. The probability of jumping the gap is worked

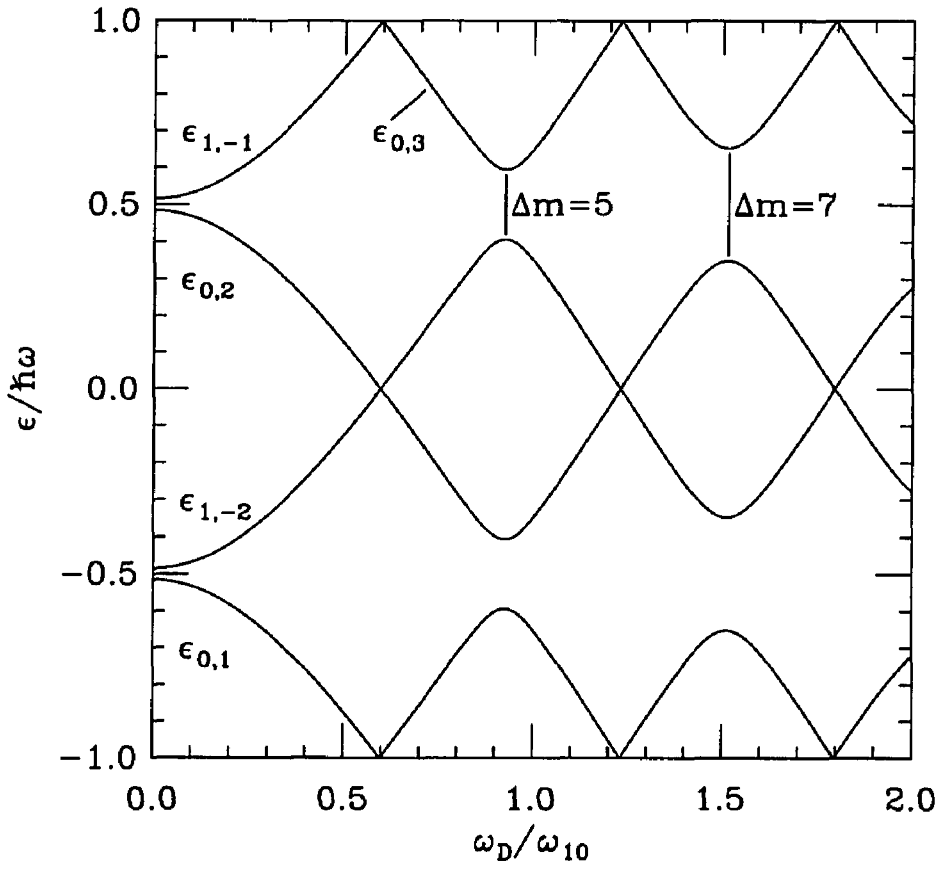

Figure 3.4: The quasi-energy plot of the two-state system described by the Hamiltonian (3.9), with $\omega/\omega_{10} = 0.33$ and $\zeta = 0$.

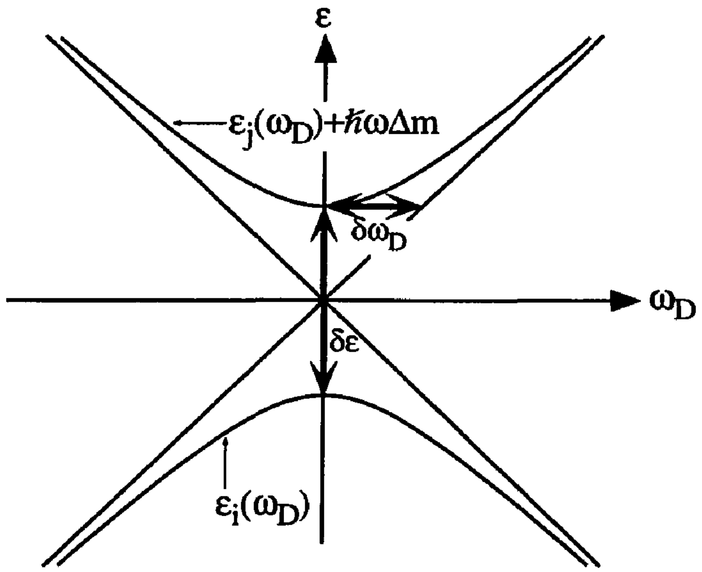

Figure 3.5: Geometric meaning of $\delta\varepsilon$ and $\delta\omega_D$ at an avoided crossing. (From Breuer and Holthaus, [12].)

out in Breuer and Holthaus [12], and is

$$P_{j\to i} = e^{\pi\eta/2}$$

where η is given by

$$\eta = \frac{1}{\hbar}\frac{\delta\varepsilon\delta\omega_D}{d\omega_D/dt}\bigg|_{\omega_D=\omega_D^*} .$$

Here, $\delta\varepsilon$ is the size of the quasienergy gap between the i^{th} and j^{th} states, $\delta\omega_D$ is the ω_D-interval over which the distance between the levels grows by $\sqrt{2}$, and ω_D^* is the ω_D-position of the avoided crossing. (See figure 3.5.)

Since the physical characteristics of the two Floquet states swap at an avoided crossing, as if it were not there, this means that the system will keep its physical characteristics if it is swept quickly enough through the crossing. Thus, in a system with many states, where there are several tiny avoided crossings riddling the quasienergy spectrum, one can ignore the smallest gaps. These are effectively "invisible," unless the system is ramped up slowly enough. In an infinite-state system, there are avoided crossings of all sizes, so that no speed is slow enough to jump all gaps. Thus, as we ramp more and more slowly, the final state of the system keeps changing, as smaller gaps become "seen" by the system. No adiabatic limit exists, then for a driven system at arbitrary field strength! How do we classify the dynamics of a strongly driven system, when there is such a dependence on the past history? This question will be explored in chapter 6.

Let us return to our simple two-state system, and look at a certain physical characteristic, namely the dipole $\langle z(t)\rangle = \langle\psi(t)|z|\psi(t)\rangle$, where $|\psi(t)\rangle$ solves Schrödinger's equation for the Hamiltonian (3.9), again with $\omega/\omega_{10} = 0.33$ and $\zeta = 0$. We will start in the ground state, and ramp up to three final values of ω_D: before, at, and after the first avoided crossing in figure 3.4. In each case, we will ramp up both very slowly and very quickly, compared with the size of the gap in the way described above. Figure 3.6 shows the results. The history dependence is clear; and we also see that *at* the avoided crossing, the dipole response is strongly fifth harmonic, which is the photon-index difference Δm between at the gap. When one ramps up the field ω_D adiabatically, so that the system follows a continuous quasienergy line $\varepsilon(\omega_D)$, then the component of the first harmonic response which is in phase with the driving field is proportional to $d\varepsilon/d\omega_D$. (See appendix A for the proof.)

We will return to this system and classify its history-dependence later in chapter 6, and also incorporate the effects of many-body interactions and dissipation. So now let us divert our attention to the modeling of many-body effects and dissipation, in the next two chapters.

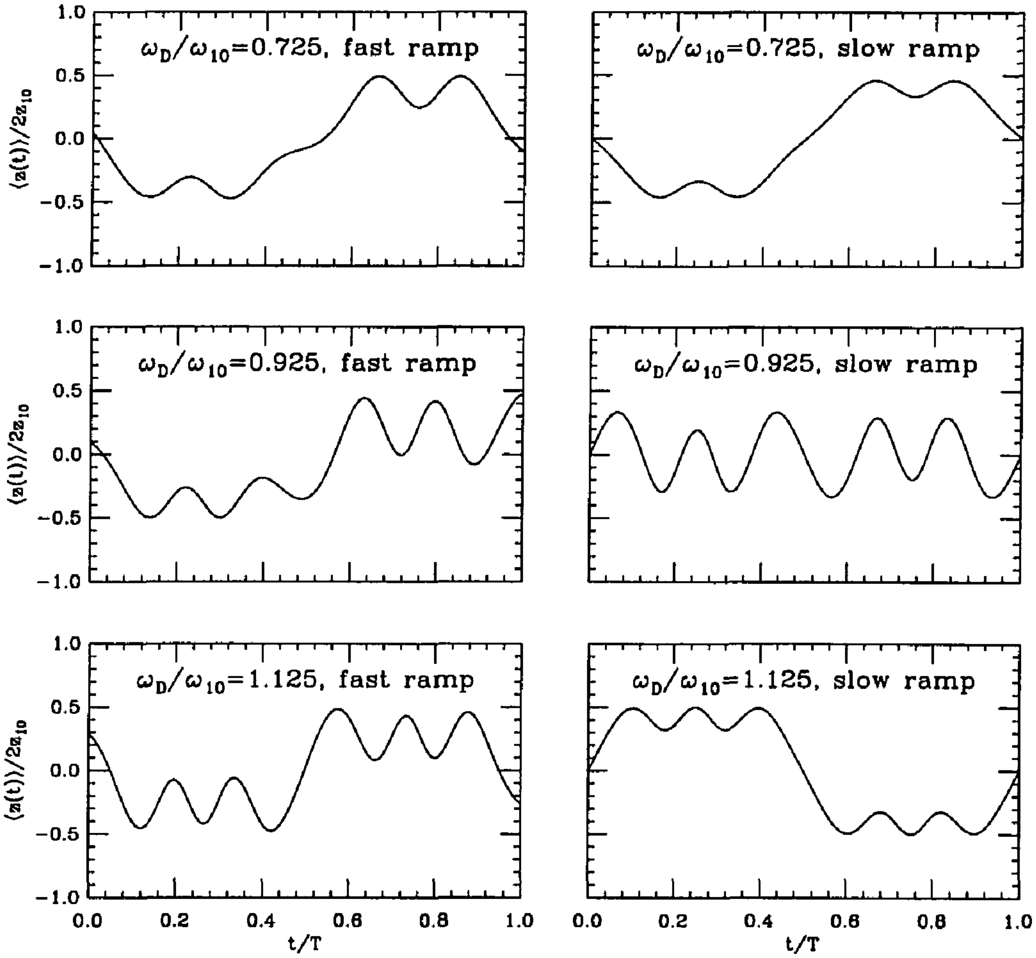

Figure 3.6: The dipole response of the two-state system described by the Hamiltonian (3.9), with $\omega/\omega_{10} = 0.33$ and $\zeta = 0$, at three different drive amplitudes, and two different ramp-up speeds.

Chapter 4

Many-Body Effects

Up until now we have ignored the electron-electron interactions in our description of the quantum well. Although the single particle picture is interesting, it is not an accurate model quantum well at doped at a typical sheet density $N_S \sim 10^{11}\text{cm}^{-2}$. In a wide quantum well, say on the order of hundreds of Angstroms, this implies a 3-D density $n \sim 10^{17}\text{cm}-3$. Thus, the typical inter-particle spacing r, defined by

$$\tfrac{4}{3}\pi r^3 n = 1, \tag{4.1}$$

which comes out to about $r \sim 10^{-6}\text{cm}$. At this distance, the Coulomb repulsion between two electrons is

$$V(r) = \frac{e^2}{\kappa r} \sim 10\text{meV}.$$

(Where $\kappa \approx 13$ is the DC dielectric constant in GaAs). This is on the order of the difference between the lowest intersubband energies! Clearly we are missing much by neglecting electron-electron interactions[1].

---

[1] In narrower quantum wells the relative Coulomb energy is lower, since the intersubband spacing goes approximately as the square of the inverse well width, but the electron density is proportional to the well width, so that the Coulomb energy goes only as the inverse width.

Density functional theory [27] lends itself to solve the time-independent many-body problem, by replacing it with a self-consistent many-body potential and single-particle Schrödinger equation [29]. The eigenstates of this Schrödinger equation may be used as the basis set for time-dependent perturbation theory, when an external driving field is applied. From this, one may calculate a many-body response function, if one is careful to include the time-dependent fields generated by the driven electron density. The first-harmonic response function, complete with the self-consistent effects due to electron-electron interaction, has been calculated by Ando [1]. He performs this calculation[2] with the time-dependent change in the electron-electron interaction potentials accounted for in a self-consistent manner. In the same spirit, we will extended this work to the second-harmonic response. The second-order change in the single-particle effective potential is self-consistently calculated, and from this we can compute the second-order susceptibility $\tilde{\chi}^{(2)}(2\omega;\omega,\omega)$. For the case where only one subband interacts significantly with the ground subband, we derive an explicit two-subband formula for $\tilde{\chi}^{(2)}(2\omega;\omega,\omega)$, and we also derive an explicit two-subband formula for the so-called linear electro-optic effect, $\tilde{\chi}^{(2)}(\omega;0,\omega)$. The latter is calculated easily from the self-consistent first-harmonic response. In both cases, the resonant frequencies appearing in the denominator are shifted, because of the electron-electron interactions, by the same amount as in the first-harmonic response.

We will end this chapter by comparing the second-harmonic response of an asymmetric quantum well, obtained experimentally by Heyman et al. [25], with the response function $\tilde{\chi}^{(2)}(2\omega;\omega,\omega)$ calculated in this chapter. Their experiment confirms

---

[2] Actually, Ando calculates the self-consistent conductivity, which differs from the susceptibility by a factor of $i\omega$.

the location of the depolarization-shifted resonant frequencies of the second order response.

4.1 The Self-Consistent Quantum Well

One can calculate the ground state of the undriven system by a Kohn-Sham self-consistent scheme (see appendix B). Assuming translational symmetry in the plane perpendicular to the growth (z) direction of the well, we reduce the problem to a one-dimensional single-particle time-independent Schrödinger equation for the z-component of the system:

$$\left[-\frac{\hbar^2}{2m^*}\frac{d^2}{dz^2} + W(z) + v(z)\right]\xi_n(z) = E_n\xi_n(z). \tag{4.2}$$

Here, E_n is the bottom of the n^{th} subband, and we now include the effective potential due to electron-electron interactions, $v(z)$. This term can be divided into two parts,

$$v(z) = v_s[n(z); z] + v_{xc}[n(z); z].$$

Here, the notation implies that the effective potential is a functional of the electronic density $n(z)$, which is the conclusion of the Hohenberg-Kohn theorem [27]. The direct, or Hartree term, is the purely classical electrostatic potential due to the density of electrons,

$$v_s[n(z); z] = -\frac{4\pi e^2}{\kappa}\int_{-\infty}^{z} dz' \int_{-\infty}^{z'} dz'' n(z'') + \frac{2\pi e^2 N_S}{\kappa} z, \tag{4.3}$$

obtained by integration of Poisson's equation. The 3-D density $n(z)$ is related to the 1-D density $\rho(z)$ by

$$n(z) = N_S \rho(z). \tag{4.4}$$

The choice of integration constants to obtain (4.3) is such that the resultant electric fields at $z = \pm\infty$ are exactly opposite:

$$\mathcal{E}_C(\infty) = -\frac{1}{e}\left.\frac{\partial v_s}{\partial z}\right|_{z=\infty} = -\mathcal{E}_C(-\infty).$$

This is the case if there is no other charge in our system, as we will assume. Any overall additive constant to the electrostatic potential has been dropped for the sake of simplicity. This of course will not change any of our results.

The so-called indirect term $v_{xc}[n(z); z]$ accounts for the effects of exchange and correlation as a local potential. (See appendix B for more on this term.) There are many approximations in the literature for this last term, most of which are valid for time-independent systems. In the derivations in this chapter, we will assume that the exchange-correlation term is frequency-independent, and that the time-dependence of this term comes merely from the time-dependent electronic density, used in the static form for the v_{xc}, that is

$$v(z,t) = v_s[n(z,t); z] + v_{xc}[n(z,t); z]. \tag{4.5}$$

This is called the *Adiabatic* approximation.

Local approximations to the static exchange-correlation potential can be found in Dreizler and Gross [19], for example, and usually have the limitation of being valid only in the slowly varying and high electronic density regime. Although this condition is not strictly met in most quantum wells, the approximations used none the less give reasonable results. The form we use is that proposed by Hedin and Lundqvist (see [19]),

$$v_{xc}[n(z,t); z] = -\left[1 + \frac{0.7734}{21}\ln\left(1 + \frac{1}{r_s(z)}\right)\right]\frac{2}{\pi}\left(\frac{4}{9\pi}\right)^{\frac{1}{3}}\frac{1}{r_s(z)}R_y^*, \tag{4.6}$$

where $r_s(z) = r(z)/a_0^*$, ($r(z)$ being defined by equation 4.1 as a function of $n(z)$), $a_0^* = \kappa\hbar^2/m^*e^2$ is the effective Bohr radius in the material, and $R_y^* = e^2/2\kappa a_0^*$ is the effective Rydberg. This form is claimed by its originators to be valid roughly in the range $r_s \sim 2 \rightarrow 6$. This is indeed the case in typical quantum wells, where $r_s \sim 3-4$. However, a frequency-dependent exchange-correlation potential[3] derived for the homogeneous electron gas by Gross and Kohn [24] shows a marked frequency-dependence for relatively low electronic densities ($r_s > 2$). It is expected, then, that our Adiabatic approximation for v_{xc} is not a good one, but will merely give qualitatively correct results, as a first correction to the Coulomb potential.

An example of the self-consistent ground and first-excited states of a doped square well are shown in figure 4.1, superimposed over the self-consistent potential. The top graph shows the empty well, the bottom graph shows the doped well, assuming only the ground state is occupied. Although the scales of the wavefunctions in these graphs are arbitrary, their asymptotes are placed at their corresponding energy eigenvalues relative to the well. As one can see, in a square well the self-consistent effects can flatten out the ground state wavefunction significantly.

4.2 The Second Harmonic

We will now calculate the second-harmonic susceptibility $\tilde{\chi}^{(2)}(2\omega;\omega,\omega)$, which will be abbreviated $\tilde{\chi}^{(2)}$ in this section. When an external electric field $\mathcal{E}(e^{-i\omega t}+e^{i\omega t})$ is applied to the system, it modifies the electronic density, which we will carry out to

---

[3] It should also be pointed out that Dobson [18] has prescribed a method which splits the motion of the electron density into two parts: a translating part, and a compressing part. The first part should be used with the *static* exchange-correlation potential, and only the second should be used in the frequency-dependent exchange-correlation potential.

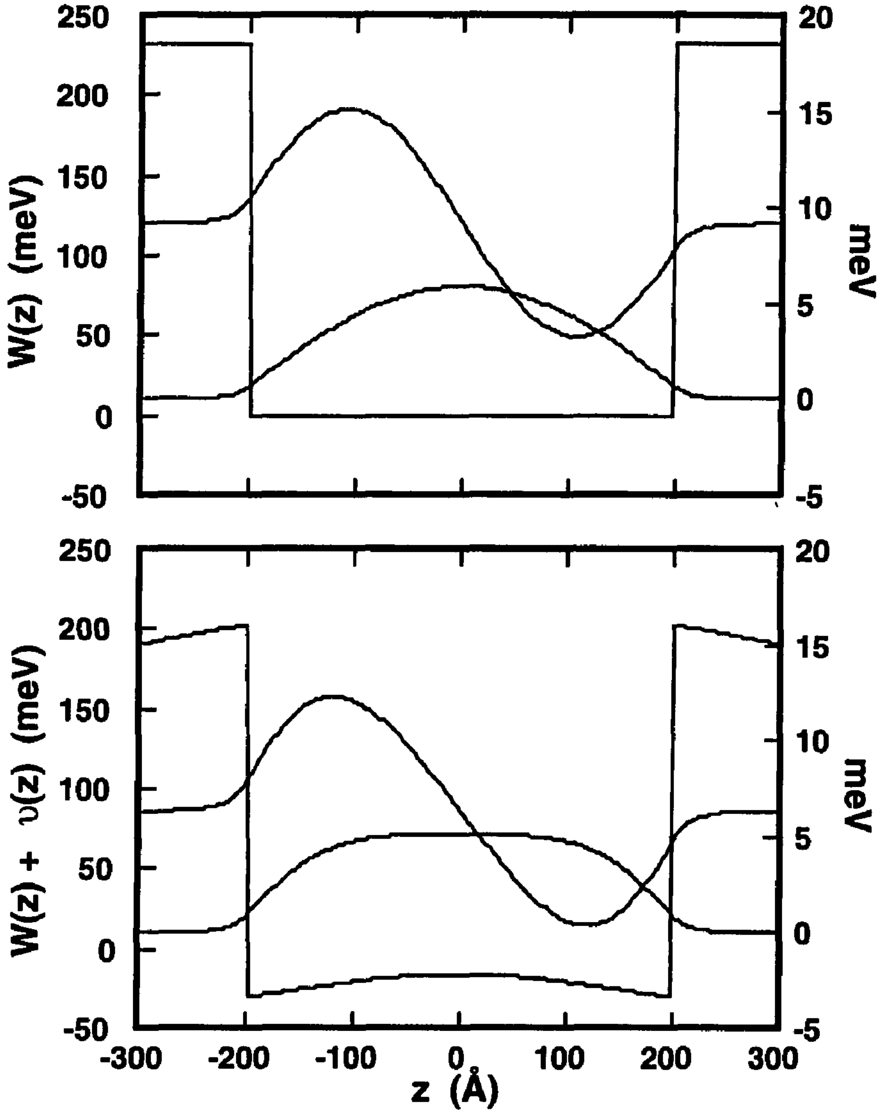

Figure 4.1: A square well, empty (top) and with an electronic sheet density $N_S = 2 \times 10^{11}\text{cm}^{-2}$ (bottom). The ground and first excited self-consistent eigenfucntions are superimposed on the well, so that their asymptotes are at their corresponding energy eigenvalues on right vertical axes, but their overall scale is arbitrary.

second order as $\delta n^{(1)}(z)(e^{-i\omega t}+e^{i\omega t})+\delta n^{(2)}(z)(e^{-2i\omega t}+e^{2i\omega t})$. This gives rise to a change in the direct and indirect potentials, which we represent as the second order perturbing potential

$$V(z,t)=V^{(1)}(z)(e^{-i\omega t}+e^{i\omega t})+V^{(2)}(z)(e^{-2i\omega t}+e^{2i\omega t}). \tag{4.7}$$

We are ignoring phase shifts here (keeping only terms in phase with the driving field), since we are assuming infinite lifetimes at present. Later, we can introduce a small imaginary components to the resonant frequencies which will give the desired phase shifts on resonance. The Fourier coefficients are given by

$$V^{(1)}(z)=e\mathcal{E}z+\delta v_s^{(1)}(z)+\delta v_{xc}^{(1)}(z) \tag{4.8}$$

and

$$V^{(2)}(z)=\delta v_s^{(2)}(z)+\delta v_{xc}^{(2)}(z), \tag{4.9}$$

where

$$\delta v_s^{(i)}(z)=-\frac{4\pi e^2}{\kappa}\int_{-\infty}^{z}dz'\int_{-\infty}^{z'}dz''\delta n^{(i)}(z'') \tag{4.10}$$

and

$$\delta v_{xc}^{(i)}(z)=\frac{\partial v_{xc}}{\partial n(z)}\delta n^{(i)}(z). \tag{4.11}$$

We should pause to justify our assumption given above concerning the form of the self-consistent potential. Second-order perturbation theory not only gives a second-harmonic response to a monochromatic external field, but also a static or secular shift. We have not included this term self-consistently. This is perfectly correct, since the secular terms are second-order in the perturbing field. Thus, the effect on either the first or second harmonic must be at least third-order, beyond the order of our calculation. Therefore we may ignore it without affecting the second-harmonic. Also, note that the second-order potential $V^{(2)}(z)$ does not affect, but only *responds*, to the first harmonic $V^{(1)}(z)$, to second order. So we may first self-consistently solve for $V^{(1)}(z)$ in response to the external field, and then self-consistently solve for $V^{(2)}(z)$ in response to $V^{(1)}(z)$.

Assuming that only the ground subband which we label $|0\rangle$ is initially occupied, time-dependent perturbation theory gives (setting $\hbar = 1$)

$$\delta n^{(1)}(z) = -2N_S \sum_n \xi_n(z)\xi_0(z)V_{n0}^{(1)} \frac{\omega_{n0}}{\omega_{n0}^2 - \omega^2}, \tag{4.12}$$

and

$$\begin{aligned} \delta n^{(2)}(z) &= -2N_S \sum_n \xi_n(z)\xi_0(z)V_{n0}^{(2)} \frac{\omega_{n0}}{\omega_{n0}^2 - (2\omega)^2} \\ &\quad + N_S \sum_{nm} \xi_n(z)\xi_m(z)V_{n0}^{(1)}V_{m0}^{(1)} \frac{1}{(\omega_{m0} - \omega)(\omega_{n0} + \omega)} \\ &\quad + N_S \sum_{nm} \xi_n(z)\xi_0(z)V_{nm}^{(1)}V_{m0}^{(1)} \left[\frac{1}{(\omega_{n0} - 2\omega)(\omega_{m0} - \omega)} + \frac{1}{(\omega_{n0} + 2\omega)(\omega_{m0} + \omega)}\right], \end{aligned} \tag{4.13}$$

where N_S is the electron sheet density, $\omega_{n0} \equiv E_n - E_0$, and $V_{nm}^{(i)} = \langle n|V^{(i)}|m\rangle$.

Now we may directly calculate the second-order susceptibility from

$$\tilde{\chi}^{(2)} = \frac{e}{\mathcal{E}^2} \int_{-\infty}^{\infty} dz\, z\delta n^{(2)}(z). \tag{4.14}$$

Using (4.13), one has

$$\begin{aligned} \tilde{\chi}^{(2)} &= -2\frac{eN_S}{\mathcal{E}^2} \sum_n z_{n0} V_{n0}^{(2)} \frac{\omega_{n0}}{\omega_{n0}^2 - (2\omega)^2} \\ &\quad + \frac{eN_S}{\mathcal{E}^2} \sum_{nm} z_{nm} V_{n0}^{(1)}V_{m0}^{(1)} \frac{1}{(\omega_{m0} - \omega)(\omega_{n0} + \omega)} \\ &\quad + \frac{eN_S}{\mathcal{E}^2} \sum_{nm} z_{n0} V_{nm}^{(1)}V_{m0}^{(1)} \left[\frac{1}{(\omega_{n0} - 2\omega)(\omega_{m0} - \omega)} + \frac{1}{(\omega_{n0} + 2\omega)(\omega_{m0} + \omega)}\right], \end{aligned} \tag{4.15}$$

where $z_{nm} = \langle n|z|m\rangle$. Now all that is left is to find the self-consistent matrix elements $V_{nm}^{(i)}$.

Starting with the first-order matrix elements, insert the first-order change in density (4.12) into (4.8) and take a matrix element of (4.8), giving

$$V_{jk}^{(1)} = e\mathcal{E}z_{jk} - 2N_S\sum_n \left(\frac{4\pi e^2}{\kappa}S_{jkn0} + X_{jkn0}\right) V_{n0}^{(1)}\frac{\omega_{n0}}{\omega_{n0}^2 - \omega^2}. \tag{4.16}$$

Here we are defining the integrals[4]

$$S_{jknm} \equiv -\int_{-\infty}^{\infty} dz\xi_j(z)\xi_k(z)\int_{-\infty}^{z} dz'\int_{-\infty}^{z'} dz''\xi_n(z'')\xi_m(z'') \tag{4.17}$$

and

$$X_{jknm} \equiv \int_{-\infty}^{\infty} dz\xi_j(z)\xi_k(z)\xi_n(z)\xi_m(z)\frac{\partial v_{xc}}{\partial n(z)}. \tag{4.18}$$

Setting $k = 0$ in (4.16) allows its solution as a linear algebra problem, then the rest of the matrix elements ($k > 0$) may be readily calculated. Now we must solve for the second order matrix elements, by inserting the second-order density (4.13) into (4.9) and taking a matrix element of (4.9), giving

$$V_{j0}^{(2)} = \zeta_j - 2N_S\sum_n \left(\frac{4\pi e^2}{\kappa}S_{j0n0} + X_{j0n0}\right) V_{n0}^{(2)}\frac{\omega_{n0}}{\omega_{n0}^2 - (2\omega)^2}. \tag{4.19}$$

Here we only need to find one column of $V^{(2)}$, since (4.15) requires no more. The vector ζ_j is

$$\zeta_j \;=\; N_S\sum_{nm}\left(\frac{4\pi e^2}{\kappa}S_{j0nm} + X_{j0nm}\right) V_{n0}^{(1)}V_{m0}^{(1)}\frac{1}{(\omega_{m0} - \omega)(\omega_{n0} + \omega)} +$$

---

[4] The integral 4.17 can be integrated by parts, giving

$$S_{jknm} = \int_{-\infty}^{\infty} dz\left[\int_{-\infty}^{z} dz'\xi_n(z')\xi_m(z')\right]\left[\int_{-\infty}^{z} dz'\xi_j(z')\xi_k(z') - \delta_{jk}\right],$$

and simplified in most cases by the identity

$$\int_{-\infty}^{z} dz'\xi_n(z')\xi_m(z') = \frac{\hbar}{2m^*\omega_{nm}}\left[\xi_n(z)\frac{d\xi_m}{dz} - \frac{d\xi_n}{dz}\xi_m(z)\right]$$

if $\omega_{nm} \neq 0$. To prove this identity, differentiate both sides by z, and use Schrödinger's equation to eliminate the second derivatives. Since both sides of the above equation are equal (to zero) in the limit $z \to -\infty$, then equal slopes imply equal values.

$$N_S \sum_{nm} \left(\frac{4\pi e^2}{\kappa} S_{j0n0} + X_{j0n0} \right) V^{(1)}_{nm} V^{(1)}_{m0} \times$$
$$\left[\frac{1}{(\omega_{n0} - 2\omega)(\omega_{m0} - \omega)} + \frac{1}{(\omega_{n0} + 2\omega)(\omega_{m0} + \omega)} \right].$$

Again, (4.19) may be solved with linear algebra.

Thus, one has a computational method for calculating the self-consistent response function $\tilde{\chi}^{(2)}$, using (4.15). We may obtain some insight into the many-body effects by looking at the system in the two-subband approximation. Then, the above linear equations may be solved trivially, (see appendix C for more detail) and after re-inserting $\hbar$, we have (assuming we have set our coördinate system so that $z_{00} = 0$, and labeling the excited subband $|1\rangle$),

$$\tilde{\chi}^{(2)}(2\omega; \omega, \omega) = \frac{3e^3 N_S}{\hbar^2} \frac{z_{10}^2 z_{11} \omega_{10}^2 (\omega_{10}^2 - \omega^2)}{(\tilde{\omega}_{10}^2 - (2\omega)^2)(\tilde{\omega}_{10}^2 - \omega^2)^2}. \tag{4.20}$$

This response function has the resonant frequency

$$\tilde{\omega}_{10}^2 = \omega_{10}^2 (1 + \alpha_{11} - \beta_{11}), \tag{4.21}$$

where

$$\alpha_{jn} = 2N_S \frac{4\pi e^2}{\kappa} S_{j0n0} (\omega_{j0} \omega_{n0})^{-1/2} \tag{4.22}$$

and

$$\beta_{jn} = -2N_S X_{j0n0} (\omega_{j0} \omega_{n0})^{-1/2}, \tag{4.23}$$

exactly the two-subband shifted resonance frequency found in the first-harmonic response [1].

4.3 The Linear Electro-Optic Effect

Whereas the function $\tilde{\chi}^{(2)}(2\omega; \omega, \omega)$ gives the response due to the addition of two like frequencies, the linear electro-optic effect is the response function $\tilde{\chi}^{(2)}(\omega; 0, \omega)$

due to the addition of the frequency ω and a zero-frequency, or static field. It is related in a simple way to the first-order susceptibility $\tilde{\chi}^{(1)}(\omega)$ by

$$\tilde{\chi}^{(2)}(\omega;0,\omega)=\frac{1}{2}\frac{\partial}{\partial\mathcal{E}^0}\tilde{\chi}^{(1)}(\omega). \qquad (4.24)$$

We employ this relation to calculate the self-consistent response $\tilde{\chi}^{(2)}(\omega;0,\omega)$ directly from the first-order self-consistent response $\tilde{\chi}^{(1)}(\omega)$ of the system described by (4.2) which has been calculated in [1]. In this section, we will confine our calculation to the two-subband approximation from the start, again labeling the excited subband $|1\rangle$.

The first-order self-consistent susceptibility for a two-subband system is

$$\tilde{\chi}^{(1)}(\omega)=\frac{2e^2N_S}{\hbar}z_{10}^2\frac{\omega_{10}}{\tilde{\omega}_{10}^2-\omega^2}. \qquad (4.25)$$

By applying time-independent perturbation theory to (4.2), (again setting $\hbar=1$) we have

$$\frac{\partial\omega_{10}}{\partial\mathcal{E}^0}=ez_{11} \qquad (4.26)$$

(the single-particle Stark shift) and

$$\frac{\partial|0\rangle}{\partial\mathcal{E}^0}=-\frac{ez_{10}}{\omega_{10}}|1\rangle,\qquad \frac{\partial|1\rangle}{\partial\mathcal{E}^0}=\frac{ez_{10}}{\omega_{10}}|0\rangle. \qquad (4.27)$$

With these identities, and (C.1), it is straightforward to differentiate (4.21) after some work:

$$\frac{1}{e}\frac{\partial(\tilde{\omega}_{10})^2}{\partial\mathcal{E}^0}=\omega_{10}z_{11}(1+\alpha_{11}-\beta_{11})+2z_{11}\omega_{10}-2z_{10}\omega_{10}\gamma$$

where γ is defined in appendix C. Using the relation derived in that appendix, $z_{10}\gamma=z_{11}(\alpha_{11}-\beta_{11})$, along with (4.21) leads to the self-consistent Stark shift,

$$\frac{\partial\tilde{\omega}_{10}}{\partial\mathcal{E}^0}=\frac{ez_{11}}{2}\frac{\omega_{10}}{\tilde{\omega}_{10}}\left(3-\frac{\tilde{\omega}_{10}^2}{\omega_{10}^2}\right). \qquad (4.28)$$

Now using (4.26), (4.27), and (4.28), we may differentiate (4.25), and (4.24) giving (re-inserting $\hbar$)

$$\tilde{\chi}^{(2)}(\omega;0,\omega) = -\frac{e^3 N_S}{\hbar^2} z_{10}^2 z_{11} \frac{3\omega_{10}^2 - \omega^2}{(\tilde{\omega}_{10}^2 - \omega^2)^2}. \tag{4.29}$$

The second harmonic $\tilde{\chi}^{(2)}(2\omega;\omega,\omega)$ and electro-optic effect $\tilde{\chi}^{(2)}(\omega;0,\omega)$ presented in this chapter have some striking features. As mentioned earlier, they have poles at the same frequencies as the first harmonic $\tilde{\chi}^{(1)}(\omega)$, as well as at half of those frequencies in the case of the second harmonic. Although this is not obvious for the full second harmonic response (4.15), calculations show that this is true, to high numerical precision. It may be possible to prove analytically that this is the case. The fact that the depolarization shift is the same in second order as in first order is may be somewhat understood intuitively, by noticing that the equation governing the second-order matrix elements (4.19) is exactly the same as that which determines the first-order matrix elements (4.16) (for $k = 0$), with two exceptions. One exception is that the driving term $e\mathcal{E}z_{j0}$ is replaced by ζ_j, which is a sum of second-order products of the first-order matrix elements. Thus, the simple poles in the first harmonic response give rise to second-order poles in the second harmonic response, at the same frequencies. The other exception is that the frequency ω appearing in (4.19) is multiplied by two, creating simple poles at half of the depolarization-shifted absorption frequencies of the first harmonic response.

Another feature of the second-harmonic response, in the two state approximation (4.20), is a node at the bare absorption frequency. In the single-particle limit, $\tilde{\omega}_{10} \to \omega_{10}$, this node dissapears, being absorbed by the numerator to give the well-known single particle result.

In any real quantum well, there are scattering and dissipation mechanisms present. These have the effect of giving a state a finite lifetime, approximately the time one expects before an electron "scatters," (because of well roughness, interaction with the lattice, etc.) into a state with a different momentum or energy. The effect of this is to broaden resonance peaks, and can be phenomenologically accounted for by adding a small imaginary part to the resonance frequency: $\omega_{10} \rightarrow \omega_{10} - i\Gamma$ (where Γ is the experimentally observed half-linewidth of the resonance peak). This prescription, applied to both the bare and dressed resonance frequencies, has been used by Heyman et al. [25] to modify both response functions in this chapter to include finite lifetimes, in excellent agreement with experimental lineshapes.

The well used by Heyman et al. is an *asymmetric double square well*, or two narrow square wells of different widths separated by a barrier. The tunnel-splitting between the ground states of the two wells creates two eigenstates whose energies are about 10 meV apart, with the next two tunnel-split states having energies about 100 meV higher. Since the FEL frequencies are in the 10 meV range, the higher states do not play a significant role, so that thier well is an effectively *two-subband* system. Thus, all of our two-state calculations are not just toy models, but good physical models in this case.

Figure 4.2 shows the experimental and calculated magnitudes of $\chi^{(2)}(2\omega, \omega, \omega)$. The dashed curve is obtained from the single-particle formula. Not only are the resonances in the wrong places (at the bare intersubband transition frequency ω_{10}, and $\frac{1}{2}\omega_{10}$), but the relative heights of the two resonance peaks are strikingly different then those of the dressed response function.

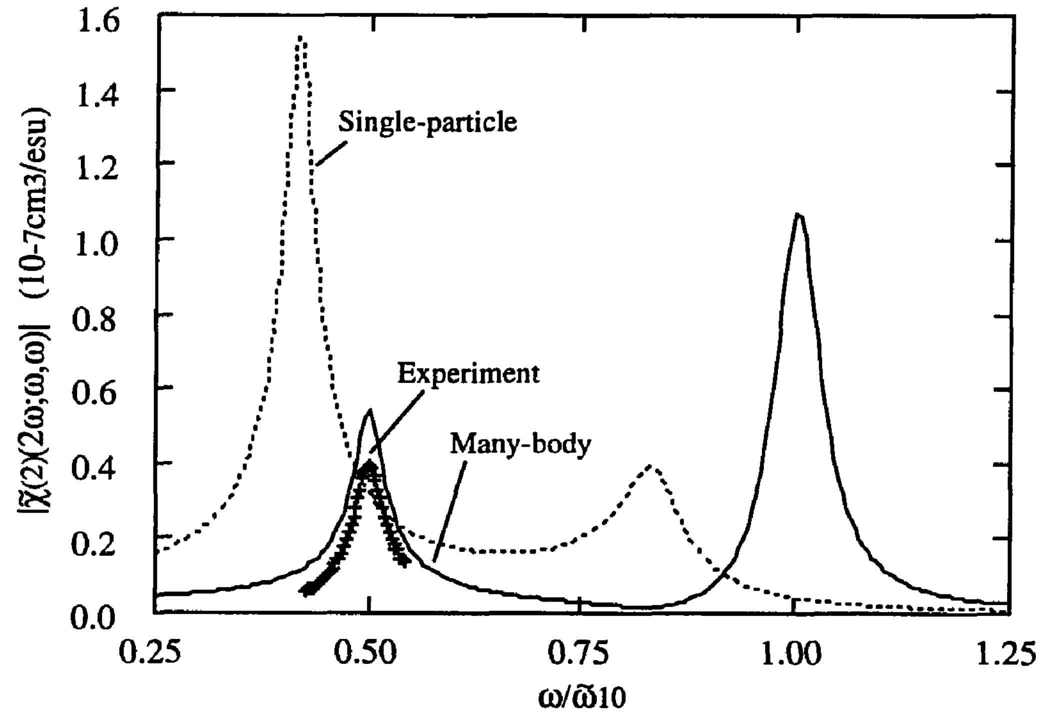

Figure 4.2: Experimental and calculated response $|\chi^{(2)}(2\omega, \omega, \omega)|$. The x's are the experimental data points of Heyman et al. [25], with an uncertainty in the vertical scale of approximately ±50%. The solid curve is obtained from equation 4.20. The dashed curve shows the prediction of the single-particle formula.

Chapter 5

Including Dissipation

One can understand the response of the system at finite temperatures, and/or in the presence of energy and momentum relaxation mechanisms, using the density matrix formulation of quantum mechanics [8, 21].

Consider an ensemble of identical systems, all described by the Hamiltonian H. If $|\xi_j\rangle$ is a complete set of states (time-independent), then the state of a particular system in the ensemble can be expanded as

$$|\xi(t)\rangle = \sum_j c_j(t)|\xi_j\rangle.$$

If one defines the matrix ρ as

$$\rho_{mn}(t) = \overline{c_n c_m^*},$$

where the bar denotes averaging over the entire ensemble, then one can show that ρ has many desirable properties, and is termed the ***density matrix*** of the system described by H. The density matrix plays the role of the state vector in single-particle quantum mechanics.

The density matrix evolves in time by the equation

$$\frac{\partial \rho}{\partial t} = -i[H, \rho],$$

(setting $\hbar = 1$, as will be the case throughout this chapter) analogous to the Liouville equation in classical mechanics. The *ensemble average* of the expectation value of any observable A may be obtained by

$$\overline{\langle A \rangle} = \mathbf{Tr}(\rho A).$$

Thus, given the initial density matrix $\rho(0)$, one can has a method for calculating any of the observable properties of the ensemble in question.

From the definition of the density matrix, and its time-evolution, it follows that ρ is Hermitian, and looking at $\overline{\langle 1 \rangle}$ gives $\mathbf{Tr}\rho = 1$. In fact, from its definition it is easy to see that the diagonal elements of ρ are the fractional populations of each basis state, while the off-diagonal elements are proportional to phase correlations between states. Of course, the elements of ρ depend on the choice of basis used, but expectation values of observables are independent of basis, since the *trace* operation is invariant under a change of basis.

Given two bases $|\xi_j\rangle$ and $|\zeta_j\rangle$ related by the unitary transformation $|\xi_j\rangle = U|\zeta_j\rangle$, the corresponding density matrices (ρ in the basis $|\xi_j\rangle$, and $\tilde{\rho}$ in the basis $|\zeta_j\rangle$) are related by

$$\tilde{\rho} = U^{\dagger}\rho U.$$

(The dagger denotes the operator adjoint.) An important special case is when one basis is the set of spatial eigenstates, $|z\rangle$. Then $U_{nz} = \xi_n(z)$, and

$$\tilde{\rho}_{z'z} \equiv \rho(z', z) = \sum_{mn} \xi_m(z)\xi_n^*(z')\rho_{nm}.$$

The spatial probability density of a single particle is the diagonal of this matrix,

$$\rho(z) = \sum_{mn} \xi_m(z)\xi_n^*(z)\rho_{nm}. \tag{5.1}$$

The initial condition for the time-evolution of the density matrix depends on the assumptions one is making concerning the past evolution or preparation of the ensemble. If one assumes that the ensemble has "decorrelated," via some scattering mechanism (impurities, coupling to a heat bath, etc.), or that the ensemble was otherwise prepared in a completely random manner, then a reasonable assumption for $\rho(0)$ is that it is diagonal, that is no phase correlations between states. The diagonal elements of the initial density matrix may reflect a thermal distribution, if one is describing a system in equilibrium coupled to a heat bath. Such is the case with the quantum well experiments we are modeling.

A simple model for energy and momentum dissipation may be incorporated in the density matrix formalism. Essentially, one merely "decays" the elements of $\rho(t)$ to an equilibrium $\bar{\rho}$, where $\bar{\rho}$ is diagonal and time-independent. To this end, a relaxation rate R_{mn} for each element of the density matrix is incorporated into a tensor operator R, as

$$R(\rho)_{mn} = R_{mn}\rho_{mn}, \tag{5.2}$$

and the time evolution of $\rho(t)$ given by

$$\frac{\partial \rho}{\partial t} = -i[H, \rho] - R(\rho - \bar{\rho}). \tag{5.3}$$

5.1 Perturbation

Let us assume that we know the equilibrium density matrix for a system which is described by the time-independent Hamiltonian H_0. Using the basis of eigenstates of H_0, we have

$$\frac{\partial \bar{\rho}}{\partial t} = -i[H_0, \bar{\rho}] - R(0) = 0, \tag{5.4}$$

since H_0 and $\bar{\rho}$ are both diagonal. This is consistent with our assumption that $\bar{\rho}$ is time-independent.

Now let us apply a the perturbation $e\mathcal{E}z(e^{-i\omega t} + e^{i\omega t})$ to the system. As in the previous chapter, we will take into account the time-dependent electric fields generated by the time-dependent densities, up to second order, so that the effective perturbing potential $V(t)$ is

$$V(t) = V^{(0)} + V^{(1)}e^{-i\omega t} + V^{(1)\dagger}e^{i\omega t} + V^{(2)}e^{-2i\omega t} + V^{(2)\dagger}e^{2i\omega t}. \tag{5.5}$$

As before,

$$\begin{aligned} V^{(0)} &= \delta v^{(0)} \\ V^{(1)} &= \delta v^{(1)} + e\mathcal{E}z \\ V^{(2)} &= \delta v^{(2)}. \end{aligned}$$

Correspondingly, the density matrix is assumed to take on the form

$$\rho(t) = \bar{\rho} + \delta\rho(t), \tag{5.6}$$

where

$$\delta\rho(t) = \delta\rho^{(0)} + \delta\rho^{(1)}e^{-i\omega t} + \delta\rho^{(1)\dagger}e^{i\omega t} + \delta\rho^{(2)}e^{-2i\omega t} + \delta\rho^{(2)\dagger}e^{2i\omega t}.$$

Given equations 4.10, 4.11, 4.4, 4.17, 4.18 and 5.1, we have

$$\delta v_{mn}^{(i)} = \tfrac{1}{2}\sum_{kl} T_{mnkl}\,\delta\rho_{mn}^{(i)},$$

where we have consolidated our integral notation somewhat:

$$T_{mnkl} \equiv 2N_S\left(\frac{4\pi e^2}{\kappa}S_{mnkl} + X_{mnkl}\right). \tag{5.7}$$

Now we may solve for the Fourier components of the density matrix, order by order, by plugging equations 5.6 and 5.5 into equation 5.3. Remember, the static *and* second harmonic components of the density matrix and the potential are *second* order effects of the external field.

The zero-order terms of 5.3 cancel by dint of 5.4. The first-order terms give

$$\omega\delta\rho^{(1)} = [H_0, \delta\rho^{(1)}] + [V^{(1)}, \bar{\rho}] - iR(\delta\rho^{(1)}), \tag{5.8}$$

and an equivalent expression for $\delta\rho^{(1)\dagger}$. Equating second-order terms gives

$$0 = [H_0, \delta\rho^{(0)}] + [V^{(0)}, \bar{\rho}] + [V^{(1)}, \delta\rho^{(1)\dagger}] + [V^{(1)\dagger}, \delta\rho^{(1)}] - iR(\delta\rho^{(0)}) \tag{5.9}$$

for the static term, and

$$2\omega\delta\rho^{(2)} = [H_0, \delta\rho^{(2)}] + [V^{(2)}, \bar{\rho}] + [V^{(1)}, \delta\rho^{(1)}] - iR(\delta\rho^{(2)}) \tag{5.10}$$

for the second-harmonic term. Defining $d_{nm} \equiv \bar{\rho}_{nn} - \bar{\rho}_{mm}$ and taking a matrix element, equation 5.8 becomes

$$(\omega_{mn} - iR_{mn} - \omega)\delta\rho^{(1)}_{mn} + \tfrac{1}{2}d_{mn}\sum_{kl} T_{mnkl}\delta\rho^{(1)}_{kl} = -d_{nm}e\mathcal{E}z_{mn},$$

equation 5.9 becomes

$$(\omega_{mn} - iR_{mn})\delta\rho^{(0)}_{mn} + \tfrac{1}{2}d_{mn}\sum_{kl} T_{mnkl}\delta\rho^{(0)}_{kl} = -[V^{(1)}, \delta\rho^{(1)\dagger}]_{mn} - [V^{(1)\dagger}, \delta\rho^{(1)}]_{mn},$$

and equation 5.10 becomes

$$(\omega_{mn} - iR_{mn} - 2\omega)\delta\rho^{(2)}_{mn} + \tfrac{1}{2}d_{mn}\sum_{kl} T_{mnkl}\delta\rho^{(2)}_{kl} = -[V^{(1)}, \delta\rho^{(1)}]_{mn}.$$

Once the self-consistent stationary states and energies of the well are found, and the relaxation rates R_{mn} given, the above equations may be solved numerically using matrix inversion. The "vector" to be solved for is ρ_{mn}, whose indices are ordered so that one has a linear system of $m \cdot n$ equations. The "matrix" T_{mnkl} thus has as its indices (mn) and (kl).

Then, the sheet susceptibilities $\tilde{\chi}^{(1)}(\omega)$, $\tilde{\chi}^{(2)}(0;\omega,-\omega)$ and $\tilde{\chi}^{(2)}(2\omega;\omega,\omega)$ may be easily calculated:

$$\tilde{\chi}^{(n)}(j\omega) = \frac{-eN_S\overline{\langle z(j\omega)\rangle}}{\mathcal{E}^n} = \frac{-eN_S}{\mathcal{E}^n}\mathrm{Tr}\, z\rho^{(j)}. \tag{5.11}$$

This calculation has been worked out in more detail for the first-order response by Ando [2], and in this case one gets a very pretty result. Momentarily setting $R_{mn} = 0$, let us define

$$\gamma_{mnkl} \equiv T_{mnkl}(d_{nm}d_{kl})^{\frac{1}{2}}(\omega_{mn}\omega_{kl})^{-\frac{1}{2}}.$$

Note that

$$\gamma_{m0k0} = (d_{0m}d_{0k})^{\frac{1}{2}}(\alpha_{mk} - \beta_{mk}), \tag{5.12}$$

from (4.22) and (4.23). These are the population-weighted depolarization shifts. Let us also define

$$A_{(m>n)(k>l)} \equiv \omega_{kl}^2\delta_{mk}\delta_{nl} + \omega_{mn}\gamma_{mnkl}\omega_{kl}.$$

Here, the "single index" $(m > n)$ denotes an ordered pair with $m > n$, so that the rank of A is $\frac{1}{2}N(N-1)$, where N is the rank of our original density matrix.

Diagonalizing A, with a similarity transformation $\tilde{A} = S^T A S$, one arrives at

$$\tilde{\chi}^{(1)}(\omega) = \frac{N_S e^2}{m^*}\sum_{m>n}\frac{\tilde{f}_{mn}}{\tilde{\omega}_{mn}^2 - \omega^2 - 2i\omega\Gamma},$$

where the line broadening Γ (corresponding finite lifetimes due to scattering and dissipation) has been re-introduced. The depolarization-shifted transition frequencies are simply given by $\tilde{\omega}_{mn}^2 = \tilde{A}_{(m>n)(m>n)}$. The oscillator strengths are given by

$$\tilde{f}_{mn} = \left[\sum_{k>l}\left(\frac{2m^*}{\hbar^2}\hbar\omega_{kl}d_{lk}\right)^{\frac{1}{2}} z_{kl}S_{(k>l)(m>n)}\right]^2.$$

Here we have re-introduced the mass m^* and $\hbar$. In the two-level approximation, one has the simple expression for the first-order response

$$\tilde{\chi}^{(1)}(\omega) = \frac{2N_S e^2}{\hbar} \frac{\omega_{10} z_{10}^2 \Delta}{\tilde{\omega}_{10}^2 - \omega^2 - 2i\omega\Gamma},$$

where we have defined $\Delta \equiv d_{01}$ as the difference in the fractional level populations. The depolarization-shifted absorption frequency becomes

$$\tilde{\omega}_{10}^2 = \omega_{10}^2(1 + \gamma_{1010}) = \omega_{10}^2[1 + (\alpha_{11} - \beta_{11})\Delta]. \tag{5.13}$$

We see that when the equilibrium populations of the two states are equal, implying very high temperatures, or large sheet density N_S, the depolarization effect vanishes. However, the magnitude of the response is also proportional to the difference in populations.

Staying within the two-level approximation, we may readily calculate explicit formulae for the self-consistent second-order response for multiply-filled subbands with dissipation. Equating, as is standard convention [38], $R_{00} = R_{11} \equiv \Gamma_1$ to the *inter*subband relaxation rate, and $R_{01} = R_{10} \equiv \Gamma_2$ to the *intra*subband relaxation rate, then we have

$$V_{10}^{(1)} = V_{01}^{(1)} = e\mathcal{E} z_{10} \frac{\omega_{10}^2 - \omega^2 - 2i\omega\Gamma_2}{\tilde{\omega}_{10}^2 - \omega^2 - 2i\omega\Gamma_2},$$

$$V_{11}^{(1)} - V_{00}^{(1)} = \frac{z_{11} - z_{00}}{z_{10}} V_{10}^{(1)},$$

and

$$\delta\rho^{(1)} = \frac{-\Delta e\mathcal{E} z_{10}}{\tilde{\omega}_{10}^2 - \omega^2 - 2i\omega\Gamma_2} \begin{pmatrix} 0 & \omega_{10} - \omega - i\Gamma_2 \\ \omega_{10} + \omega + i\Gamma_2 & 0 \end{pmatrix}.$$

The zeros on the diagonal tell us that there is no first order change in the level populations, due to the external field.

From these matrix elements we may readily solve 5.9 and 5.10,to find $\delta\rho^{(0)}$ and $\delta\rho^{(2)}$. Then equation 5.11 gives for second-order susceptibilities, (in the limit where $\omega_{10}, \omega \gg \Gamma_1, \Gamma_2$):

$$\tilde{\chi}^{(2)}(0;\omega,-\omega) = -\frac{4e^3 N_S}{\hbar^2} \frac{\omega_{10}^2 \left[\omega^2 - \omega^2 + \frac{\Gamma_2}{\Gamma_1}(\omega_{10}^2 + \omega^2)\right] z_{10}^2 (z_{11} - z_{00})\Delta}{\tilde{\omega}_{10}^2 \left[(\tilde{\omega}_{10}^2 - \omega^2)^2 + 4\omega^2\Gamma_2^2\right]},$$

and

$$\tilde{\chi}^{(2)}(2\omega;\omega,\omega) = -\frac{3e^3 N_S}{\hbar^2} \frac{\omega_{10}^2(\omega_{10}^2 - \omega^2 - 2i\omega\Gamma_2) z_{10}^2 (z_{11} - z_{00})\Delta}{(\tilde{\omega}_{10}^2 - \omega^2 - 2i\omega\Gamma_2)^2(\tilde{\omega}_{10}^2 - (2\omega)^2 - 4i\omega\Gamma_2)}.$$

This may be compared with 4.20, keeping in mind the depolarization-shifted resonance frequency is now defined by equation 5.13, which includes the difference in populations. The overall effect of multiply-filled subbands on the second harmonic is again to reduce the size of the depolarization shift, and to reduce the total response with the multiplicative factor Δ. The poles of the second-harmonic response are *still* at the same frequency as the first-harmonic pole, and half of that frequency, even with multiply-filled subbands.

The static shift $\tilde{\chi}^{(2)}(0;\omega,-\omega)$ shows a striking feature if $\Gamma_1 > \Gamma_2$. In this case, the sign of the shift *changes* at

$$\omega^2 = \omega_{10}^2 \frac{\Gamma_1 + \Gamma_2}{\Gamma_1 - \Gamma_2}.$$

This occurs because, when the decoherence rate is less than the energy relaxation rate, the states can electrons can remain in "pure" enough states so that interference between the two wavefunctions can occur. In this case, the mean position of the electron density is not simply the weighted sum of z_{00} and z_{11}; cross-terms must be included. Since it is of questionable meaning to speak of an electron relaxing coherently, it is generally assumed that $\Gamma_1 \leq \Gamma_2$ [8], in which case the sign change in the static shift will not occur.

5.2 The Subband Filling Fractions

In the time-independent system, the equilibrium subband filling fractions are determined by the sheet density N_S and the temperature T. When the system is driven with a small field, we may assume that the filling fractions are perturbed from their undriven values by a small amount, as calculated in the last section. In order to calculate the undriven equilibrium filling fractions, one must integrate the Fermi distribution in the plane for each subband. The filling fractions may be obtained by solving for the (unique) positive root of an N^{th} degree polynomial, where N is the number of subbands considered.

We start by counting electrons. Integrating the Fermi distribution in each subband, weighted by the density of states, and summing over all subbands gives us the total number of electrons, n_e:

$$n_e = \sum_j \int_{E_j}^{\infty} dE \frac{P(E)}{e^{(E-\mu)/k_B T} + 1}, \tag{5.14}$$

where μ is the chemical potential, and must be determined. Since each subband corresponds to a two-dimensional free electron gas, we have

$$P(E)dE = P(k) 2\pi k\, dk,$$

where $\vec{k}$ is the momentum in the plane, and $k = |\vec{k}|$. We may imagine the gas to reside in a large box with sides of length L, and with periodic boundary conditions, so that $k_x = 2\pi n/L$, where n is an integer, and there is a similar quantization in the y-direction. Then the 2-D states are spaced $2\pi/L$ apart in k-space. Since we have two possible spin orientation for each spatial quantum number, this gives

$$P(k) = 2\left(\frac{L}{2\pi}\right)^2.$$

And since $E(k) = \hbar^2 k^2/2m^*$, we then have

$$P(E) = \frac{m^* L^2}{\pi \hbar^2},$$

the well-known constant 2-D energy density of states. With this density of states, equation 5.14 may be integrated exactly to give

$$N_S = \frac{n_e}{L^2} = \frac{m^* k_B T}{\pi \hbar^2} \sum_j \ln\left(1 + e^{-(E_j - \mu)/k_B T}\right). \tag{5.15}$$

The population of each subband is

$$N_j = \frac{m^* k_B T}{\pi \hbar^2} \ln\left(1 + e^{-(E_j - \mu)/k_B T}\right),$$

and the only thing we need to know now is the chemical potential μ. Multiplying both sides of 5.15 by $\pi\hbar^2/m^* k_B T$, exponentiating both sides, and defining

$$r \equiv e^{\pi \hbar^2 N_S/m^* k_B T}, \qquad s_j \equiv e^{-E_n/k_B T}, \qquad u \equiv e^{\mu/k_B T},$$

gives us

$$r = \prod_j (1 + s_j u).$$

This is a polynomial equation in u, with a unique positive solution, providing us with the chemical potential μ.

These filling fractions may be used as the diagonal equilibrium density matrix,

$$\bar{\rho}_{jj} = N_j/N_S.$$

For the case of two subbands, the filling factors may be explicitly solved for, and one finds the excited subband to have the fractional population

$$\frac{N_1}{N_S} = \frac{\tau}{\sigma} \ln\left(\sqrt{\left(\frac{s+1}{2}\right)^2 + s(r-1)} - \frac{s-1}{2}\right),$$

where $s \equiv s_1/s_0$. We may write r and s as

$$r = e^{\sigma/\tau}, \qquad s = e^{-1/\tau},$$

where σ and τ are the reduced sheet densities and temperatures, defined by

$$\sigma = \frac{\pi\hbar N_S}{m^* \omega_{10}}, \qquad \tau = \frac{k_B T}{\hbar\omega_{10}}.$$

The reduced density σ is defined such that $\sigma = 1$ when the electronic filling in the ground subband *just* reaches the bottom of the excited subband, at $T = 0$.

A plot of N_1/N_S as a function of the reduced temperature at several values of the reduced density, when only two subbands are considered, is shown in figure 5.1.

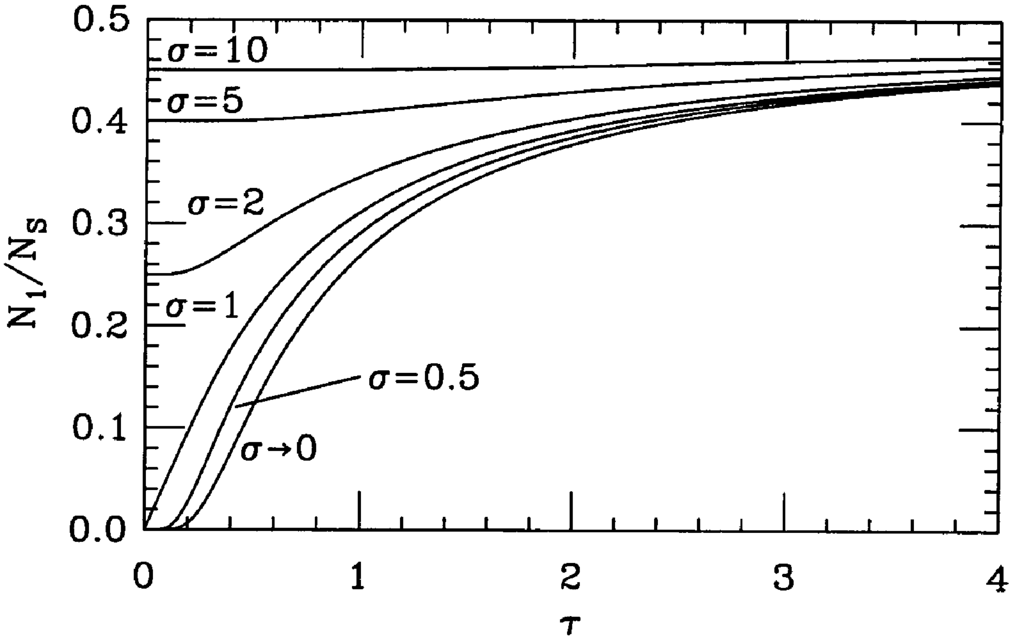

Figure 5.1: Excited subband filling fraction as a function of the reduced temperature at several values of the reduced density.

Chapter 6

Nonperturbative Effects

We have approached the quantum mechanical system in several ways so far. The Floquet basis provided us with a useful time-dependent basis, whose quasienergy spectrum gave insight into the response of the system as a function of drive amplitude. In the chapters that followed, we derived first and second order response functions, which included the effects of many-body interactions, relaxation, and multiply-filled subbands. The well-defined response function owes its usefulness to its history-independence, due to its definition in terms of an adiabatic turning-on of the external field. However, adiabatically turning on the field is a problematic concept when the final drive amplitude is nonperturbative in strength, as was discussed in chapter 3. For strong drive amplitudes, there is a natural history-dependence due to the presence of avoided crossings in the quasienergy spectrum, and one might ask, "Is there a well-defined response of a quantum mechanical system which one can find for arbitrary driving fields?"

Without dissipation, it appears that the answer to this question is *no*, considering our discussion so far. However, we shall see in this chapter that there is a concept from classical mechanics, the Poincaré section, which will describe all of the system's history-dependence in a picture. A picture is worth an infinity of histories. In this chapter, we will confine our study to the two-state, or two-subband system. The concepts presented here are completely generalizable to a larger number of states, however not as presentable on a two-dimensional sheet of paper. We shall see that when one includes many-body effects in the way we have been thus far, one arrives at a nonlinear set of equations of motion which exhibit chaos. This is of course an approximation to the true linear quantum-mechanical equations of motion, however it implies complicated response to the driving field. Not only is there history-dependence, but there is also *sensitive* history dependence, in the sense of exponentially diverging phase-space trajectories, as is typical in driven Hamiltonian systems. Although driven dissipative systems can also display chaos, typically in the form of strange attractors, actual quantum wells have enough dissipation to collapse the dynamics to a small number of non-chaotic attractors which are simple closed orbits. A typical response might show hysteresis, as the system jumps from one basin of attraction to another, however the small number of fixed points allows us to describe those fixed points, as a function of the external drive parameter, to be the multi-valued response function of the system[1].

6.1 A True Quantum Phase Space

Let us view the dynamics of the quantum system in a slightly different light now. Since Schrödinger's equation is first-order in time, knowledge of the state vector at any time completely determines the future evolution of the system. Measurement

---

[1] If one waits long enough in a physical system, one might expect it to tunnel, via interactions with its environment, to a single global attractor. The time for this tunneling is not known, however, and there is no reason to expect that hysteretic behavior will not be observable in quantum well experiments.

of the electrons' motion (via emission of classical EM fields) does not interfere with the quantum evolution as governed by Schrödinger's equation.

The Hamiltonian under consideration depends explicitly on time in a periodic fashion. Thus, the dynamical phase space in which the state-vector evolves is time-periodic, and a Poincaré section of the system (taking the "cut" to be in time) will give all of the topological information of the dynamical flow.

Consider a two-state system. The state vector contains two complex quantities,

$$\psi(t) = \begin{pmatrix} r_0 e^{-i\theta_0} \\ r_1 e^{-i\theta_1} \end{pmatrix},$$

with the normalization constraint $r_0^2 + r_1^2 = 1$, and the fact that the overall phase of the state vector is not observable allows us one more constraint, e.g. $\theta_0 = 0$. Thus our state vector has only two real degrees of freedom, which we may define as

$$\Delta \equiv r_0^2 - r_1^2,$$

and

$$\theta \equiv \theta_0 - \theta_1.$$

Therefore the phase space of the dynamical system governed by Schrödinger's equation is three-dimensional: Δ, θ, and t. Actually, the equations of motion take on a rather nice form if we replace θ by a *complex* variable, whose real and imaginary parts are obviously not independent of one another! The motivation for this will become even clearer later, when we introduce dissipation. Let

$$\rho_{10} \equiv \tfrac{1}{2}\sqrt{1-\Delta^2}\,e^{-i\theta}. \tag{6.1}$$

(This nomenclature makes the obvious connection with the density matrix.) Then one may check that Schrödinger's equation, including the self-consistent Coulomb potential but neglecting exchange-correlation, becomes (see appendix D)

$$\begin{aligned} \dot{\rho}_{10} &= -i\left(\omega_{10} + \zeta V_{10}\right)\rho_{10} - iV_{10}\Delta, \\ \dot{\Delta} &= 4V_{10}\mathbf{Im}\rho_{10} \end{aligned} \tag{6.2}$$

where $\zeta \equiv (z_{11} - z_{00})/z_{10}$, and

$$V_{10} = e\mathcal{E}z_{10}\sin\omega t + \alpha_{11}\omega_{10}\left[\mathbf{Re}\rho_{10} - \tfrac{1}{4}\zeta(\Delta - \bar{\Delta})\right].$$

Here, α_{11} is the standard depolarization shift integral (equation 4.22), and $\bar{\Delta}$ is the equilibrium value of Δ, before the driving field is introduced. (The off-diagonal $\bar{\rho}_{10} = 0$, since $\bar{\rho}$ is time-independent.) We have set $\hbar = 1$, as will be the case throughout this chapter.

6.2 The Single-Particle Case

Evolving these equations in time for several selected initial states, we may sample every drive cycle and plot out the (θ, Δ) Poincaré section. For the single particle case ($\alpha_{11} = 0$), we see in figure 6.1 sections at several different drive amplitudes, $\omega_D = e\mathcal{E}z_{10}$ for the case $\omega = 0.33\omega_{10}$, and $\zeta = 0$. The first plot shows zero drive, where the populations don't change, but the phase difference rotates with time, so that the Poincaré section consists of horizontal lines. The other three plots correspond to values of drive which are before, on and after the first avoided crossing shown in figure 3.4. For any finite drive amplitude, two fixed points appear, and the invariant surfaces bend into curves: regular motion of the state trajectories oscillates about each fixed point, and also circulates between them. The equations of motion are completely linear, so there are no chaotic trajectories.

Each fixed point is a Floquet state. The Poincaré mapping is area conserving, and therefore the Floquet states are marginally stable. All of the history-dependence

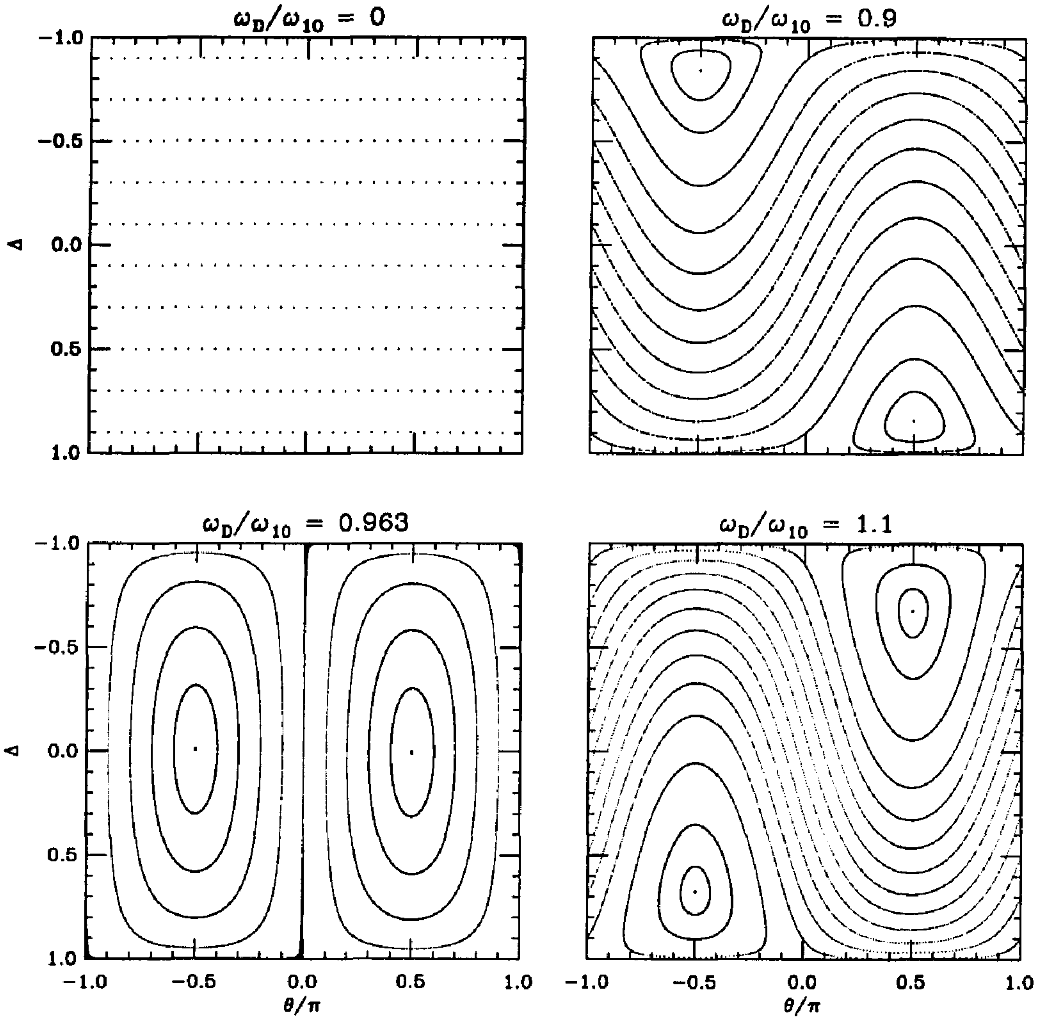

Figure 6.1: Poincaré sections of the driven single-particle two-state system.

of the system for a given value of drive amplitude is encapsulated in the Poincaré section, merely selecting an initial value and therefore a trajectory which is sampled by the section. Notice that at the value of drive which corresponds to an avoided crossing, the phase space develops massive vertical structures, and a new symmetry develops between the two fixed points. After an avoided crossing, the two fixed points swap places in the phase space, corresponding to the swapping of the Floquet states after an avoided crossing.

6.3 The Many-Particle Case

Now let us introduce many-body effects, by setting $\alpha_{11} > 0$. This introduces nonlinearities into the dynamics, as we already know. The upshot of this is dissipationless chaos in the phase space. This can be seen readily in figure 6.2, where we have set $\alpha_{11} = 1.0$, and are again driving at frequency $\omega = 0.33\omega_{10}$.

This phase portrait shows all of the generic features of dissipationless chaos, including harmonic and subharmonic resonances surrounded by islands of regular motion, interlaced with chaotic trajectories. Now the past history of the system can place the system into a dynamically regular trajectory, or a chaotic trajectory. Subharmonic generation is possible also, if one begins on a regular trajectory surrounding an $m : n$ resonance. The dipole response of the system is shown in figure 6.3, given the two initial conditions A and B shown in the figure 6.2.

Thus we have the possibility of very interesting behavior arising from our system, due to many-body interactions. In order to realize such a system experimentally, however, the dissipation channels would have to be seriously suppressed in order to make our dissipationless approximation a useful one. Doing a time-resolved mea-

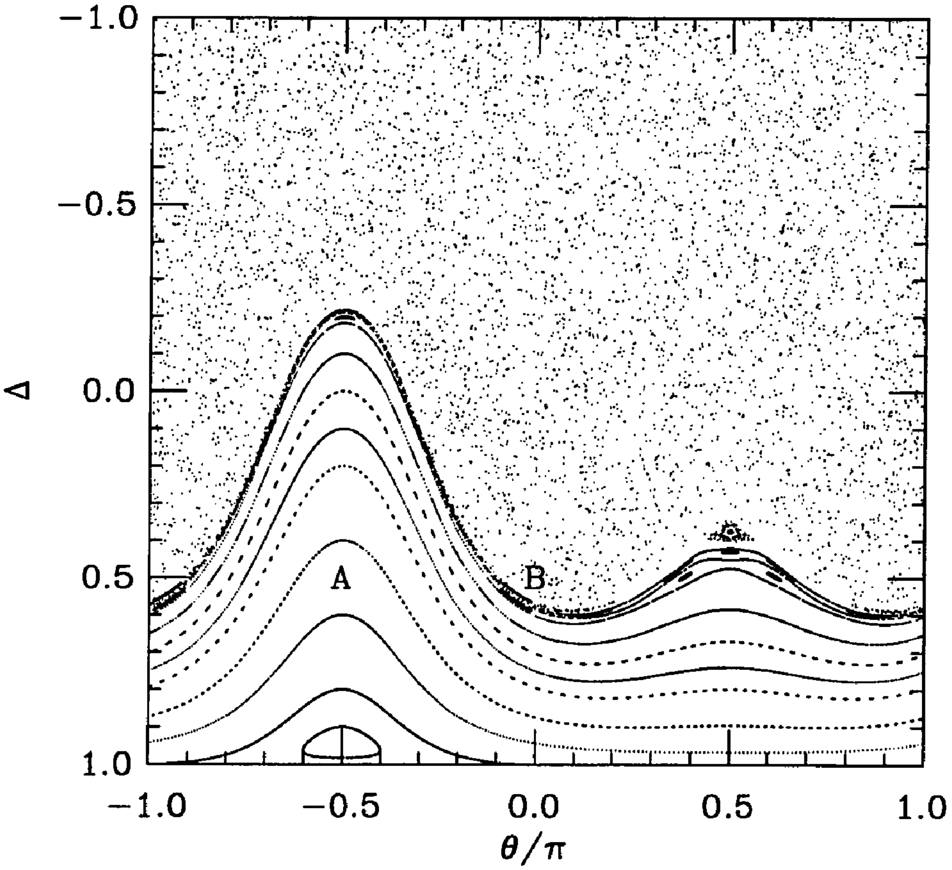

Figure 6.2: A Poincaré section of the driven many-body two-state system, at $\omega_D = 0.9\omega_{10}$.

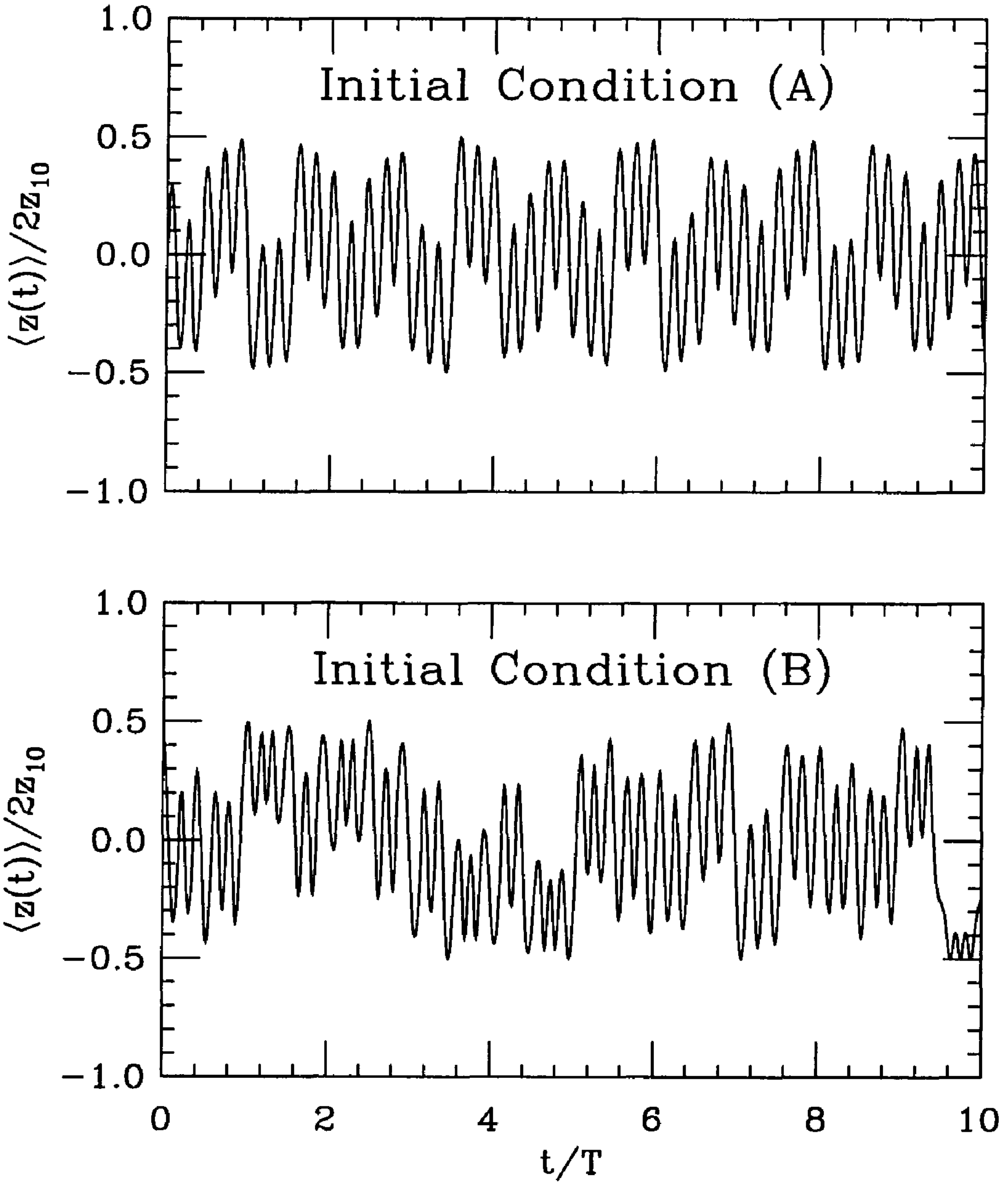

Figure 6.3: The dipole response of the system shown in figure 6.2, given the initial conditions A and B shown in that figure.

surement on time scales much less than a typical scattering time, one might be able to notice a preparation-dependent response.

6.4 Including Relaxation

Now we will introduce relaxation mechanisms into the system, in the way we did in the previous chapter. For this we will again employ the density matrix, and now instead of considering the time-evolution of the state vector under Schrödinger's equation, we will consider the time-evolution of the density matrix under the Liouville equation. Again, considering a two-state system, we see that the density matrix now contains *three* independent real quantities, since it is Hermitian, and has unit trace. We will now choose those quantities to be the real variable

$$\Delta \equiv \rho_{00} - \rho_{11},$$

and the complex off-diagonal element of the density matrix ρ_{10}. In the absence of dissipation mechanisms, these quantities become exactly what they were defined to be in the last section. Introducing dissipation as in equation 5.3, with $R_{00} = R_{11} = \Gamma_1$, and $R_{01} = R_{10} = \Gamma_2$, one finds that the damped Liouville equation becomes

$$\begin{aligned} \dot{\rho}_{10} &= -i\left(\omega_{10} + \zeta V_{10}\right)\rho_{10} - iV_{10}\Delta - \Gamma_2\rho_{10}, \\ \dot{\Delta} &= 4V_{10}\mathrm{Im}\rho_{10} - \Gamma_1(\Delta - \bar{\Delta}). \end{aligned}$$

This should be compared with 6.2, and we see that the effect of dissipation on the variables we have chosen is to add a simple linear damping term to each. Now, the real and imaginary parts of ρ_{10} are independent, i.e. equation 6.1 no longer holds. Thus, we have a *four* dimensional phase space: Δ, the phase *and* magnitude of ρ_{10}, and t.

With dissipation, the marginally stable fixed points of the Poincaré map become truly stable *sinks*. Any initial condition will evolve into some sink, corresponding to a trajectory which can be thought of as the response of the system to the external drive. Since there is in general more than one sink, there may be more than one response, and we may think of the system as having a multi-valued response function. This may manifests itself as a hysteretic response, if one sweeps through a driving parameter, as the system hops from one stable fixed point to another. An example of this is seen in figure 6.4, where the real part of the conductivity $\sigma_{zz}(\omega) \propto \omega\langle z(\omega)\rangle/\omega_D$ is plotted as a function of ω. The system parameters are: depolarization shift $\alpha_{11} = 1.0$, damping $\Gamma_1 = 0.001\omega_{10}$, and $\Gamma_2 = 0.025\omega_{10}$. Two cases are shown, the limiting case as $\omega_D \rightarrow 0$, and a finite field case, where $\omega_D = 0.01\omega_{10}$. The frequency is swept through slowly in each case, letting the system relax to its fixed response and then changing the frequency by a small amount. The low field response shows the standard perturbative resonance behavior. For the larger driving field, the frequency is swept both forwards and backwards, revealing the hysteretic response. For most values of ω in the high field case there is only one stable phase space trajectory, except in the hysteretic region, where there appears another stable trajectory and also an unstable one, which of course is not found by the system's time evolution.

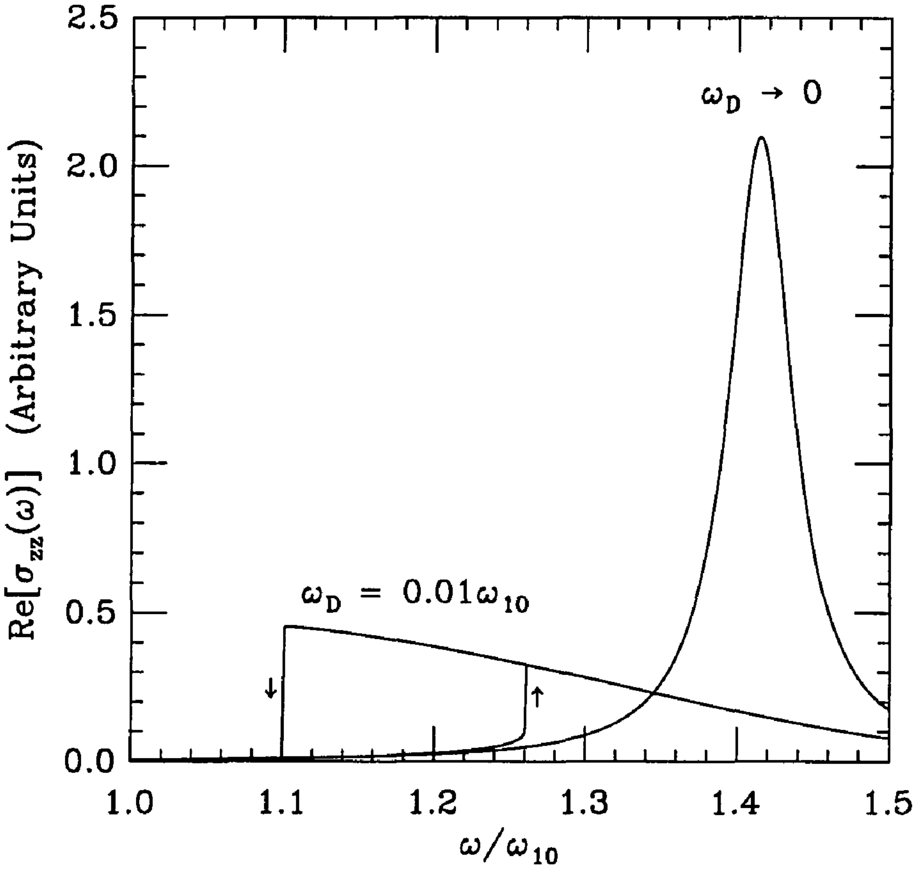

Figure 6.4: The real part of the conductivity $\sigma_{zz}(\omega)$ of the damped two-state many-body system as a function of frequency, swept through slowly in both directions. Two drive amplitudes are shown. In the high amplitude case, we see hysteretic behavior.

Chapter 7

Time-Periodic Kohn-Sham

In this chapter, we will describe another explicitly time-dependent method for solving for the dynamics of the driven many-body system described by equation 4.2. In previous chapters, we have calculated perturbative response functions, assuming low driving amplitudes, and a method for calculating nonperturbative responses using the density matrix formalism. The method described here uses the Schrödinger formalism, and takes advantage of the properties of Floquet states. It is a special case of time-dependent density functional theory [34], when we restrict ourselves to densities which are periodic in time.

The solution to the full N-body Schrödinger equation

$$i\hbar\frac{\partial\Psi}{\partial t} = H(\vec{p}_1,\ldots,\vec{p}_N,\vec{r}_1,\ldots,\vec{r}_N,t)\Psi(\vec{r}_1,\ldots,\vec{r}_N,t),$$

with initial condition $\Psi(t=0)=\Psi_0$, corresponds to a stationary point of the action integral

$$A = \int_{t_0}^{t_1} dt\,\langle\Psi(t)|\left(H(t) - i\hbar\tfrac{\partial}{\partial t}\right)|\Psi(t)\rangle$$

(where we have suppressed the coördinate-dependence of Ψ). Time-dependent density functional theory proves that the there is a one-to-one correspondence between the density $n(\vec{r},t)$ and the external potential[1] $v(\vec{r},t)$, up to an additive potential that only depends on time. (This additive potential only produces an overall phase factor in the wavefunction which does not change the density.) It follows that the wavefunctions are functionals of the density, and so is the action $A = A[n]$.

Solving for a stationary point of A,

$$\frac{\delta A[n]}{\delta n} = 0$$

gives [24]

$$i\hbar\frac{\partial \psi_j}{\partial t} = \left[-\frac{\hbar^2}{2m}\nabla^2 + v(\vec{r},t) + e\int d^3r'\,\frac{n(\vec{r}',t)}{|\vec{r}-\vec{r}'|} + \frac{\delta A_{xc}[n]}{\delta n(\vec{r},t)}\right]\psi_j(\vec{r},t). \tag{7.1}$$

The terms on the right-hand side are just the terms one expects, including the Coulomb potential from the electronic density, which is given by

$$n(\vec{r},t) = \sum_{j=1}^{N} |\psi_j(\vec{r},t)|^2.$$

The very last term in brackets in (7.1) is the time-dependent exchange-correlation term. It is guaranteed to exist, but there is in general no explicit exact form for it, and we must settle for an approximation when performing calculations.

We restrict ourselves here to only calculating time-periodic densities. Remember, Floquet's theorem tells us that the wavefunctions describing a periodically driven system can be expanded in a time-dependent orthonormal basis called the Floquet states, of the form

$$|\varphi_j(t)\rangle = e^{-i\epsilon_j t/\hbar}|u_j(t)\rangle, \tag{7.2}$$

where $u_j(\vec{r},t+T) = u_j(\vec{r},t)$ is a time-periodic function with the same period T as the driving field, and ϵ_j is the so-called "quasienergy" associated with the Floquet

---

[1] The only constraint on the external potential is that it be Taylor-expandable about some finite time t_0, with a non-zero radius of convergence.

state with quantum number j. Floquet states are eigenstates of the one-period time-evolution propagator $\mathcal{P}$,

$$\mathcal{P}|\varphi_j(0)\rangle = e^{-i\epsilon_j T/\hbar}|\varphi_j(0)\rangle, \tag{7.3}$$

and have time-periodic expectation values for any observable O, $\langle\varphi_j(t)|O|\varphi_j(t)\rangle$, if $[O,t] = 0$.

Assuming the external potential is periodic in time, and restricting ourselves to the many-body Floquet states, we prove (for reasonably localized wavefunctions) that the time-averaged expectation value of the energy

$$\langle\langle E\rangle\rangle = \frac{1}{T}\int_0^T dt\langle\varphi(t)|H(t)|\varphi(t)\rangle \tag{7.4}$$

is bounded from below. (The integrand of (7.4) is periodic in time, because of (7.2)). It follows that there exists a wavefunction with a time-periodic density which minimizes the mean energy. Let us break up the external potential into a static confining potential and the external driving field:

$$v(\vec{r},t) = W(\vec{r}) + V_L(\vec{r},t).$$

Then,

$$\begin{aligned}\langle\langle E\rangle\rangle &= \frac{1}{T}\int_0^T dt\int d^3r_1\ldots d^3r_N\,\langle\varphi(\vec{r}_1,\ldots,\vec{r}_N,t)|H_0|\varphi(\vec{r}_1,\ldots,\vec{r}_N,t)\rangle \\ &\quad+\sum_{j=1}^{N}\frac{1}{T}\int_0^T dt\int d^3r_1\ldots d^3r_N\,|\varphi(\vec{r}_1,\ldots,\vec{r}_N,t)|^2V_L(\vec{r}_j,t). \end{aligned}\tag{7.5}$$

Here, we have written out the N-electron wavefunction in its full coördinate representation, and have written the time-independent part of the Hamiltonian as H_0:

$$H_0 = \sum_{j=1}^{N}\left[\frac{-\hbar^2}{2m}\nabla_j^2 + W(\vec{r}_j)\right] + \tfrac{1}{2}e^2\sum_{i\neq j}\frac{1}{|\vec{r}_i - \vec{r}_j|}.$$

Since $\langle\varphi|H_0|\varphi\rangle$ is bounded below by the ground state energy of H_0, the first term on the righthand side of (7.5) is also bounded below by this ground state energy. Now we only need to show that the second term on the righthand side of (7.5) is bounded from below. If we restrict ourselves to confined systems, so that

$$\varphi(\vec{r}_1,\ldots,\vec{r}_N,t)=0 \quad \text{if } |\vec{r}_j|>a \text{ for any } 1\leq j\leq N,$$

then we have our sought-after lower bound if $V_L(\vec{r}_j,t)$ is reasonably well behaved. That is, if there exists a finite Λ such that

$$V_L(\vec{r},t)>\Lambda \quad \text{if } |\vec{r}|\leq a, \ \text{ for all } t.$$

This is indeed the case for the classical radiation field, even in the electric dipole approximation.

The method described in this chapter is a numerical scheme for computing the self-consistent Floquet subband in a quantum well which minimizes the mean energy, assuming that only a single Floquet subband is occupied. By using the mean energy instead of the quasienergy to label Floquet states, we avoid the pitfall of contending with a quasienergy spectrum which is unbounded from below. One expects this scheme to reproduce the perturbative response for low driving fields, and so in section 7.2 we compute the first and second-harmonic susceptibility of a doped, tilted square well at far-infrared frequencies. For low driving fields, the susceptibility computed using self-consistent Floquet states agrees with the results of time-dependent perturbation theory. The depolarization shift is implicit in this explicitly time-dependent method; it is not necessary to compute the shift separately, as we did in chapter 4.

7.1 The Numerical Method

We use a one-dimensional spatial model, assuming translational symmetry in the plane perpendicular to the growth direction of the GaAs/AlGaAs. The growth direction is taken to be parallel to the z-axis. The design potential, defined by the valence band as a function of z, is $W(z)$. We assume planar doping sites, whose z-coordinates are given by $z_1, \ldots, z_{n_d}$. The corresponding donor sheet densities at each site are $N_1, \ldots, N_{n_d}$. The total electronic sheet density in the valence band, assuming all donors to be ionized, is then $N_S = \sum_{j=1}^{n_d} N_j$. We assume all of the carriers to be confined within the region $|z| < a$, i.e. hard wall boundary conditions at $z = \pm a$. The time dependent Schrödinger equation (including the external laser field) is given by equation 4.2. Again, this equation has a limited domain of validity, and the reader is advised to review the discussion which follows it.

We perform all calculations on a m_z by m_t grid, explicitly including time as an extra dimension. Typically, the spatial grid size m_z is between 50 and 100, giving a resolution on the order of one to ten Angstroms. The temporal grid size m_t is on the order of thousands or tens of thousands, and covers one drive period. Subharmonic behavior can be studied by propagating over more than one drive cycle, but this is not done here.

The modeling proceeds as follows:

- We perform time *independent* Kohn-Sham iteration on a 1-D lattice of size m_z. The self-consistent potential obtained from this calculation is used as the starting potential for the time dependent iteration, i.e. we let $v(z,t) = v(z)$ from the time independent calculation.

- Then we repeat the following steps:

1. Integrate the Schrödinger equation (3.1) to find the one period propagator $\mathcal{P}$ (Poincaré map), using the latest guess for the time periodic potential $v(z,t)$. We propagate each time step using a Crank-Nicholson method.
2. Diagonalize $\mathcal{P}$ to find the Floquet states, (equation 7.3). Here, we assume that only one Floquet state is occupied (ignoring the x and y quantum numbers.) We further assume that this state is identified by having the lowest time-averaged expected energy, $\langle\langle E\rangle\rangle = \frac{1}{T}\int_0^T dt\langle\varphi|H|\varphi\rangle$, and call this state φ_0.
3. Calculate a new interaction potential $v'(z,t)$ using equation (4.5), and the density $n(z,t) = N_S|\varphi_0(z,t)|^2$, and replace the old potential: $v(z,t) \leftarrow v'(z,t)$.

Steps 1-3 are repeated until the interaction potential $v(z,t)$ converges sufficiently[2]. Time dependent properties of the system can then be calculated by propagating the Floquet state φ_0 through its self-consistent potential[3].

The procedure outlined above is not always convergent, i.e. the fixed point of the iteration is not always stable. This is an artifact of the procedure, not of physics. In most cases the unstable manifold is of a low enough dimension that the fixed point may be approached by "backtracking" in the case of a divergent iteration. That is, a few iterates are used to estimate the unstable manifold, and then to deduce the position of the fixed point on this manifold. This method is given in detail in

---

[2] If the desired electric field E_f is not small, it helps to increase E_f from zero in small increments, letting $v(z,t)$ converge for each increment. This roughly models turning on the field slowly, as well as helping to improve the convergence of the iterative process.

[3] This model overcomes the shortcomings of the model of Birnir et al. [7], who interlaced a Hartree iteration with each time iteration. Here the whole Poincaré map over one period is Hartree iterated until it becomes self-consistent in space and time.

appendix F. In the case of small driving amplitudes we show in appendix E the necessary and sufficient condition for stability. We also show in the near-resonance approximation that for each Fourier mode of the interaction potential, the unstable manifold is only one-dimensional, if it exists.

7.2 Checking with Perturbation Theory

As a simple first example, we compute the first and second-harmonic susceptibility of a doped, tilted, infinite square well driven by far-infrared radiation. The parameter values were chosen to be realistic and accessible to experiments on GaAs/AlGaAs quantum wells: width $2a = 400$ Å, dielectric constant $\kappa = 13$, electronic effective mass $\mu = m_e/15$ where m_e is the bare electron mass, and carrier density $N_S = 10^{11}\text{cm}^{-2}$. In order to give the system an appreciable second harmonic, the potential was given an overall tilt:

$$W(z) + V_d(z) = \begin{cases} \infty, & |z| \geq a \\ (0.05\text{meV}/\text{Å}) \cdot z, & |z| < a \end{cases}$$

The susceptibilities were computed for a range of far-infrared frequencies, at a very small drive-field strength $\mathcal{E} = 10^{-3}$ statV/cm.

For each parameter value, the iterations were continued until the response had sufficiently converged. The resulting Floquet state was propagated through one drive cycle, and the dipole $P(t) = \langle ez(t) \rangle$ was recorded at each time step. The Fourier transform $P(\omega)$ was then used to calculate the susceptibilities $\chi^{(1)}(\omega) \equiv 2P(\omega)N_S/\mathcal{E}$, and $\chi^{(2)}(\omega) \equiv 4P(2\omega)N_S/\mathcal{E}^2$. The factors of two and four come from the fact that we are using $\cos(\omega t)$ driving instead of $\exp(i\omega t)$. Plotted in figure 7.1 are $\chi^{(1)}$ and $\chi^{(2)}$. The lines represent the dressed susceptibilities calculated using

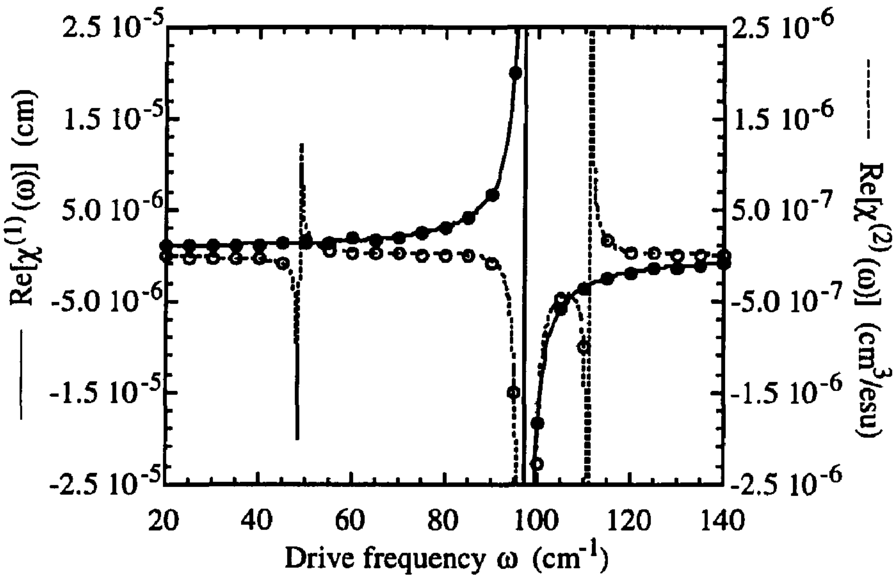

Figure 7.1: The first and second-harmonic susceptibilities $\chi^{(1)}(\omega)$ (solid line) and $\chi^{(2)}(\omega)$ (dashed line) for the doped tilted infinite square well, calculated from perturbation theory. The dots and circles represent the calculations from our model.

self-consistent perturbation theory applied to the wave functions of the undriven system calculated using the same simulation parameters on a grid of size m_z. The points are the susceptibilities calculated from our model.

The first-order response has a pole at the depolarization shifted frequency $\tilde{\omega}_{10} \approx 97.5\ \mathrm{cm}^{-1}$, representing a dressed transition from the ground to first excited state [1]. The second-order response has a simple pole at $\frac{1}{2}\tilde{\omega}_{10}$, and a second-order pole at $\tilde{\omega}_{10}$, as expected from perturbation theory. figure 7.1 also shows $\chi^{(2)}$ to have a simple pole at $\frac{1}{2}\tilde{\omega}_{20} \approx 112\ \mathrm{cm}^{-1}$, where $\tilde{\omega}_{20}$ is the dressed transition frequency from the ground to second excited state.

As one expects, our nonperturbative method agrees with perturbation theory for sufficiently small fields, with discrepancies attributable to finite temporal resolution m_t, and higher-order corrections to the response functions which our model picks up. Since the periodic oscillations of $v(z,t)$ are included from the beginning, absorption occurs at the depolarization-shifted frequency - it is not necessary to compute the shift separately.

7.3 Conclusion

In chapter 3, we used single particle Floquet states to model a GaAs/AlGaAs quantum well driven by very intense far-infrared radiation [6]. We found nonperturbative resonances in energy absorption as a function of the electric field amplitude at fixed frequency, and showed that these resonances occurred at avoided crossings of quasienergies. Birnir, Johnson and Gudmundsson [7] incorporated electron-electron interactions into Floquet theory by interlacing time iterations with Kohn-Sham iterations and indeed observed nonperturbative resonances. The model presented in this chapter is on a firmer footing, in that the Kohn-Sham iteration is performed on the entire Poincaré map, and thus eliminates the question of relaxation time scales which determine the validity of the method of interlacing.

At large field strengths one expects, for example, avoided crossings of quasienergies. However, new issues arise at nonperturbative field strengths. For example, several Floquet states may be significantly occupied. It is not clear that there exists a universal distribution, such as the Fermi distribution, which describes the population of a driven system coupled to a heat bath. In fact, the steady-state characteristics of driven systems may depend on the exact nature of the coupling to the energy reservoir [20], which runs counter to the arguments made in standard statistical mechanics of closed systems.

We have assumed that the physical system will relax to a the state which minimizes the time-averaged energy. This is an unproven, but reasonable, assumption. One must also be aware that this method may easily converge to a *local*, and not a global, minimum in mean energy. This is consistent with the hysteretic behavior found in the last chapter, but it brings to mind the possibility that the physical system would eventually tunnel, through interaction with its external environment, to a different local minimum. The time scale for this tunneling is not known. If it is much longer than a typical experiment, one would still expect to find history-dependent dynamics. In the long time limit, if a dynamic equilibrium exists, one of course expects no history dependence to remain.

Chapter 8

Conclusions and Questions

We have explored several methods for modeling quantum wells, and have included the effects of strong driving, electron-electron interactions, and a simple form of dissipation. Certainly the models presented thus far have a range of validity, as they have been useful for modeling experiments at UCSB. However, it would be useful to know what the range of validity is for these models, and to know what must be done to extend this range.

A confirmation of the validity of any model is a first-principles treatment, such as quantum Monte-Carlo. I will leave this for future work. Certainly, more can be done within the Schrödinger and density-matrix formalism. In this final chapter, we will look at the dissipation and scattering mechanisms in more detail, since they are crucial to pin down, if we are to understand the steady-state dynamics of the system, or lack thereof.

One problem with the dissipation mechanism such as the one used in equation 5.3, is that it assumes the system is always trying to relax to an incoherent population of the stationary states of the undriven system. But these states no longer have any meaning to the driven system, except when the driving field is small and so perturbation theory can be used.

The natural replacements for stationary states are the Floquet states, when the system is driven periodically. But what role do the quasienergies play? how do they relate to the energies in the driven, and undriven system? One reason that quasienergies are so troublesome is that they are only defined modulo one photon energy. Even in the extended Hilbert space formalism, where the "photon number" becomes an important quantum number, we face a spectrum of eigenvalues which is unbounded from below. Any attempt at calculating statistics of states with such a spectrum would seem fruitless.

At this point, it is good to look back at our model Hamiltonian (1.2), and give it a scrutinizing eye. When using that Hamiltonian in Schrödinger's equation, we have quantized the system, but *not* the radiation field. Certainly, this is a fine approximation for most cases, but as a result of using this approximation from the start, we have been left with the quasienergy spectrum, unbounded from below, and are at a loss to interpret it.

The *true* quantized radiation field has a ground state, that of zero photons, and thus the coupled system-plus-field has a ground state. We expect that in the limit of high photon numbers, then, the coupled system will have energies spaced a photon energy apart, and take on the appearance of our quasienergy spectrum. But far below in energy, there will lie a ground state. If this is true, we have certainly interpreted the quasienergies as the "classical radiation field" approximation to the eigenvalue spectrum of the coupled system and quantized radiation field. Let us look at some examples, to demonstrate this[1].

---

[1] The identification of Floquet states with eigenstates of the fully quantized system coupled radiation field, was made by Shirley [36].

8.1 Quantizing the Radiation Field

In order to quantize the radiation field, we consider each mode of light (wavevector and polarization) to be a modeled by a single harmonic oscillator [31, 4]. The number of photons in a mode corresponds to the state of the oscillator, the ground state representing zero photons in that mode. The Hamiltonian of the radiation field is then

$$H_R = \sum_{\vec{k},\vec{\lambda}} \left(\frac{P^2_{\vec{k}\vec{\lambda}}}{2M} + \tfrac{1}{2} M \omega^2_{\vec{k}\vec{\lambda}} X^2_{\vec{k}\vec{\lambda}} \right), \tag{8.1}$$

where we have created a coördinate system and arbitrarily choosen a mass M for each oscillator, and in a vacuum the frequencies are given by the dispersion relation $\omega_{\vec{k}\vec{\lambda}} = c|\vec{k}|$, where c is the speed of light in a vacuum. The sum runs over all wavevectors $\vec{k}$ and polarizations $\vec{\lambda}$. It is useful to second-quantize (8.1), with the lowering and raising operators $b_{\vec{k}\vec{\lambda}}$ and $b^\dagger_{\vec{k}\vec{\lambda}}$:

$$b_{\vec{k}\vec{\lambda}} = \sqrt{\frac{M\omega_{\vec{k}\vec{\lambda}}}{2\hbar}} \left(X_{\vec{k}\vec{\lambda}} + \frac{i}{M\omega_{\vec{k}\vec{\lambda}}} P_{\vec{k}\vec{\lambda}} \right), \quad b^\dagger_{\vec{k}\vec{\lambda}} = \sqrt{\frac{M\omega_{\vec{k}\vec{\lambda}}}{2\hbar}} \left(X_{\vec{k}\vec{\lambda}} - \frac{i}{M\omega_{\vec{k}\vec{\lambda}}} P_{\vec{k}\vec{\lambda}} \right).$$

Then, (8.1) becomes

$$H_R = \sum_{\vec{k},\vec{\lambda}} \hbar\omega_{\vec{k}\vec{\lambda}} \left(b^\dagger_{\vec{k}\vec{\lambda}} b_{\vec{k}\vec{\lambda}} + \tfrac{1}{2} \right). \tag{8.2}$$

Notice that the zero-point energy of each harmonic oscillator, $\frac{1}{2}\hbar\omega_{\vec{k}\vec{\lambda}}$. These terms will sum to infinity, but this infinite energy is merely an additive constant and may be subtracted from the Hamiltonian[2].

The final piece of the system-plus-radiation Hamiltonian is the interaction term coupling the undriven system to the radiation. This is well known, [31, 4] and is

---

[2] The zero-point energy becomes important in general relativity, where the absolute energy density is a key physical quantity.

given by

$$H_I = -e\sqrt{\frac{2\pi\hbar}{\omega_{\vec{k}\vec{\lambda}}V}}\sum_{\vec{k},\vec{\lambda}}\left(\vec{j}_{-\vec{k}}\cdot\vec{\lambda}b_{\vec{k}\vec{\lambda}}+\vec{j}_{\vec{k}}\cdot\vec{\lambda}^{*}b^{\dagger}_{\vec{k}\vec{\lambda}}\right), \tag{8.3}$$

where

$$\vec{j}_{\vec{k}} = \tfrac{1}{2}\left(\frac{\vec{p}}{m^*}e^{-i\vec{k}\cdot\vec{r}}+e^{-i\vec{k}\cdot\vec{r}}\frac{\vec{p}}{m^*}\right),$$

V is the volume of radiative cavity, and m^*, $\vec{p}$, and $\vec{r}$ are the effective mass, momentum operator, and position operator, respectively, in the sytsem which is coupled to the light. Let us only consider one mode of radiation, since we are considering the field to be polarized monochromatic light. Thus, we will keep only a single term in (8.2), and drop the $\vec{k}, \vec{\lambda}$ subscripts. The system may radiate in other modes, but we will not quantize those modes. The radiation Hamiltonian becomes simply

$$H_R = \hbar\omega b^\dagger b,$$

where we have subtracted out the zero-point energy $\frac{1}{2}\hbar\omega$, and the interaction Hamiltonian becomes

$$H_I = -e\sqrt{\frac{2\pi\hbar}{\omega V}}\left(j_{-k}b+j_k b^\dagger\right),$$

where

$$j_k = \tfrac{1}{2}\left(\frac{p_z}{m^*}e^{-ikz}+e^{-ikz}\frac{p_z}{m^*}\right),$$

and we have used the fact that the light is polarized in the system's z coördinate. One further approximation must be made in order that our quantized radiation field correspond to the classical term (1.1). This term is the classical field in the electric dipole approximation, where we assume that the system length is much smaller than the radiation wavelength $2\pi/k$. We then make the approximation that $e^{-ikz}\approx 1$, so that the interaction term takes on the simple form

$$H_I = -\frac{e}{m^*}\sqrt{\frac{2\pi\hbar}{\omega V}}p_z(b+b^\dagger). \tag{8.4}$$

The total Hamiltonian is

$$H = H_S + H_R + H_I, \tag{8.5}$$

where H_S is the Hamiltonian of the undriven system. Equation 8.5 replaces equation 1.2.

As an example, let us again consider the two-state system in section 3.4. The undriven system is represented as

$$H_S = \tfrac{1}{2}\hbar\omega_{10}\begin{pmatrix} -1 & 0 \\ 0 & 1 \end{pmatrix},$$

and has eigenstates

$$|\xi_0\rangle = \begin{pmatrix} 1 \\ 0 \end{pmatrix}, \quad |\xi_1\rangle = \begin{pmatrix} 0 \\ 1 \end{pmatrix}.$$

The radiation field has harmonic oscillator eigenstates, which we will represent as $|m\rangle$:

$$H_R|m\rangle = m\hbar\omega|m\rangle.$$

If we work in the product-space of the the spaces spanned by $|\xi_n\rangle$ and $|m\rangle$, the eigenstates of H_R, and define a new set of states by

$$|n, m\rangle \equiv |\xi_n\rangle \otimes |m\rangle,$$

which are the eigenstates of the uncoupled Hamiltonian of the system and radiation

$$(H_S + H_R)|n, m\rangle = E_{nm}|n, m\rangle,$$

where

$$E_{nm} = E_n + m\hbar\omega,$$

and $E_1 = -E_0 = \frac{1}{2}\hbar\omega_{10}$. The momentum operator p_z for the two state system may be represented as

$$p_z = p_{10}\begin{pmatrix} 0 & -i \\ i & 0 \end{pmatrix}.$$

Using this, our interaction Hamiltonian (8.4) can be written

$$H_I = \hbar\omega_I\begin{pmatrix} 0 & i \\ -i & 0 \end{pmatrix}(b + b^\dagger).$$

Here we have compressed all of the constants into the interaction energy $\hbar\omega_I$,

$$\omega_I \equiv \frac{ep_{10}}{m^*}\sqrt{\frac{2\pi}{\hbar\omega V}}. \tag{8.6}$$

With this interaction, in the $|n, m\rangle$ basis, our coupled Hamiltonian (8.5) may be represented as

$$H = \hbar\left(\begin{array}{ccccccc} -\frac{1}{2}\omega_{10} & 0 & 0 & i\omega_I & & & \mathbf{0} \\ 0 & \frac{1}{2}\omega_{10} & -i\omega_I & 0 & & & \\ 0 & i\omega_I & \omega - \frac{1}{2}\omega_{10} & 0 & 0 & i\sqrt{2}\omega_I & \\ -i\omega_I & 0 & 0 & \omega + \frac{1}{2}\omega_{10} & -i\sqrt{2}\omega_I & 0 & \\ & & 0 & i\sqrt{2}\omega_I & 2\omega - \frac{1}{2}\omega_{10} & 0 & \\ & & -i\sqrt{2}\omega_I & 0 & 0 & 2\omega + \frac{1}{2}\omega_{10} & \\ \mathbf{0} & & & & & & \ddots \end{array}\right). \tag{8.7}$$

Here we have used the well-known property of the raising and lowering operators,

$$b|m\rangle = \sqrt{m}|m-1\rangle, \quad b^\dagger|m\rangle = \sqrt{m+1}|m+1\rangle.$$

We wish to digonalize (8.7) exactly,

$$H|\varphi_{nm}\rangle = \varepsilon_{nm}|\varphi_{nm}\rangle,$$

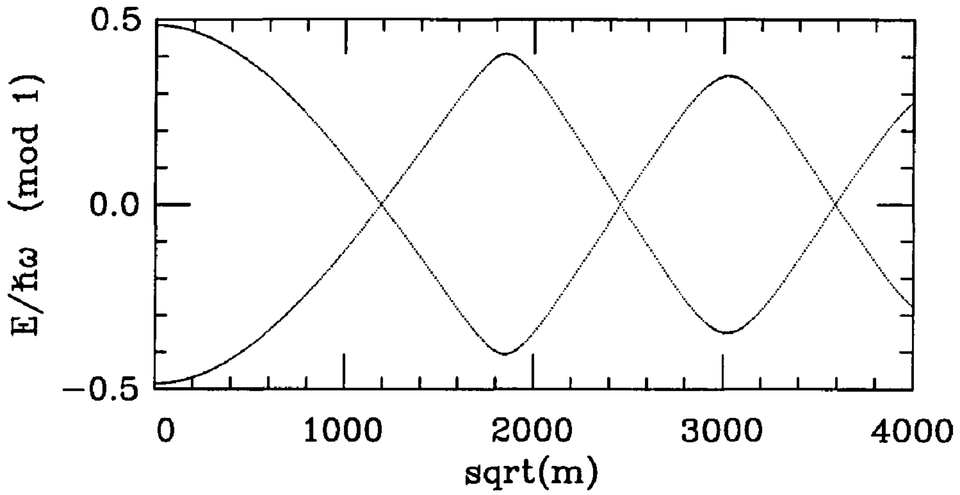

Figure 8.1: The energy eigenvalues, modulo $\hbar\omega$, of the coupled two-state system and radation field, as a function of the square root of the photon number m. The interaction strength has been adjusted so that the horizontal scale matches that of figure 3.4.

to find the energy eigenvalues ε_{nm}. To find a very large range of eigenvalues, we will sweep a large "window" across H by diagonalizing only a reasonably large submatrix H_m at a time, where H_m is centered on the m-photon elements in the diagonal of H. We can assume that the central eigenvalues of H_m are reasonably accurate. We will plot these energies as a function of $\sqrt{m}$, since the magnitude of the classical electric field $\mathcal{E}$ is proportional to $\sqrt{m}$. Picking a small coupling $\omega_I \ll \omega_{10}$, and $\omega = 0.33\omega_{10}$, figure 8.1 shows the coupled two-state system and radiation field energy eigenvalues, modulo $\hbar\omega$, as a function of the $\sqrt{m}$. Comparing with figure 3.4, there is no doubt we have found the quasienergy spectrum.

8.2 The Rotating Wave Approximation

In order to check an exactly soluble case, we may approximate the interaction term H_I in the following way. Noting that

$$p_z = ip_{10}\begin{pmatrix} 0 & 1 \\ -1 & 0 \end{pmatrix} = ip_{10}(a - a^\dagger),$$

where a and $a^\dagger$ are the lowering and raising operators for the two-state system,

$$a = \begin{pmatrix} 0 & 1 \\ 0 & 0 \end{pmatrix}, \quad a^\dagger = \begin{pmatrix} 0 & 0 \\ 1 & 0 \end{pmatrix},$$

the interaction term can be written

$$H_I = i\hbar\omega_I \left(ab + ab^\dagger - a^\dagger b - a^\dagger b^\dagger\right).$$

If we keep only the $ab^\dagger$ and $a^\dagger b$ terms, we make what is known as the *rotating wave approximation*. It has this name because it corresponds to, in the classical-field case, splitting the linearly polarized light into a sum of two terms, each circularly polarized in opposite directions, then keeping only one of the circularly polarized terms. Making this approximation, the total Hamiltonian takes on the block-diagonal form

$$H^{RWA} = \hbar \left(\begin{array}{ccccccc} -\frac{1}{2}\omega_{10} & 0 & 0 & 0 & & & {\huge 0} \\ 0 & \frac{1}{2}\omega_{10} & -i\omega_I & 0 & & & \\ 0 & i\omega_I & \omega - \frac{1}{2}\omega_{10} & 0 & 0 & 0 & \\ 0 & 0 & 0 & \omega + \frac{1}{2}\omega_{10} & -i\sqrt{2}\omega_I & 0 & \\ & & 0 & i\sqrt{2}\omega_I & 2\omega - \frac{1}{2}\omega_{10} & 0 & \\ & & 0 & 0 & 0 & 2\omega + \frac{1}{2}\omega_{10} & \\ {\huge 0} & & & & & & \ddots \end{array}\right) \tag{8.8}$$

which may be trivially diagonalized. If we name the two-by-two blocks down the diagonal of H^{RWA} as

$$H_m = \hbar \begin{pmatrix} m\omega + \frac{1}{2}\omega_{10} & -i\sqrt{m+1}\omega_I \\ i\sqrt{m+1}\omega_I & (m+1)\omega - \frac{1}{2}\omega_{10} \end{pmatrix}, \tag{8.9}$$

then we have for each block the pair of eigenvalues given by

$$\det(H_m - \varepsilon) = 0,$$

whose solution is

$$\varepsilon_{\pm} = \left(m + \tfrac{1}{2}\right)\hbar\omega \pm \tfrac{1}{2}\hbar\sqrt{(\omega_{10} - \omega)^2 + 4(m+1)\omega_I^2}. \tag{8.10}$$

This may be compared with the quasienergies of the classically driven two-state system in the rotating wave approximation. This is obtained by taking the Hamiltonian (3.9), with $\zeta = 0$, and splitting the driving term into a *rotating* and a *counterrotating* field:

$$V_L(t) = \tfrac{1}{2}\hbar\omega_D \left\{ \begin{pmatrix} 0 & -ie^{i\omega t} \\ ie^{-i\omega t} & 0 \end{pmatrix} + \begin{pmatrix} 0 & ie^{-i\omega t} \\ -ie^{i\omega t} & 0 \end{pmatrix} \right\}. \tag{8.11}$$

The second term in the curly brackets is dropped in the RWA. The quasienergies and Floquet states of (3.9) under this approximation may be found exactly (See appendix G). The quasienergies are

$$\varepsilon_{\pm}^{cd} = m\hbar\omega \pm \tfrac{1}{2}\hbar\sqrt{(\omega_{10} - \omega)^2 + \omega_D^2} \quad (\mathrm{mod}\ \hbar\omega).$$

Compating with (8.10), we see that the classical correspondence is

$$\omega_D^2 = 4m\omega_I^2. \tag{8.12}$$

(Where we have let $m+1 \rightarrow m$ in the limit of large m.) Using the definitions of ω_D (3.10) and ω_I (8.6), equation 8.12 gives

$$\frac{\mathcal{E}^2}{8\pi} = \frac{\hbar}{\omega}\frac{m}{V}\left(\frac{p_{10}}{m^* z_{10}}\right)^2.$$

This is the classical energy density in the field, and is proportional to the number of photons m per unit volume, as we expect.

In order to recover the time-dependence of the Floquet states which we expect in a driven system, one can assume the state of the photon field to be initially a *coherent superposition* of pure photon eigenstates

$$|\alpha\rangle = e^{-\frac{1}{2}|\alpha|^2}\sum_{m=0}^{\infty}\frac{\alpha^m}{\sqrt{m!}}|m\rangle.$$

Here, α is any complex number. The coherent states have a Poisson distribution over photon eigenstates, with mean value $\langle m\rangle = |\alpha|^2$, and width $\Delta m = |\alpha|$. The complex phase of α determines the phase of the corresponding classical drive in the limit as $\langle m\rangle \rightarrow \infty$. Also in this limit, the quantum fields gives the correct classical sinusoidal behavior [36].

8.3 An Open Question

The form of dissipation used in this work has been the very simple relaxation operator (5.2) introduced in chapter 5. This operator is not just empirically motivated; one can deduce its form from physical arguments [8]. It would be most satisfying to have a form of dissipation derived from a detailed physical model. Indeed, this has been accomplished by Caldeira and Leggett [14]. By coupling a single particle system to a bath of harmonic oscillators, through a linear coupling term, they were able to derive in the end a density matrix equation of motion which only involved the system (bath variables were integrated out). Their model assumes that the system couples with phonons of virtually all frequencies (their upper cut-off in frequency is mildly enforced, and taken to infinity when it will allow an integral to be solved explicitly). Their derivation for a general damped system was valid only in the high-temperature limit, but we may also write down an explicit solution of their model in the zero temperature case. This is done in appendix H. There, we also apply the zero-temperature formula to the two state system, and compare it with the dissipation used in this work. In this case, we see that the phonon model cannot capture the two relaxation time scales which we use in our two-state calculations. But it is satisfying to derive a similar form to the dissipation we are using from a first-principles model.

Our ability to charactarize and understand the dynamics of strongly driven quantum systems depends on our understanding of the coupling of such systems to their environment. I believe that a superior model of a periodically driven system coupled to an external environment can be derived in terms of single-particle Floquet states. As was shown in the last section, Floquet states are the correct eigenstates of a system coupled to the radiation field. The obvious next step would be to derive a dynamic equilibrium distribution over Floquet states. As far as I know, this has not been yet accomplished. It stands as an open problem to be solved, when (if at all) such a distribution exists, and if so, what it is.

Appendix A

The Adiabatic Limit

When one prepares a finite-state system in an energy eigenstate $|\xi\rangle$ with energy E, and then ramps up the electric field $\mathcal{E}$ in the potential (1.1) slowly, the system will "adiabatically" remain in one Floquet state $|\varphi\rangle$ whose associated quasienergy began at $\varepsilon = E \pmod{\hbar\omega}$ when $\mathcal{E} = 0$, and changes continuously as a function of $\mathcal{E}$. Using the extended Hilbert space formalism (see section E.1), we may easily derive a first-order differential equation in $\mathcal{E}$ for Floquet states and their associated quasienergies. Since we have an initial condition for each, $|\varphi(\mathcal{E} = 0)\rangle = |\xi\rangle$ and $\varepsilon(\mathcal{E} = 0) = E$, their values are uniquely defined for all drive amplitudes.

The extended Hilbert space formalism re-casts Schrödinger's equation as an eigenvalue problem,

$$\left(H - i\hbar\frac{\partial}{\partial t}\right) u_{n\nu}(z,t) = \varepsilon_{n\nu} u_{n\nu}(z,t),$$

with ν being the photon index associated with each representative of the quasienergy, (see equations 3.3 and 3.4), so that the physical Floquet state is ν *− independent*. Notice that our index notation will change as we ramp through each avoided crossing adiabatically, by our (physically motivated) convention of labeling the Floquet states and quasienergies *as if the quasienergy lines* had *crossed*. Thus, to avoid confusion, we will use a different index scheme in this appendix. Each Floquet state and quasienergy will be labeled by the eigenstate and energy they *adiabatically* evolve from.

First-order perturbation theory, in its time-independent form, may be applied to the states $u_{n\nu}(z,t)$, with the inner product given in section E.1. Thus, if we are at some field value $\mathcal{E}$, and we change the electric field by $\delta\mathcal{E}$, we change the Hamiltonian by

$$\delta H(z,t) = e\delta\mathcal{E} z \sin\omega t.$$

This change in the quasienergy is then

$$\delta\varepsilon_{n\nu} = \langle\langle u_{n\nu}|\delta H(z,t)|u_{n\nu}\rangle\rangle,$$

implying

$$\frac{\partial\varepsilon_{n\nu}}{\partial\mathcal{E}} = \langle\langle u_{n\nu}|ez\sin\omega t|u_{n\nu}\rangle\rangle = e\frac{1}{T}\int_0^T dt\,\sin\omega t\int_{-\infty}^{\infty} dz\, z|u_{n\nu}|^2.$$

Since $|u_{n\nu}(z,t)|^2 = |\phi_{n\nu}(z,t)|^2$ the right-hand side of the above equation is just the $\sin\omega t$ Fourier component of the polarization $\langle ez(t)\rangle$. Thus, the slope of the quasienergy with respect to the driving field $\mathcal{E}$ is equal to the component of the first-harmonic response which is in phase with the driving field.

Applying perturbation theory to the eigenvectors $u_{n\nu}(z,t)$,

$$\delta u_{n\nu}(z,t) = \sum_{m\mu\neq n\nu}\frac{\langle\langle u_{m\mu}|\delta H(z,t)|u_n\nu\rangle\rangle}{\varepsilon_{n\nu}-\varepsilon_{m\mu}}u_{m\mu}(z,t),$$

or

$$\frac{\partial u_{n\nu}}{\partial\mathcal{E}} = e\sum_{m\mu\neq n\nu}\frac{\langle\langle u_{m\mu}|z\sin\omega t|u_{n\nu}\rangle\rangle}{\varepsilon_{n\nu}-\varepsilon_{m\mu}}u_{m\mu}(z,t).$$

These equations define the evolution of the system in the adiabatic limit, as the ramping speed of the electric field E goes to zero. They are perfectly well-behaved for any finite-state system, but for an infinite-state system the sums may diverge, corresponding to an absence of the adiabatic limit.

Appendix B

The Kohn-Sham Self-Consistent Scheme

The Kohn-Sham self-consistent scheme [29] for finding the ground state properties of an interacting system of electrons is of central interest in our work. It reduces the problem of finding the solution of the full many-body Schrödinger equation to that of solving one nonlinear single-particle Schrödinger equation. It was shown by Hohenberg and Kohn [27] that the ground state energy a system of interacting electrons, in a static potential $V(\vec{r})$, can be written as

$$E = T[n] + \int d^3r\, V(\vec{r})n(\vec{r}) + \tfrac{1}{2}e^2 \int d^3r \int d^3r' \, \frac{n(\vec{r})n(\vec{r}')}{|\vec{r} - \vec{r}'|} + E_{xc}[n],$$

where $n(\vec{r})$ is the ground state density, and $T[n]$ and $E_{xc}[n]$ are functionals of the density. The first term on the right-hand side, $T[n]$, is by definition the kinetic energy of a system of non-interacting electron with density $n(\vec{r})$. The next two terms are obviously due to the static potential $V(\vec{r})$, and the classical electrostatic energy of the electronic density. The last term, $E_{xc}[n]$, is by definition everything else, and is called the *exchange-correlation* energy. This term incorporates all quantum correlations which are neglected in the classical electrostatic energy.

The name "exchange-correlation" is an unfortunate choice of words. Indeed, everything $E_{xc}[n]$ accounts for is a form of electron correlation, including the "exchange" part, which comes from the fact that the electrons are Fermions, and therefore the total many-body wavefunction must be antisymmetric with respect to exchange of any two electrons. This exchange piece, $E_x[n]$, may be calculated exactly (see, for example, Ashcroft and Mermin [3]) and is

$$E_x[n] = -\tfrac{1}{2}e^2 \int d^3r \int d^3r' \, \frac{n_1(\vec{r},\vec{r}')n_1(\vec{r}',\vec{r})}{|\vec{r}-\vec{r}'|},$$

where $n_1(\vec{r},\vec{r}')$ is the single-particle density matrix,

$$n_1(\vec{r},\vec{r}') \equiv \sum_{j=1}^{N} \xi_j(\vec{r})\xi_j^*(\vec{r}'),$$

the $\xi_j's$ are the single-electron wavefunctions, and N is the number of electrons.

The field of study known as *Density Functional Theory* is primarily devoted to finding expressions for $E_{xc}[n]$. A common approximation is the Local Density Approximation (LDA) which assumes that the electronic density is slowly varying so that we may write

$$E_{xc}[n] = \int d^3r \, n(\vec{r})\epsilon_{xc}\left(n(\vec{r})\right),$$

where $\epsilon_{xc}(n)$ is the exchange-correlation energy per electron in a uniform electron gas with density n, and for which there are several approximations available [19]. From this it follows [29, 19] that one may solve for the ground state density via a set of effective single-particle wavefunction $\xi_n(\vec{r})$, which are the solutions of the nonlinear Schrödinger equation

$$\left[-\frac{\hbar^2}{2m}\nabla^2 + V(\vec{r}) + v_s(\vec{r}) + v_{xc}(\vec{r})\right]\xi_n(\vec{r}) = E_n\xi_n(\vec{r}).$$

Here, $v_s(\vec{r})$ is simply the electrostatic potential

$$v_s(\vec{r}) = e\int d^3r' \, \frac{n(\vec{r}')}{|\vec{r}-\vec{r}'|},$$

and $v_s(\vec{r})$ is defined as

$$v_{xc}(\vec{r}) \equiv \frac{d(n\epsilon_{xc})}{dn},$$

and

$$n(\vec{r}) = \sum_{j=1}^{N} |\xi_n(\vec{r})|^2.$$

(In a quantum well, this last sum becomes a sum over subbands, with each summand weighted by the fractional occupation of the subbands.)

The local density approximation, which we use, is valid in both the slowly varying density and high density regimes. In the first case, one may show that the LDA $E_{xc}[n]$ is the first term in a gradient expansion for the full exchange-correlation energy, so that when the density is slowly varying, and therefore the gradients relatively small, the higher order terms may be neglected. In the second case, the exchange-correlation energy becomes much smaller than the kinetic energy, so that corrections to the LDA become negligible.

The self-consistent equations above have been used with great success in finding the static properties of systems such as atoms, molecules, and quantum wells. If the system is time-dependent, Gross and Kohn [24] have employed a generalization of density functional theory [34] to show that that derive a time-dependent exchange-correlation term, valid in the linear response regime. Their results show that in either the high density, or low frequency regimes, the static exchange-correlation term does not fair to badly. In quantum wells, neither of these conditions are met. We therefore expect the Gross-Kohn generalization to be of use in modeling driven quantum wells, but as of yet their exchange-correlation term has not been incorporated our studies.

Appendix C

Details of the Two-Level Calculations

For a two-subband system, solving (4.16) and (4.19) and plugging into (4.15) is tedious but straightforward, and gives

$$\begin{aligned}\tilde{\chi}^{(2)} &= \tfrac{3}{2}e^3 N_S \times \\ &\frac{2z_{10}^2 z_{11}(\tilde{\omega}_{10}^2\omega_{10}^2 - 2\omega^2\omega_{10}^2 + \omega^2\tilde{\omega}_{10}^2) - z_{10}^3\omega_{10}^2[\gamma(2\omega_{10}^2 + 4\omega^2) + \gamma'(\omega_{10}^2 - \omega^2)]}{(\tilde{\omega}_{10}^2 - (2\omega)^2)(\tilde{\omega}_{10}^2 - \omega^2)^2}.\end{aligned}$$

The factors γ and γ' are defined as

$$\gamma \equiv \frac{2N_S}{\omega_{10}}\left[\frac{4\pi e^2}{\kappa}(S_{1110} - S_{0010}) - (X_{1110} - X_{0010})\right]$$

and

$$\gamma' \equiv \frac{2N_S}{\omega_{10}}\left[\frac{4\pi e^2}{\kappa}(S_{1011} - S_{1000}) - (X_{1011} - X_{1000})\right].$$

However, much simplification is still possible as we have identities amongst the integrals S_{jknm} which can be proven with integration by parts, and are generally useful so we give more here than are needed for this calculation:

$$\begin{aligned} S_{jknm} - S_{nmjk} &= 0 && \text{if } j \neq k \text{ and } n \neq m, \\ S_{kknm} - S_{nmkk} &= z_{nm} && \text{if } n \neq m, \\ S_{kk11} - S_{11kk} &= z_{11} - z_{kk}. \end{aligned} \tag{C.1}$$

From these identities it is easy to see that $\gamma = \gamma'$, and one arrives at (assuming our coördinate system is such that $z_{00} = 0$),

$$\tilde{\chi}^{(2)} = 3e^3 N_S z_{10}^2 \omega_{10}^2 \frac{z_{11}(\omega_{10}^2 - \omega^2) + [z_{11}(\alpha_{11} - \beta_{11}) - z_{10}\gamma](\omega_{10}^2 + \omega^2)}{(\tilde{\omega}_{10}^2 - (2\omega)^2)(\tilde{\omega}_{10}^2 - \omega^2)^2}. \tag{C.2}$$

We may simplify (C.2) by noting that

$$\alpha_{11} - \beta_{11} = \langle 1|f|0\rangle,$$

and

$$\gamma = \langle 1|f|1\rangle - \langle 0|f|0\rangle,$$

where the brackets denote the usual Hilbert space inner product, and

$$f(z) \equiv \frac{2N_S}{\omega_{10}} \left[-\frac{4\pi e^2}{\kappa} \int_{-\infty}^{z} dz' \int_{-\infty}^{z'} dz'' \xi_1(z'')\xi_0(z'') \;+\; \xi_1(z)\xi_0(z) \frac{\partial v_{xc}}{\partial n(z)} \right].$$

Since $f(z)$ commutes with z, then $\langle 1|fz|0\rangle = \langle 1|zf|0\rangle$. Completeness of the two-subband system then gives

$$\langle 1|f|1\rangle\langle 1|z|0\rangle + \langle 1|f|0\rangle\langle 0|z|0\rangle = \langle 1|z|1\rangle\langle 1|f|0\rangle + \langle 1|z|0\rangle\langle 0|f|0\rangle,$$

or $z_{10}\gamma = z_{11}(\alpha_{11} - \beta_{11})$, cancelling out the bracketed term in (C.2) to give (4.20).

Appendix D

The Density Matrix Equations of Motion

The equation of motion for the density matrix of a time-dependent system

$$\frac{\partial\rho}{\partial t} = -i[H_0 + V(t), \rho(t)]$$

(where H_0 is time-independent, and we have set $\hbar = 1$) take on a rather nice form in the basis of eigenstates of H_0. This is because, for any diagonal matrix D, and an arbitrary matrix A,

$$[D, A]_{nm} = \sum_k (D_{nk}A_{km} - A_{nk}D_{km}) = (D_{nn} - D_{mm})A_{nm}.$$

In the basis of energy eigenstates $\xi_n(z)$, $[H_0]_{nn} = E_n$, and we have

$$[H_0, \rho(t)]_{nm} = \omega_{nm}\rho_{nm}(t)$$

where $\omega_{nm} = E_n - E_m$. One is then left with evaluating $[V(t), \rho(t)]_{nm}$. In general, this requires carrying out the full matrix multiplications between V and ρ.

If we absorb all of the static potential in H_0, including the static self-consistent potential of the undriven system, then

$$V(t) = e\mathcal{E}z\sin\omega t + \delta v_s(z,t) + \delta v_{xc}(z,t).$$

Where the last two terms are the changes in the Coulomb and exchange-correlation potentials due to the driving. Since the Coulomb potential (4.3) is a linear functional of the density, then

$$\begin{aligned} \delta v_s(z,t) &= -\frac{4\pi e^2}{\kappa}\int_{-\infty}^{z} dz' \int_{-\infty}^{z'} dz'' \delta n(z'',t) \\ &= -\frac{4\pi e^2 N_S}{\kappa}\sum_{jk}\delta\rho_{jk}(t)\int_{-\infty}^{z} dz' \int_{-\infty}^{z'} dz'' \xi_j(z'')\xi_k(z''). \end{aligned}$$

Taking a matrix element gives

$$\delta v_{s,nm} = \frac{4\pi e^2 N_S}{\kappa}\sum_{kj}\delta\rho_{kj}(t)S_{nmkj}, \tag{D.1}$$

by definition of (4.17). We will assume that when the system is undriven, the equilibrium density matrix is time-independent (and therefore diagonal), which we will label $\bar{\rho}$, so that

$$\delta\rho(t) = \rho(t) - \bar{\rho}. \tag{D.2}$$

That there exists a time-dependent exchange-correlation potential $v_{xc}(z,t)$ which allows us to calculate the time-evolution of the electron density self-consistently, is a result of time-dependent density functional theory [24]. An approximation for this term is $v_{xc}(z,t) = v_{xc}[n(z,t);z]$, that is, using the static exchange-correlation potential, and merely plugging in the time-dependent density. This is valid in the high density regime, and also when the drive frequency is very low (compared to the effective Rydberg frequency in the material), for small drive amplitudes (linear response). In this case, we may linearize the exchange-correlation potential, so that

$$\delta v_{xc}(z,t) = \frac{\partial v_{xc}}{\partial n}\delta n(z,t),$$

then a similar treatment to the Coulomb potential gives

$$\delta v_{xc,kj} = N_S\sum_{kj}\delta\rho_{kj}(t)X_{nmkj},$$

by definition of (4.18). The range of validity of this treatment for high driving amplitudes is certainly questionable. Of course, we may perform these calculations in an arbitrary basis, and include the full many-body potentials explicitly. Then, one might expect the static exchange-correlation potential to be valid for any drive strength, as long as the density is high or the drive frequency is low (as are the frequencies of the dominant harmonics in the electron polarization!) This has not been proven rigorously, however.

In order to keep our computations simple, and be valid for all driving fields, we remain in the basis of self-consistent eigenstates and drop the exchange-correlation potential. The equations of motion for the density matrix elements become

$$\dot{\rho}_{nm} = -i\omega_{nm}\rho_{nm} - i[V(t),\rho]_{nm}, \tag{D.3}$$

where

$$V_{nm}(t) = e\mathcal{E}z_{nm}\sin\omega t + \delta v_{s,nm}(z,t). \tag{D.4}$$

D.1 The Two-Subband System

If we approximate our system with only two subbands, the equations of motion become very simple. Defining $\Delta \equiv \rho_{00} - \rho_{11}$, equation D.3 gives

$$\begin{aligned} \dot{\Delta} &= -i\left([V(t),\rho]_{00} - [V(t),\rho]_{11}\right), \\ \dot{\rho}_{10} &= -i\omega_{10}\rho_{10} - i[V(t),\rho]_{10}. \end{aligned} \tag{D.5}$$

Since $\rho_{01} = \rho_{10}^*$, and $V_{10}(t) = V_{01}(t)$, carrying out the commutators gives

$$\begin{aligned} [V(t),\rho]_{00} - [V(t),\rho]_{11} &= 4iV_{10}(t)\mathrm{Im}\rho_{10}, \\ [V(t),\rho]_{10} &= \left(V_{11}(t) - V_{00}(t)\right)\rho_{10} + V_{10}(t)\Delta. \end{aligned} \tag{D.6}$$

This may be simplified when we notice that $V(z,t)$ commutes with z, so that $\langle 1|Vz|0\rangle = \langle 1|zV|0\rangle$. Completeness of the two-subband system then gives

$$\langle 1|V|1\rangle\langle 1|V|0\rangle + \langle 1|V|0\rangle\langle 0|V|0\rangle = \langle 1|z|1\rangle\langle 1|f|0\rangle + \langle 1|z|0\rangle\langle 0|f|0\rangle,$$

or $V_{11}(t) - V_{00}(t) = \zeta V_{10}(t)$, where we have defined $\zeta = (z_{11} - z_{00})/z_{10}$. With this, (D.5) and (D.6) become

$$\begin{aligned} \dot{\Delta} &= 4V_{10}(t)\mathbf{Im}\rho_{10}, \\ \dot{\rho}_{10} &= -i(\omega_{10} + \zeta V_{10}(t))\rho_{10} - iV_{10}(t)\Delta. \end{aligned}$$

The matrix element $V_{10}(t)$ is (using equations D.4, D.1, and D.2),

$$\begin{aligned} V_{10}(t) &= e\mathcal{E}z_{10}\sin\omega t \\ &+ \frac{4\pi e^2 N_S}{\kappa}\left[(\rho_{10}(t) + \rho_{01}(t))\, S_{1010} + (\rho_{00}(t) - \bar{\rho}_{00})\, S_{1000} + (\rho_{11}(t) - \bar{\rho}_{11})\, S_{1011}\right]. \end{aligned}$$

Now, using $\mathbf{Tr}\rho = 1$, defining $\bar{\Delta} \equiv \bar{\rho}_{00} - \bar{\rho}_{11}$, and using the fact that

$$S_{1011} - S_{1000} = \zeta S_{1010},$$

(see appendix C) we have

$$\begin{aligned} V_{10}(t) &= e\mathcal{E}z_{10}\sin\omega t + \frac{4\pi e^2 N_S}{\kappa} S_{1010}\left[(\rho_{10}(t) + \rho_{01}(t)) - \tfrac{1}{2}\zeta(\Delta - \bar{\Delta})\right] \\ &= e\mathcal{E}z_{10}\sin\omega t + \alpha_{11}\omega_{10}\left[\mathbf{Re}\rho_{10} - \tfrac{1}{4}\zeta(\Delta - \bar{\Delta})\right]. \end{aligned}$$

On the last line above, α_{11} is the depolarization-shift integral (4.22).

Appendix E

Stability of the TPKS Method

We may determine stability of the procedure outlined in chapter 7 in the linear (small driving amplitude) regime by using the specific time-dependent solution as the known fixed-point of the iteration, and iterating a "nearby" interaction potential which differs slightly from the solution. In the linear driving regime, the time-dependent solution may be found self-consistently by solving a linear set of equations [1]. We may then find the Floquet states associated with the nearby potential by perturbation theory, and generate an updated interaction potential from the perturbed Floquet states. Our criterion for stability is that the updated potential is nearer to the true solution than the initial potential.

E.1 Extended Hilbert Space Formalism

We will take advantage of the *extended* Hilbert space [35] formulation of Floquet theory, in which time is an additional dimension, with periodic boundary conditions in that dimension. If $\varphi_n(t)$ is a normalized Floquet state solution of Schrödinger's equation (setting $\hbar = 1$)

$$i\frac{\partial \varphi_n}{\partial t} = H(t)\varphi_n(t),$$

where $H(t+T) = H(t)$, then we may decompose $\varphi_n(t)$ in a countably infinite number of ways indexed by the "photon number" ν:

$$\varphi_n(t) = e^{-i\varepsilon_{n\nu}t} u_{n\nu}(t)$$

where $u_{n\nu}(t+T) = u_{n\nu}(t)$. The index ν says which Brillouin zone the Floquet state lives in, and consequently adds an integer number of photon energies to the quasienergy, $\varepsilon_{n\nu} = \nu\omega + \varepsilon_{n0}$, where $\omega = 2\pi/T$. If we define an *Extended Hilbert space Hamiltonian*

$$\mathcal{H} \equiv H - i\tfrac{\partial}{\partial t},$$

then the functions $u_{n\nu}$ and the quasienergies $\varepsilon_{n\nu}$ are solutions of the eigenvalue equation

$$\mathcal{H}u_{n\nu} = \varepsilon_{n\nu}u_{n\nu}.$$

The advantage of this formalism is that all of the standard tools of time-independent quantum mechanics, in particular perturbation theory, carry directly over into the extended Hilbert space as long as one uses the inner product

$$\langle\langle f|g\rangle\rangle \equiv \frac{1}{T}\int_0^T dt \langle f|g\rangle,$$

where the single brackets denote the standard inner product in the original Hilbert space, and f and g must be periodic functions in time with period T. The functions $u_{n\nu}$ are orthonormal with respect to the double-bracket inner product,

$$\langle\langle u_{n\nu}|u_{m\mu}\rangle\rangle = \delta_{nm}\delta_{\nu\mu}.$$

E.2 Representing The Fixed Point

Let us assume we know the solution to the time-dependent Schrödinger equation (3.1). Writing this in the extended Hilbert space formalism,

$$\bar{\mathcal{H}}\bar{u}_{n\nu} = \bar{\varepsilon}_{n\nu}\bar{u}_{n\nu}$$

where

$$\bar{\mathcal{H}} = \bar{H} - i\tfrac{\partial}{\partial t},$$

and

$$\bar{H} = -\frac{1}{2}\frac{\partial^2}{\partial z^2} + v_0(z) + e\mathcal{E}z(e^{-i\omega t} + e^{i\omega t}) + \bar{v}(z,t).$$

(Note we have altered notation somewhat from that of equation (3.1), and have set the effective mass μ to unity.) Here, the bars indicate that the solution (both potential *and* wave functions) are self-consistent, that is the fixed point of the iteration.

If we assume that only the state corresponding to the ground subband is initially filled in the undriven system, and that the drive is turned on adiabatically, then this translates in the Floquet picture to only one Floquet subband occupied, which we label φ_0. Each other subband also turns into a corresponding Floquet subband, and for small drive amplitudes we know their solutions from time-dependent perturbation theory [1]. In terms of the undriven self-consistent stationary states (which we take to be real), $\bar{H}^{(\mathcal{E}=0)}\xi_n = E_n\xi_n$, the Floquet states are

$$\varphi_n(z,t) = e^{-iE_n t}\left[\xi_n(z) - \sum_m V_{mn}\xi_m(z)\left(\frac{e^{-i\omega t}}{\omega_{nm} - \omega} + \frac{e^{i\omega t}}{\omega_{nm} + \omega}\right)\right] \tag{E.1}$$

where $\omega_{nm} \equiv E_n - E_m$. The matrix elements V_{mn} are found by solving the linear set of equations

$$V_{mn} = e\mathcal{E}z_{mn} - 2N_S\sum_n \left(\frac{4\pi e^2}{\kappa}S_{mnk0} + X_{mnk0}\right)V_{k0}\frac{\omega_{k0}}{\omega_{k0}^2 - \omega^2},$$

where S_{mnkj} and X_{mnkj} are defined by (4.17) and (4.18), and $z_{mn} = \langle \xi_m | z | \xi_n \rangle$ is the dipole matrix element. From (E.1) we may read off the functions and quasienergies:

$$\bar{u}_{n\nu} = e^{i\nu\omega t}\left[\xi_n(z) - \sum_m V_{mn}\xi_m(z)\left(\frac{e^{-i\omega t}}{\omega_{nm} - \omega} + \frac{e^{i\omega t}}{\omega_{nm} + \omega}\right)\right]$$

and

$$\bar{\varepsilon}_{n\nu} = \nu\omega + E_n.$$

We may obtain the density from any ground state representative $\bar{u}_{0\nu}$, and for this discussion we choose the $\nu = 0$ representative:

$$\bar{n}(z,t) = N_S|\bar{u}_{00}(z,t)|^2.$$

E.3 Linear Stability Analysis

Now we start with an interaction potential $v(z,t)$ which departs from the true solution by a small amount,

$$v(z,t) = \bar{v}(z,t) + \delta v(z,t)$$

where $\delta v(z, t+T) = \delta v(z,t)$. Then

$$\mathcal{H} = \bar{\mathcal{H}} + \delta v(z,t),$$

and we may apply perturbation theory *in a time-independent form* to find the quasienergies and Floquet states associated with $\mathcal{H}$:

$$\varepsilon_{n\nu} = \bar{\varepsilon}_{n\nu} + \langle\langle \bar{u}_{n\nu}|\delta v|\bar{u}_{n\nu}\rangle\rangle + \mathcal{O}(\delta v^2)$$

and

$$u_{n\nu} = \bar{u}_{n\nu} + \sum_{m\mu\neq n\nu} \bar{u}_{m\mu}\frac{\langle\langle \bar{u}_{m\mu}|\delta v|\bar{u}_{n\nu}\rangle\rangle}{\bar{\varepsilon}_{n\nu} - \bar{\varepsilon}_{m\mu}} + \mathcal{O}(\delta v^2).$$

The electronic density is then

$$n(z,t) = N_S|u_{00}(z,t)|^2 = \bar{n}(z,t) + \delta n(z,t), \tag{E.2}$$

where

$$\delta n(z,t) = 2N_S\mathrm{Re}\left[\sum_{m\mu\neq 00} e^{i\mu\omega t}\xi_m(z)\xi_0(z)\frac{\langle\langle\xi_m|e^{-i\mu\omega t}\delta v|\xi_0\rangle\rangle}{\bar{\varepsilon}_{00}-\bar{\varepsilon}_{m\mu}}\right] + \mathcal{O}(\delta v^2) + \mathcal{O}((e\mathcal{E}z)^2).$$

Breaking δv into Fourier modes,

$$\delta v(z,t) = \sum_{\eta} \delta v(z,\eta)e^{i\eta\omega t},$$

and defining $\delta v_{mn}(\mu) \equiv \langle\xi_m|\delta v(z,\mu)|\xi_n\rangle$, we arrive at

$$\delta n(z,t) = -N_S \sum_{m\mu\neq 00} \xi_m(z)\xi_0(z)\left(e^{i\mu\omega t}\delta v_{m0}(\mu) + e^{-i\mu\omega t}\delta v_{m0}(-\mu)\right)\frac{1}{\omega_{m0}+\mu\omega}.$$

(In the above equation, we have used the fact that $\delta v(z,t)$ is real, so that $\delta v^*(z,\mu) = \delta v(z,-\mu)$.) Updating our interaction potential using (4.5) and the density (E.2) gives

$$v'(z,t) = \bar{v}(z,t) + \delta v'(z,t)$$

where

$$\delta v'(z,t) = -\frac{4\pi e^2}{\kappa}\int_{-\infty}^{z} dz' \int_{-\infty}^{z'} dz''\delta n(z'',t) + \frac{\partial v_{xc}}{\partial n(z)}\delta n(z,t). \tag{E.3}$$

We may Fourier transform (E.3) and take a matrix element, to get

$$\delta v'_{nl}(\eta) = -2N_S\sum_{m}\delta v_{m0}(\eta)\frac{\omega_{m0}}{\omega_{m0}^2-(\eta\omega)^2}\left(\frac{4\pi e^2}{\kappa}S_{nlmo} + X_{nlm0}\right). \tag{E.4}$$

This is a linear mapping, mode by mode, from one interaction potential to the next.

We may relate the map (E.4) to the depolarization-shifted absorption frequencies, which may be found by defining [1]

$$\alpha_{nm} - \beta_{nm} = -2N_S\left(\frac{4\pi e^2}{\kappa}S_{n0mo} + X_{n0m0}\right)(\omega_{n0}\omega_{m0})^{-1/2},$$

and

$$A_{nm} = \omega_{m0}^2 \delta_{nm} + \omega_{n0}(\alpha_{nm} - \beta_{nm})\omega_{m0}.$$

Then, the depolarization-shifted resonance frequencies are the square roots of the eigenvalues of the matrix $[A_{nm}]$.

If we define the vector $\vec{a}$ with components $a_n \equiv \omega_{n0}^{1/2} \delta v_{n0}(\eta)$, then (E.4) becomes (for $l = 0$)

$$\vec{a}' = M\vec{a},$$

where M is the matrix with elements

$$M_{nm} = \frac{\omega_{m0}^2 \delta_{nm} - A_{nm}}{\omega_{m0}^2 - (\eta\omega)^2}.$$

Thus, the iterative procedure is stable if and only if the spectrum of M lies inside the unit circle, since the $l \neq 0$ components of $\delta v_{nl}(\eta)$ are linear combinations of the components of $\vec{a}$, from equation (E.4).

We may gain further insight into the stability criterion with the near-resonance approximation, which is valid when $\eta\omega \sim \omega_{n0}$ for some state n and Fourier mode η. This is in fact where instability is very much a problem, as can be seen by the definition of the matrix M. In this approximation, $A_{nn} = \tilde{\omega}_{n0}^2$, the square of the depolarization-shifted absorption frequency, and all other elements of A are zero. This gives us the mapping

$$\delta v_{n0}'(\eta) = \frac{\omega_{n0}^2 - \tilde{\omega}_{n0}^2}{\omega_{n0}^2 - (\eta\omega)^2} \delta v_{n0}(\eta).$$

This map is stable if and only if

$$|(\eta\omega)^2 - \omega_{n0}^2| > |\tilde{\omega}_{n0}^2 - \omega_{n0}^2|.$$

That is, the map is stable if and only if there is no harmonic of ω which lies in a frequency range which is quadratically centered about the bare absorption frequency

ω_{n0} (where the map is most unstable), and which extends up to the depolarization-shifted absorption frequency $\tilde{\omega}_{n0}$.

Therefore in the near-resonance approximation, the unstable manifold for each Fourier mode, if it exists, is one-dimensional.

Appendix F

The Method of "Backtracking"

When solving for a the self-consistent wavefunctions and potential iteratively, one wishes to find a fixed point of the iterative process; this is the self-consistent solution. If we consider the discretized potential to be a finite-dimensional vector $\vec{a}$, and the self-consistent iteration to be a mapping $\mathcal{M}$ from one potential to another,

$$\vec{a}_{n+1} = \mathcal{M}(\vec{a}_n),$$

then our desired solution is a fixed point of $\mathcal{M}$. In some cases, as we have seen, this fixed point is *not* stable. However, as we have shown in the previous appendix, in many cases the unstable manifold (which we will label W_u from now on) is very low, and often $\dim W_u = 1$. It would be a pity if one unstable direction prevented us from finding the fixed point, when all of the other directions are stable. Fortunately, it is rather simple to stablize the iteration process in this case, if one is near enough to the fixed point to begin with.

Let us assume we are near the fixed point, $\vec{a}^*$. We know that the map $\mathcal{M}$ becomes linear near a fixed point,

$$\mathcal{M}(\vec{a}) \approx \vec{a}^* + M(\vec{a} - \vec{a}^*) \tag{F.1}$$

Consider a sequence of vectors, obtained from a repeated application of $\mathcal{M}$:

$$\vec{a}_1 = \mathcal{M}(\vec{a}_0), \quad \vec{a}_2 = \mathcal{M}(\vec{a}_1), \ \ldots \text{ etc.}$$

One expects each iterate $\vec{a}_n$ to be exponentially closer to the unstable manifold than the previous iterate, and soon each subsequent vector will be "running away" along the unstable manifold. This behavior clearly reveals not only the direction but also the distance to the fixed point. In fact, if $\dim W_u = 1$, then only two applications of $\mathcal{M}$ to an initial vector $\vec{a}_0$ will give enough information to estimate where the fixed point $\vec{a}^*$ lies. Then we may reset our vector to the estimate of the fixed point. If we are successful, we will be even closer to the fixed point, so that two iterates later our estimation process will be even more accurate. Thus, the mapping augmented with backtracking is effectively a *new* map, with a *stable* fixed point at $\vec{a}^*$. We will now derive the algorithm, for the cases $\dim W_u = 1$ and 2.

F.1 $\dim W_u = 1$

Let us assume we are near the fixed point $\vec{a}^*$, so that equation F.1 holds, and work in a coördinate system such that one coördinate is in the direction of W_u, and all other coördinates are perpendicular to W_u. (Since our mapping is now linear, W_u is a straight line.) This is depicted in figure F.1.

Since we become closer to W_u on each iteration, a good estimate for the direction of W_u is merely $\vec{a}_2 - \vec{a}_1$. Our task then becomes estimating the *distance* in this direction from $\vec{a}^*$ to a known vector, say $\vec{a}_1$. Defining

$$\begin{aligned} \vec{\delta}_1 &\equiv \vec{a}_1 - \vec{a}_0, \\ \text{and } \vec{\delta}_2 &\equiv \vec{a}_2 - \vec{a}_1, \end{aligned}$$

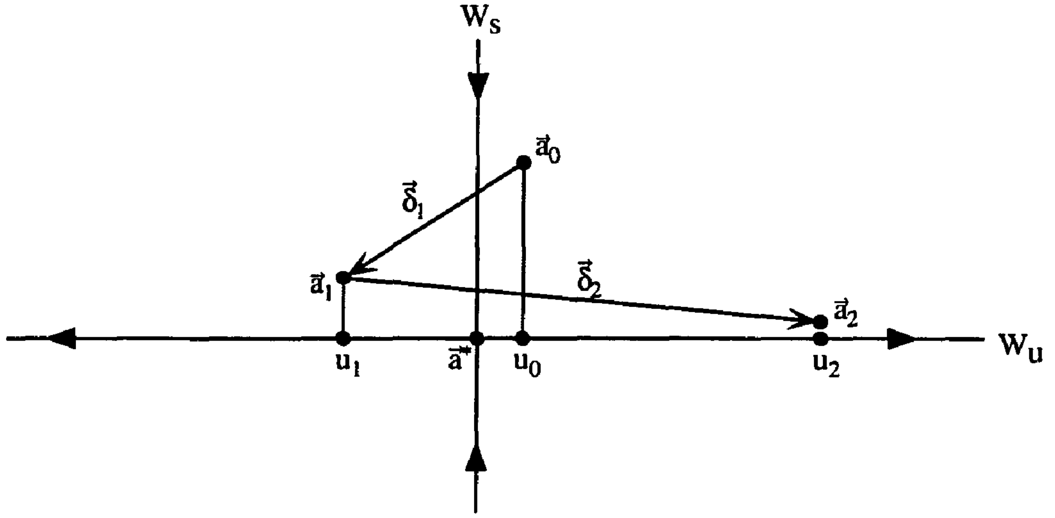

Figure F.1: The iterates resulting from the repeated mapping by $\mathcal{M}$, dim $W_u = 1$, near the fixed point $\vec{a}^*$. The stable manifold W_s, which are all coördinates perpendicular to W_u, are rolled into the vertical axis.

and making the approximation that $\vec{a}_2$ and $\vec{a}_1$ both in fact lie *on* W_u, then the projections of the vectors $\vec{a}_n$, labeled u_n, have the following relations:

$$\begin{aligned} u_2 - u_1 &= |\vec{\delta}_2|, \\ \text{and } u_1 - u_0 &= \vec{\delta}_1 \cdot \vec{\delta}_2 / |\vec{\delta}_2|. \end{aligned} \tag{F.2}$$

The linear mapping M gives the following relations involving the position of the fixed point on W_u, labeled u^*:

$$\begin{aligned} u_2 - u^* &= g(u_1 - u^*), \\ \text{and } u_1 - u^* &= g(u_0 - u^*), \end{aligned}$$

where the constant factor g is the eigenvalue of M corresponding to the unstable direction, so that $|g| > 1$. Since

$$\begin{aligned} u_2 - u_1 &= (u_2 - u^*) - (u_1 - u^*) &= (g-1)(u_1 - u^*), \\ \text{and} \quad u_1 - u_0 &= (u_1 - u^*) - (u_0 - u^*) &= (g-1)(u_0 - u^*), \end{aligned}$$

we may divide these two equations to get

$$\frac{u_2 - u_1}{u_1 - u_0} = \frac{u_1 - u^*}{u_0 - u^*}. \tag{F.3}$$

Substituting $u_0 - u^*$ by $u_1 - u^* - (u_1 - u_0)$ in equation F.3, and solving for $u_1 - u^*$ gives

$$u_1 - u^* = \left(\frac{u_2 - u_1}{u_1 - u_0} - 1\right)^{-1} (u_2 - u_1),$$

or, using equations F.2,

$$u^* - u_1 = \left(1 - \frac{|\vec{\delta}_2|}{\vec{\delta}_1 \cdot \vec{\delta}_2 / |\vec{\delta}_2|}\right)^{-1} |\vec{\delta}_2|.$$

This is the relative position of $\vec{a}^*$ compared with $\vec{a}_1$, in the direction of $\vec{\delta}_2$. Multiplying this by the unit vector $\vec{\delta}_2/|\vec{\delta}_2|$ gives their vector difference, so

$$\vec{a}^* = \vec{a}_1 + \left(1 - \frac{\vec{\delta}_2 \cdot \vec{\delta}_2}{\vec{\delta}_1 \cdot \vec{\delta}_2}\right)^{-1} \vec{\delta}_2. \tag{F.4}$$

Equation F.4 estimates the position of $\vec{a}^*$, which may be substituted for the current iterate, if the iterates are diverging ($|\vec{\delta}_2| > |\vec{\delta}_1|$). If the map still fails to converge, then it is possible that: (i) the initial vector $\vec{a}_0$ was too far from the fixed point, (ii) the growth factor g was too close to unit magnitude, or (iii) $\dim W_u > 1$. In the first case, the only thing that can help is to choose a better initial vector. If one is ramping a parameter, say turning up the driving amplitude slowly in the Time-Periodic Kohn-Sham algorithm, then this corresponds to ramping more slowly. In the second case, it may help to iterate the map a few more times before backtracking, so that the iterates are closer to being along W_u. Strong divergence

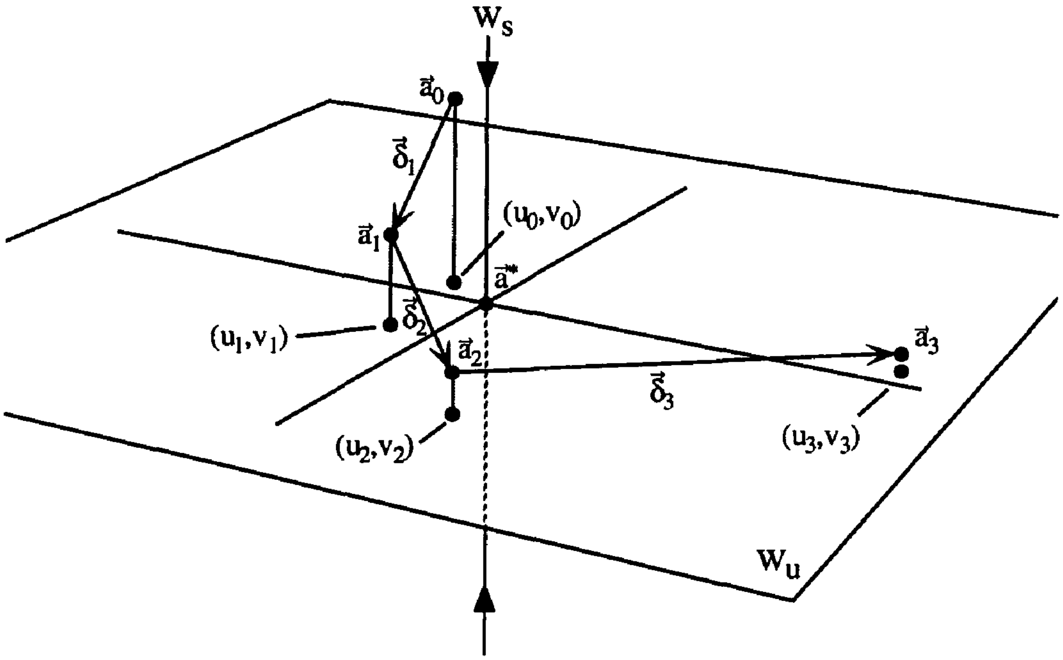

Figure F.2: The iterates resulting from the repeated mapping by $\mathcal{M}$, $\dim W_u = 2$, near the fixed point $\vec{a}^*$. As in figure F.2, the all coördinates in the stable manifold W_s are depicted here as a single dimension.

actually helps in backtracking! In the third case, one must try a higher-dimensional algorithm. The case of $\dim W_u = 2$ is treated next.

F.2 $\dim W_u = 2$

If one wishes to backtrack to a fixed point with a two-dimensional unstable manifold, more information is needed. In particular, three iterates of $\mathcal{M}$ and an initial vector $\vec{a}_0$ is needed, in order to approximate the plane W_u near the fixed point. Figure F.2 shows the coördinate labeling in this case.

We have labeled the third iterate $\vec{a}_3$, and defined

$$\vec{\delta}_3 \equiv \vec{a}_3 - \vec{a}_2.$$

Our approximation is now that $\vec{\delta}_1$, $\vec{\delta}_2$, and $\vec{\delta}_3$ all lie in the plane W_u. We will set up an orthogonal coördinate system in the plane, (u, v), with $\hat{u}$ lying along $\vec{\delta}_2$:

$$\begin{aligned} \hat{u} &\equiv \vec{\delta}_2/|\vec{\delta}_2|, \\ \hat{v} &\equiv \vec{v}/|\vec{v}|, \end{aligned}$$

where

$$\vec{v} = \vec{\delta}_3 - \left(\frac{\vec{\delta}_2 \cdot \vec{\delta}_3}{\vec{\delta}_3 \cdot \vec{\delta}_3}\right)\vec{\delta}_2.$$

The coördinates in the W_u plane of our iterates (as shown in figure F.2) become

$$\begin{aligned} (u_1 - u_0, v_1 - v_0) &= (\vec{\delta}_1 \cdot \hat{u}, \vec{\delta}_1 \cdot \hat{v}), \\ (u_2 - u_1, v_2 - v_1) &= (|\vec{\delta}_2|, 0), \\ (u_3 - u_2, v_3 - v_2) &= (\vec{\delta}_3 \cdot \hat{u}, |\vec{v}|). \end{aligned}$$

And the linear mappings

$$\begin{aligned} (u_1 - u^*, v_1 - v^*) &= G(u_0 - u^*, v_0 - v^*) \\ (u_2 - u^*, v_2 - v^*) &= G(u_1 - u^*, v_1 - v^*) \\ (u_3 - u^*, v_3 - v^*) &= G(u_2 - u^*, v_2 - v^*), \end{aligned}$$

where G is a 2×2 projection of M onto W_u, in the (u, v) coördinate system, so that $|\det G| > 1$.

The algebra is lengthy, but in the end we may eliminate the matrix G and arrive at a formula for the position of the fixed point $\vec{a}^*$ in terms of the differences $\vec{\delta}_n$ and the iterate $\vec{a}_2$:

$$\vec{a}^* = \vec{a}_2 + \frac{\vec{\delta}_2}{c_2 - 1} + \frac{\vec{\delta}_3}{c_3 + 1}, \qquad \text{(F.5)}$$

where

$$c_2 = \frac{(\vec{\delta}_1 \cdot \vec{\delta}_3)(\vec{\delta}_2 \cdot \vec{\delta}_2 - \vec{\delta}_3 \cdot \vec{\delta}_2) + (\vec{\delta}_1 \cdot \vec{\delta}_2)(\vec{\delta}_3 \cdot \vec{\delta}_3 - \vec{\delta}_3 \cdot \vec{\delta}_2)}{(\vec{\delta}_2 \cdot \vec{\delta}_2)(\vec{\delta}_3 \cdot \vec{\delta}_3) - (\vec{\delta}_2 \cdot \vec{\delta}_3)^2}$$

and

$$c_3 = \frac{(\vec{\delta}_3 \cdot \vec{\delta}_2)(\vec{\delta}_1 \cdot \vec{\delta}_3 - \vec{\delta}_3 \cdot \vec{\delta}_2) + (\vec{\delta}_3 \cdot \vec{\delta}_3)(\vec{\delta}_2 \cdot \vec{\delta}_2 - \vec{\delta}_1 \cdot \vec{\delta}_2)}{(\vec{\delta}_3 \cdot \vec{\delta}_2)(\vec{\delta}_1 \cdot \vec{\delta}_2) - (\vec{\delta}_2 \cdot \vec{\delta}_2)(\vec{\delta}_1 \cdot \vec{\delta}_3)}.$$

Equation F.5 is our estimate for the position of $\vec{a}^*$. If backtracking with this estimate for our current iterate still fails to converge to the fixed point, then again it is possible that: (i) the initial vector $\vec{a}_0$ was too far from the fixed point, (ii) the determinant $\det G$ was too close to unit magnitude, or (iii) $\dim W_u > 2$. The remedies for each of these cases is the same as for the corresponding cases described at the end of the last section. However, it is questionable whether or not it is useful to employ an algorithm for $\dim W_u > 2$. As we continue to iterate $\mathcal{M}$, the resultant vectors will eventually be so far away from $\vec{a}^*$ that equation F.1 is no longer valid. This means we may have to start impractically close to $\vec{a}^*$ to begin backtracking. For the two-dimensional case where we need three iterates, this could already be a problem. For a higher dimensional W_u, even more iterates would be needed.

Appendix G

The Rotating Wave Approximation

The Rotating Wave Approximation (RWA) is an integrable approximation to the sinusoidally-driven two state system described by the Hamiltonian (3.9), with $\zeta = 0$. Splitting the the driving term in this Hamiltonian, as is done in equation 8.11, and dropping the second term in the curly brackets in that equation, one obtains the Schrödinger equation

$$i\hbar\frac{\partial\psi}{\partial t} = \left[\tfrac{1}{2}\hbar\omega_{10}\begin{pmatrix} -1 & 0 \\ 0 & 1 \end{pmatrix} + \tfrac{1}{2}\hbar\omega_D\begin{pmatrix} 0 & -ie^{i\omega t} \\ ie^{-i\omega t} & 0 \end{pmatrix}\right]\psi(t). \tag{G.1}$$

The trick is to find a unitary transformation that turns the Hamiltonian for the system time-independent[1]. The transformation here is simply

$$\psi(t) = \begin{pmatrix} e^{-i\omega t} & 0 \\ 0 & 1 \end{pmatrix}\chi(t).$$

---

[1] By Floquet's theorem, for a periodically driven system, there *always* exists such a transformation, however, only in the exactly integrable systems can such a transformation be written down in closed form.

Plugging this transformation into the above Schrödinger equation, one obtains

$$i\hbar\frac{\partial\chi}{\partial t} = G\chi(t),$$

where

$$G = \tfrac{1}{2}\hbar(\omega_{10} - \omega)\begin{pmatrix} -1 & 0 \\ 0 & 1 \end{pmatrix} + \tfrac{1}{2}\hbar\omega_D\begin{pmatrix} 0 & i \\ -i & 0 \end{pmatrix} - \tfrac{1}{2}\hbar\omega$$

is the Hamiltonian equation for a time-independent system, and whose stationary states and energy eigenvalues are the Floquet states and quasienergies of (G.1). Diagonalizing G,

$$\det(G - \varepsilon) = 0,$$

yields two quasienergies

$$\varepsilon_{\pm} = -\tfrac{1}{2}\hbar\omega \pm \tfrac{1}{2}\hbar\sqrt{(\omega_{10} - \omega)^2 + \omega_D^2}.$$

Of course, there are an infinite number of representatives for each quasienergy, indexed by an integer m, obtained by adding an integer multiple of photon energies $m\hbar\omega$. The RWA quasienergies (over two $\hbar\omega$-zones) are plotted in figure G.1, for $\omega/\omega_{10} = 0.33$. Notice there are *no* avoided crossings in this figure, since the RWA Hamiltonian is integrable. Therefore, the Rotating Wave Approximation is a fine approximation for a mildly driven system, that is, with driving field strengths below those in which one expects the strong field avoided crossings to play an important role.

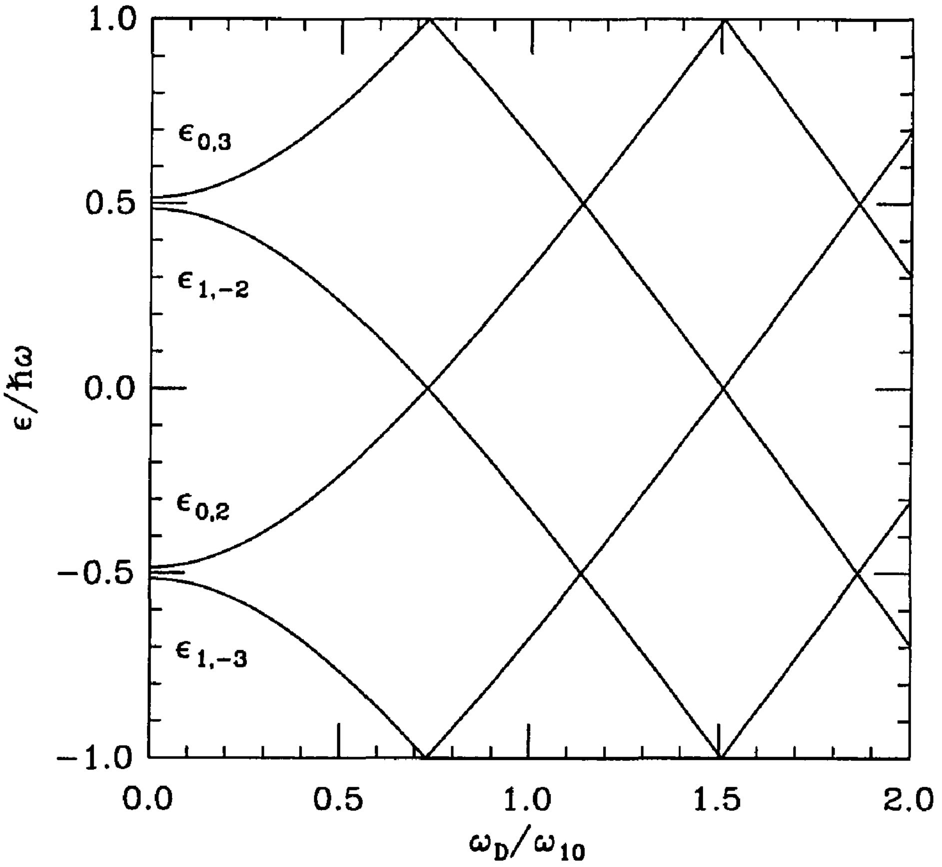

Figure G.1: The quasi-energy plot of the two-state system in the Rotating Wave Approximation, described by the Hamiltonian (G.1), with $\omega/\omega_{10} = 0.33$.

Appendix H

The Zero-Temperature Phonon Bath

We wish to derive a zero-temperature formula for the time evolution of the reduced density matrix of an arbitrary system coupled with a bath of harmonic oscillators. We will extend the result of Caldeira and Leggett [14] who derived a *high*-temperature formula of this sort. Although Dekker [17] has derived a formula valid for zero temperatures, his derivation is only for a damped harmonic oscillator, and uses "quantal noise" to bring about the damping. However, our result will look formally similar to Dekker's.

We begin with system coupled linearly to a bath of harmonic oscillators:

$$H = H_A + H_I + H_B = \frac{p^2}{2M} + v(x) + x\sum_k C_k R_k + \sum_k \frac{p_k^2}{2m} + \tfrac{1}{2}\sum_k m\omega_k^2 R_k^2.$$

The system coördinate is x, and the coördinate of the k^{th} harmonic oscillator is R_k. This can be solved exactly [21, 22], and the reduced density operator for the system (tracing over bath variables) $\tilde{\rho}(x,y,t)$ evolves by

$$\tilde{\rho}(x,y,t) = \int dx'dy' J(x,y,t;x',y',0)\tilde{\rho}(x',y',0),$$

where

$$\begin{aligned} J(x,y,t;x',y',0) &= \int\!\!\int \mathcal{D}x\mathcal{D}y \exp \frac{i}{\hbar}\Big\{S_A[x] - S_A[y] - \int_0^t \int_0^\tau [x(\tau) - y(\tau)] \\ &\quad \times \alpha_I(\tau - s)[x(s) + y(s)]d\tau ds\Big\} \\ &\quad \times \exp -\frac{1}{\hbar}\int_0^t \int_0^\tau [x(\tau) - y(\tau)]\alpha_R(\tau - s)[x(s) - y(s)]d\tau ds. \end{aligned}$$

This contains the action of the system,

$$S_A = \int_0^t \left(\tfrac{1}{2}M\dot{x}^2 - v(x)\right),$$

and the influence functionals

$$\alpha_R(\tau - s) = \sum_k \frac{C_k^2}{2m\omega_k} \coth \frac{\hbar\omega_k}{2k_BT} \cos \omega_k(\tau - s)$$

and

$$\alpha_I(\tau - s) = -\sum_k \frac{C_k^2}{2m\omega_k} \sin \omega_k(\tau - s).$$

Up until now, everything has been exact. The only temperature dependence is in α_R, which becomes in the limit as $T \to 0$,

$$\alpha_R(\tau - s) = \sum_k \frac{C_k^2}{2m\omega_k} \cos \omega_k(\tau - s).$$

In order to make progress, we approximate the sums over the reservoir as integrals. Doing so,

$$\alpha_R(\tau - s) \approx \frac{1}{2m}\int_0^\infty \rho_D(\omega)\frac{C^2(\omega)}{\omega} \cos \omega(\tau - s)d\omega,$$

and we must decide on the oscillator density $\rho_D(\omega)$ and the coupling strengths $C(\omega)$. This is already done in Caldeira and Leggett, obtained from taking the high-temperature case and matching the result with the known classical theory of Brownian motion. They also introduce a frequency cutoff Ω, so that

$$\rho_D(\omega)C^2(\omega) = \begin{cases} \frac{2m\eta\omega^2}{\pi}, & \omega < \Omega, \\ 0 & \omega > \Omega, \end{cases}$$

where η is the viscous damping constant for the classically damped case, obtained in the high-T limit. This gives us

$$\alpha_R(\tau - s) = \frac{\eta}{\pi}\int_0^{\Omega} \omega \cos\omega(\tau - s)d\omega,$$

and

$$\alpha_I(\tau - s) = -\frac{\eta}{\pi}\int_0^{\Omega} \omega \sin\omega(\tau - s)d\omega = \frac{\eta}{2\pi}\frac{d}{\tau - s}\int_{-\Omega}^{\Omega} \cos\omega(\tau - s)d\omega.$$

This term becomes the derivative of a δ-function in the limit of high Ω. This is a tricky point. We will not assume that Ω actually is taken to infinity, but we will assume that it is larger than any other frequency in the problem. Thus, we will *sometimes* send $\Omega \to \infty$, but only as a mathematically convenient approximation. Other times, it will be kept finite, as is necessary. For instance, taking the limit $\eta \to \infty$ gives

$$\alpha_I(\tau - s) \to \eta\frac{d}{\tau - s}\delta(\tau - s).$$

Substituting this in the propagator integral and integrating that term by parts gives an $\eta\delta(0)$ coefficient. Looking at the origin of the δ-function more carefully, we see that this coefficient is actually

$$\frac{1}{\pi}\lim_{\Omega \to \infty} \eta\Omega.$$

This will be taken to be a finite constant, so that it would *appear* that we are taking $\eta \to 0$. Since η is our damping constant, this is clearly not the case. We are merely saying that η is very much less than any other frequency in the problem.

The net result of the $\eta\delta(0)$ term is to add a small harmonic term to the potential energy terms in S_A, which we will take to be the effective, or renormalized system S_R. Thus the propagator reads

$$J(x, y, t; x', y', 0) \;=\; \int\!\!\int \mathcal{D}x\mathcal{D}y \exp\frac{i}{\hbar}\Big\{S_R[x] - S_R[y]$$

$$-\frac{\eta}{2}\int_0^t(x\dot{x}-y\dot{y}+x\dot{y}-y\dot{x})d\tau\Big\}$$
$$\times\exp-\frac{1}{\hbar}\frac{\eta}{\pi}\int_0^\Omega\int_0^t\int_0^\tau[x(\tau)-y(\tau)]\omega\cos\omega(\tau-s)[x(s)-y(s)]d\tau ds d\omega.$$

We are left with the task of evaluating the last integral.

Evaluating the ω-ingtegal before taking $\Omega\to\infty$,

$$\int_0^\Omega\omega\cos\omega(\tau-s)d\omega=\Omega\left\{\frac{\sin\Omega(\tau-s)}{\tau-s}+\frac{1}{\Omega(\tau-s)^2}\left[\cos\Omega(\tau-s)-1\right]\right\}.$$

Taking the limit as $\Omega\to\infty$ gives δ-functions,

$$\lim_{\Omega\to\infty}\frac{\sin\Omega(\tau-s)}{\tau-s}=\pi\delta(\tau-s),$$

and

$$\lim_{\Omega\to\infty}\frac{1}{\Omega(\tau-s)^2}\left[\cos\Omega(\tau-s)-1\right]=-\tfrac{1}{2}\pi\delta(\tau-s).$$

This gives us the final expression for the propagator,

$$J(x,y,t;x',y',0)=\int\int\mathcal{D}x\mathcal{D}y\exp\frac{i}{\hbar}\Big\{S_R[x]-S_R[y]$$
$$-\frac{\eta}{2}\int_0^t(x\dot{x}-y\dot{y}+x\dot{y}-y\dot{x})d\tau\Big\}$$
$$\times\exp-\frac{1}{\hbar}\frac{\eta\Omega}{2}\int_0^t[x(\tau)-y(\tau)]^2d\tau.$$

This propagator is of the same form as that derived by Caldeira and Leggett, with the substitution

$$\frac{\eta k_BT}{\hbar^2}\to\tfrac{1}{2}\eta\Omega.$$

In fact, this is what Dekker derived for the damped harmonic oscillator at $T=0$. We have derived this for a general damped system, at $T=0$. Making the above substitution in the reduced density matrix equation of motion, we have

$$\dot{\tilde{\rho}}=\frac{1}{i\hbar}[H_R,\tilde{\rho}]+\frac{\gamma}{i\hbar}(xp\tilde{\rho}-\tilde{\rho}px+x\tilde{\rho}p-p\tilde{\rho}x)-\frac{\eta\Omega}{2\hbar}[x,[x,\tilde{\rho}]].$$

Here, we have used the equation found in Caldeira and Leggett, noting that $\gamma = \frac{\eta}{2M}$, and using the relation $[x, p] = i\hbar$.

H.1 The Two-State System

Well-known damping results are available for the two-state system, and we would like to compare the calculations shown here with them. To this end, let us work in the two-state system,

$$\tilde{\rho} = \begin{pmatrix} \rho_{00} & \rho_{01} \\ \rho_{10} & \rho_{11} \end{pmatrix}.$$

Let us assume that the x and p operators can be written as

$$x = x_{10}\begin{pmatrix} 0 & 1 \\ 1 & 0 \end{pmatrix}, \quad p = p_{10}\begin{pmatrix} 0 & -i \\ i & 0 \end{pmatrix}.$$

Then the equation of motion becomes

$$\dot{\tilde{\rho}} = \frac{1}{i\hbar}[H_R, \tilde{\rho}] + \frac{2\gamma x_{10} p_{10}}{\hbar}\begin{pmatrix} 1 & 0 \\ 0 & -1 \end{pmatrix} + \frac{\eta\Omega x_{10}^2}{\hbar}\begin{pmatrix} \Delta & -2iq \\ 2iq & -\Delta \end{pmatrix},$$

Where $\Delta \equiv \rho_{00} - \rho_{11}$, and $\rho_{10} \equiv p + iq$. These last two terms are damping terms, and may be cast in the form

$$-\Gamma\begin{pmatrix} \rho_{00} - \rho_{00}^0 & -iq \\ iq & \rho_{11} - \rho_{11}^0 \end{pmatrix},$$

(where ρ_{00}^0 and ρ_{11}^0 are the undriven equilibrium values of the ρ_{00} and ρ_{11},) with the substitutions

$$\frac{2\gamma x_{10} p_{10}}{\hbar} = \frac{\eta\Omega x_{10}^2}{\hbar} = \tfrac{1}{2}\Gamma,$$

and taking advantage of the fact that $\rho_{00} + \rho_{11} = 1$.

This should be compared with the relaxation operator used in this work (5.2) for the two-state system,

$$-\begin{pmatrix} \Gamma_1(\rho_{00}-\rho_{00}^0) & \Gamma_2\rho_{01} \\ \Gamma_2\rho_{10} & \Gamma_1(\rho_{11}-\rho_{11}^0) \end{pmatrix}.$$

We see two differences between the phonon bath model and the above relaxation matrix. First, there is only *one* characteristic damping rate, Γ, instead of two. The second is that the phonon model only damps the *imaginary* part of the off-diagonal elements. Thus, it appears that the model proposed by Caldeira and Leggett, when applied to the two-state system, captures the population relaxation mechanisms quite well, but leaves something to be desired when modeling the correlation relaxation mechanisms.

Bibliography

[1] T. Ando. Electronic properties of two-dimensional systems. *Rev. Mod. Phys.*, 54:437, 1982.

[2] T. Ando. Self-consistent results for a GaAs/Al$_x$Ga$_{1-x}$As heterojunction. I. Subband structure and light-scattering spectra. *J. Phys. Soc. Jpn.*, 51:3893–3899, 1982.

[3] N. W. Ashcroft and N. D. Mermin. *Solid State Physics.* Saunders, 1976.

[4] G. Baym. *Lectures on Quantum Mechanics.* Benjamin/Cummings, California, 1973.

[5] F. Benvenuto, G. Casati, I. Guarneri, and D. L. Shepelyanski. A quantum transistion from localized to extended states in a classically chaotic system. *Z. Physik B*, 84:N1:159–163, 1990.

[6] B. Birnir, B. Galdrikian, M. Sherwin, and R. Grauer. Nonperturbative resonances in periodically driven quantum wells. *Phys. Rev. B*, 47:6795–6798, 1993.

[7] B. Birnir, V. Gudmundsson, and K. Johnson. To be published.

[8] K. Blum. *Density Matrix Theory and Applications.* Plenum Press, New York, 1981.

[9] H. P. Breuer, K. Dietz, and M. Holthaaus. On the classical dynamics of strongly driven anharmonic oscillators. *Physica D*, 46:N3:317–341, 1990.

[10] H. P. Breuer, K. Dietz, and M. Holthaus. The role of avoided crossings in the dynamics of strong laser field - matter interactions. *Z. Phys. D*, 8:349, 1988.

[11] H. P. Breuer, K. Dietz, and M. Holthaus. Strong laser fields interacting with matter i. *Z. Phys. D*, 10:13, 1988.

[12] H. P. Breuer and M. Holthaus. Adiabatic processes in the ionization of highly excited hydrogen atoms. *Z. Phys. D*, 11:1–14, 1989.

[13] H. P. Breuer and M. Holthaus. A semiclassical theory of quasienergies and floquet wave functions. *Annals of Physics*, V221:N2:249–291, 1991.

[14] A. O. Caldeira and A. J. Leggett. Path integral approach to quantum brownian motion. *Physica A*, 121:587–616, 1983.

[15] B. V. Chirikov. A universal instability of many-dimensional oscillator systems. *Physical Reports*, 52(5):263–379, 1979.

[16] E. A. Coddington and N. Levinson. *Theory of Ordinary Differential Equations.* McGraw-Hill, New York, 1955.

[17] H. Dekker. Quantization of the linearly damped harmonic oscillator. *Phys. Rev. A*, 16:2126–2134, 1977.

[18] J. F. Dobson. The harmonic-potential theorem: Implications for approximate many-body theories. Submitted to Phys. Rev. Lett.

[19] R. M. Dreizler and E. K. U. Gross. *Density Functional Theory.* Springer-Verlag, Berlin; Heidelberg, 1990.

[20] M. I. Dykman and V. N. Smelyanskiĭ. Quantum theory of transitions between stable states of a nonlinear oscillator interacting with a medium in a resonant field. *Sov. Phys. JETP*, 67:1769, 1988.

[21] R. P. Feynman. *Statistical Mechanics; a set of lectures.* Benjamin, Reading, Massachusetts, 1972.

[22] R. P. Feynman and A. R. Hibbs. *Quantum Mechanics and Path Integrals.* McGraw-Hill, New York, 1965.

[23] J. M. Greene. A method for determining a stochastic transition. *J. Math. Physics*, 20(6):1183–1201, 1979.

[24] E. K. U. Gross and W. Kohn. Time-dependent density-functional theory. *Advances in Quantum Chemistry*, 21:255, 1990.

[25] J. N. Heyman et al. Resonant harmonic generation and dynamic screening in a double quantum well. *Phys. Rev. Lett.*, 72:2183–2186, 1994.

[26] M. Hillery, R. F. O'Connell, M. O. Scully, and E. P. Wigner. Distribution functions in physics: Fundamentals. *Physics Reports*, 106(3):121–167, 1984.

[27] P. Hohenberg and W. Kohn. Inhomogeneous electron gas. *Phys. Rev.*, 136:864–871, 1964.

[28] R. V. Jensen, M. M. Sanders, M. Saraceno, and B. Sundaram. Inhibition of quantum transport due to scars of unstable periodic orbits. *Phys. Rev. Lett.*, 63:2771–2775, 1989.

[29] W. Kohn and L. J. Sham. Self-consistent equations including exchange and correlation effects. *Phys. Rev.*, 140:1133–1138, 1965.

[30] W. A. Lin and L. E. Reichl. External field induced chaos in an infinite square well potential. *Physica D*, 19:145–152, 1986.

[31] R. Loudon. *The Quantum Theory of Light.* Oxford University Press, New York, 1973.

[32] R. S. MacKay and J. D. Meiss. Relation between quantum and classical thresholds for multiphoton ionization of excited atoms. *Phys. Rev. A*, 37:4702, 1988.

[33] I. L. Mayer, L. C. M. Miranda, B. Y. Tong, and R. M. O. Galvao. On the stochastic ionisation of electrons in quantum well structures. *J. Phys. B*, 18:3835–3847, 1985.

[34] E. Runge and E. K. U. Gross. Density-functional theory for time-dependent systems. *Phys. Rev. Lett.*, 52:997, 1984.

[35] H. Sambé. Steady states and quasienergies of a quantum-mechanical system in an oscillating field. *Phys. Rev. A*, 7:2203, 1973.

[36] J. H. Shirley. Solution of the schrödinger equation with a hamiltonian periodic in time. *Phys. Rev.*, V138(4B):B979–B987, 1965.

[37] J. M. T. Thompson, A. R. Bokaian, and R. Ghaffari. Subharmonic resonances and chaotic motions of a bilinear oscillator. *IMA Journal of Applied Mathematics*, 31:207–234, 1983.

[38] M. Załużny. Influence of the depolarization effect on the nonlinear intersubband absorption spectra of quantum wells. *Phys. Rev. B*, 47:3995–3998, 1993.